

Dissertation zu Erlangung des Doktorgrades  
der Fakultät für Chemie und Pharmazie  
der Ludwig-Maximilians-Universität München



## **Defective DNA Repair in EGFR-mutant Lung Cancer**

### **Opportunities for Targeted Therapy**

Heike Natalie Pfäffle  
aus Esslingen am Neckar, Deutschland

2013

## Erklärung

Diese Dissertation wurde im Sinne von § 7 der Promotionsordnung vom 28. November 2011 von Herrn Prof. Dr. Henning Willers betreut und von Frau Prof. Dr. Angelika Vollmar von der Fakultät für Chemie und Pharmazie vertreten.

## Eidesstattliche Versicherung

Diese Dissertation wurde eigenständig und ohne unerlaubte Hilfe erarbeitet.

München, den 20. September, 2013

Heike Natalie Pfäffle 

-----  
Heike Natalie Pfäffle

Dissertation eingereicht am:	15.10.2013
1. Gutachterin:	Prof. Dr. Angelika M. Vollmar
2. Gutachter:	Prof. Dr. Henning Willers
Mündliche Prüfung am:	5.11.2013

# **Meiner Familie**

# **TABLE OF CONTENTS**

<b>1. INTRODUCTION.....</b>	<b>5</b>
<b>1.1. Significance and Objective.....</b>	<b>6</b>
<b>1.2. Lung cancer .....</b>	<b>8</b>
1.2.1. Characteristics of lung cancer .....	8
1.2.2. EGFR and lung cancer .....	11
1.2.2.1. EGFR function .....	11
1.2.2.2. Mutant EGFR in lung cancer .....	13
<b>1.3. DNA repair.....</b>	<b>16</b>
1.3.1. Defective DNA repair – Promoter and “Achilles Heel” of cancers .....	16
1.3.2. DNA Interstrand Crosslink (ICL) Repair .....	17
1.3.2.1. DNA damaging agents: cisplatin and MMC.....	17
1.3.2.2. ICL repair by Fanconi Anemia (FA) pathway and Homologous Recombination Repair (HRR).....	19
1.3.3. Targeting defects in DNA repair .....	24
1.3.3.1. Concept of targeted therapies .....	24
1.3.3.2. Targeted therapy with PARP inhibitors .....	24
1.3.3.2.1. PARP1 function.....	25
1.3.3.2.2. PARP inhibitors .....	25
<b>2. MATERIALS AND METHODS .....</b>	<b>29</b>
<b>2.1. Materials.....</b>	<b>30</b>
2.1.1. Drugs, chemicals, antibodies.....	30
2.1.2. Equipment .....	33
2.1.3. Company Addresses .....	35
<b>2.2. Methods.....</b>	<b>36</b>
2.2.1. Cell lines .....	36
2.2.2. Cell culture.....	38
2.2.3. Freezing, thawing, storage .....	38
2.2.4. Creating EGFR TKI resistant cell lines .....	38
2.2.5. Long-term cell survival: Colony formation assay .....	39
2.2.6. Short-term cell survival: Syto60 staining .....	40
2.2.7. Foci formation assay .....	40
2.2.7.1. Immunofluorescent staining in cell lines.....	40
2.2.7.2. Immunofluorescent staining in tissue .....	41
2.2.8. Flow Cytometry.....	42
2.2.9. Western Blot.....	43
2.2.9.1. Isolation of proteins .....	43
2.2.9.2. Protein quantification: The Bio-Rad protein assay .....	43
2.2.9.3. SDS-PAGE .....	44
2.2.9.3.1. Sample preparation.....	44
2.2.9.3.2. Electrophoresis .....	44
2.2.9.4. Transfer .....	44
2.2.9.5. Detection .....	45
2.2.10. Chromatid aberrations .....	45
2.2.11. Transfections .....	46

2.2.11.1. Plasmids.....	46
2.2.11.2. Plasmid amplification.....	46
2.2.11.2.1. Transformation.....	46
2.2.11.2.2. DNA Purification.....	47
2.2.11.3. Plasmid identification.....	48
2.2.11.4. Plasmid transfection.....	49
2.2.12. Gene silencing.....	49
2.2.13. Modified alkaline comet assay.....	50
2.2.14. Alkaline comet assay.....	51
2.2.15. Gene expression analysis.....	52
2.2.16. Statistical Analysis.....	52
<b>3. RESULTS .....</b>	<b>53</b>
<b>3.1. EGFR-mutant cell lines are impaired in repairing DNA damage         resulting in a Fanconi Anemia like cellular phenotype .....</b>	<b>54</b>
3.1.1. EGFR-mutant cell lines exhibit increased sensitivity to ICL inducing agents.....	54
3.1.2. EGFR mutation sensitizes to ICL inducing agents.....	55
3.1.3. EGFR-mutant cell lines show increased unrepaired DNA damage upon treatment with cisplatin.....	56
3.1.4. EGFR-mutant cells arrest in G2 phase when challenged with MMC...58	
3.1.5. Increased chromosomal radials can be found in EGFR-mutant cells treated with MMC.....	60
3.1.6. EGFR mutation is associated with increased ATM activity.....	61
<b>3.2. Mutated EGFR impairs FA/HRR pathway resulting in lack of repair         protein RAD51 in response to ICL.....</b>	<b>63</b>
3.2.1. EGFR-mutant cells, like FA-deficient ones, do not form RAD51 repair foci in response to ICL.....	63
3.2.2. EGFR-mutant cells contain normal levels of RAD51 protein.....	65
3.2.3. RAD51 foci defect in EGFR-mutant cells is specific for ICL damage..	65
3.2.4. EGFR nuclear translocation does not correlate with the observed FA/HRR defect.....	66
3.2.5. DNA-PKcs activity does not affect sensitivity to cisplatin.....	67
3.2.6. Overactive EGFR signaling in mutant cells does not account for lack of RAD51 foci.....	68
3.2.7. EGFR impairs FANCD2/RAD51 pathway kinase-independently.....	70
<b>3.3. Repair defect is downstream of FANCD2 at the stage of ICL         unhooking involving failed recruitment of FAN1 .....</b>	<b>71</b>
3.3.1. EGFR mutation is epistatic to FANCD2.....	71
3.3.2. Increased replication fork stalling in EGFR-mutant cells.....	73
3.3.3. Defect downstream of BRCA1.....	74
3.3.4. Defect downstream of core complex, FANCD2.....	74
3.3.5. Impaired ICL unhooking.....	75
3.3.6. EGFR-mutant cells have low FAN1 gene expression.....	77
3.3.7. FAN1 protein levels tend to be reduced in EGFR-mutant cells.....	77
3.3.8. EGFR-mutant cells fail to recruit FAN1 to ICL.....	78

<b>3.4. Impaired FAN1 recruitment and HRR sensitizes EGFR-mutant cells to PARP inhibitors</b> .....	<b>79</b>
3.4.1. EGFR-mutant cells fail to form FAN1 foci in response to PARP inhibitor olaparib.....	79
3.4.2. EGFR-mutant cells are impaired in RAD51 foci resolution after PARP inhibitor treatment.....	80
3.4.3. EGFR-mutant cells treated with olaparib contain large amounts of unrepaired DNA damage.....	81
3.4.4. EGFR-mutant cell lines exhibit increased sensitivity to olaparib .....	83
3.4.5. EGFR-mutant sensitizes to olaparib in vivo.....	83
<b>3.5. Treatment with DNA damaging agents: Effect of EGFR TKI resistance on sensitivity</b> .....	<b>85</b>
3.5.1. EGFR TKI resistance may not result in cisplatin resistance.....	85
3.5.2. EGFR TKI resistance might sensitize to IR .....	86
3.5.3. EGFR TKI-resistance sensitizes to PARP inhibitors possibly due to more endogenous SSB .....	88
<b>4. DISCUSSION</b> .....	<b>91</b>
4.1. Cells with mutant EGFR show impaired ICL repair and a FA-like phenotype .....	92
4.2. Defect in FA/HRR pathway is independent of EGFR-mutant kinase function .....	94
4.3. EGFR-mutant cells show reduced FAN1 recruitment and impaired ICL unhooking.....	97
4.4. DNA repair defect in EGFR-mutant cells is exploitable with PARP inhibitors .....	99
4.5. DNA damaging treatments: No adverse influence of EGFR TKI resistance on sensitivity.....	101
4.6. Implications of findings for the clinic: .....	103
<b>5. SUMMARY</b> .....	<b>104</b>
5.1. Summary of findings.....	105
5.2. Model .....	107
<b>6. REFERENCES</b> .....	<b>108</b>
<b>7. APPENDIX</b> .....	<b>116</b>
7.1. Abbreviations .....	117
7.2. Publications .....	119
7.3. Curriculum vitae .....	120
7.4. Acknowledgments.....	121

# **1. INTRODUCTION**

## 1.1. Significance and Objective

Lung cancer is the leading cause of cancer deaths in the US and worldwide. It is the most common cancer found in both men and women in the US after prostate and breast cancer [1]. Lung cancer outlooks in Germany are similarly dire [2] (Figure 1). Given these grim statistics there is a great urgency to improve treatment outcome.

Traditional cancer therapy is based on a “one treatment fits all” theory. The mainstay treatment for locally, advanced lung cancer has long been radiation combined with chemotherapy [1]. Outcomes of this treatment regime are however unsatisfactory. Hallmarks of traditional cancer therapy are severe side effects and poor survival rates, especially in patients with advanced tumors. The 5-year survival rate for patients with non-small cell lung cancer (NSCLC) is as low as 16% [1].

Across the field of cancer therapies, there has been a recent trend towards utilizing newly discovered targeted agents. These drugs target specific features in the tumor and advance the field towards more “personalized medicine”. They tend to be less toxic to normal cells and thus better tolerable by patients.

One great example for this concept is poly ADP-ribose polymerase (PARP) inhibitors. These drugs interfere with DNA repair by inhibiting the DNA repair enzyme PARP, thus leading to prolonged DNA damage. Normally other repair pathways can repair the damage, but some cancer cells harbor defects in the DNA repair machinery, rendering them specifically sensitive to PARP inhibitors. Promising results with PARP inhibitors have been achieved in breast, ovarian and prostate cancers, which contain those DNA repair defects [3].

Another example of targeted therapy is inhibitors against the tyrosine kinase of epidermal growth factor receptor (EGFR). These drugs are very effective in a subset of lung cancer patients, which harbor activating mutations in EGFR. Such cancers are dependent on the overactive survival and growth signaling of mutated EGFR; thus disruption with EGFR inhibitors leads to cancer cell death and impressive decrease of tumor size [4]. Despite great initial success, unfortunately, nearly all patients experience tumor progression, posing the need for yet another treatment strategy [5].

Our group is particularly interested in the treatment of lung cancer and the study of DNA repair pathways. With the need to find new treatment approaches for EGFR-mutant lung cancer patients, we aimed to find DNA repair defects exploitable for targeted therapy.

We built our hypothesis on the following information: Our previous findings showed, that NSCLC are enriched for DNA repair defects. Birkelbach et al. found a prevalence of homologous recombination repair (HRR) defects in NSCLC in vitro and in vivo [6]. Furthermore, it has been observed in the clinic that EGFR-mutant NSCLC exhibit increased sensitivity to platinum-based DNA damaging agents [7] [8] [9]. Thus we speculated to find new targets within the DNA repair machinery, and we hypothesized the following:

“EGFR-mutant lung cancers harbor a common DNA repair defect, exploitable for targeted therapy.”

A secondary aim was to investigate the influence of acquired resistance to EGFR tyrosine kinase inhibitors (TKI) on sensitivity to DNA damaging treatments in EGFR-mutant lung cancer cell lines.

**Aims of this Ph.D. thesis:**

1. To characterize the response of EGFR-mutant lung cancer cells to DNA damaging therapy:
  - a. Elucidate the mechanism of defective DNA repair in EGFR-mutant lung cancers
  - b. Exploit defective DNA repair for targeted treatment
2. To determine whether acquired resistance to EGFR TKI alters the sensitivity of EGFR-mutant lung cancer cells to DNA damaging agents.

## 1.2. Lung cancer

### 1.2.1. Characteristics of lung cancer

Lung cancers are classified according to their histology: Non-small cell lung cancers (NSCLC) and small-cell lung cancers (SCLC) [5]. This study will focus on the more common type of NSCLC, which accounts for 84% of lung cancer cases [5] [1].

The number one risk factor for developing lung cancer is smoking. The relative risk in men is 23. This means men, who smoke, are 23x more likely to develop lung cancer than their non-smoking fellows [1]. Furthermore there is a strong causal relationship between passive smoking and lung cancer [10]. Second in the rank is radon gas released from soil and building materials [1]. Other risk factors include asbestos, certain metals (chromium, cadmium, arsenic), some organic chemicals, radiation, air pollution, diesel exhaust and paint [1]. While all these risk factors can be avoided - especially smoking – this last one cannot: genetic susceptibility [1]. So far we have a very limited understanding of how genetic background could influence lung cancer development. Germline mutations in the epidermal growth factor receptor (EGFR), for example, may increase the risk to develop lung cancer [11]. EGFR is a cell surface receptor involved in growth and survival signaling; for more details see chapter 1.2.2.1. An ongoing study is further elucidating the association between EGFR germline mutations and increased lung cancer risk (ClinicalTrials.gov Identifier #: NCT01754025). Somatic EGFR activating mutations, on the other hand, seem to cluster in non-smokers of East-Asian ethnicity [12] [5] [13]. However, the cause of this remains elusive.

Unfortunately by the time lung cancer is detected, it has usually metastasized. Only 15% are diagnosed in an early stage [1]. For 2013, 228,190 new cases are expected in the US alone, which accounts for 14% of all cancer diagnoses [1]. This makes lung cancer, after prostate and breast cancer, the most common tumor type in both men and women [14]. In Germany lung cancer ranks third in incidence after prostate/breast and colon cancer [2] (Figure 1B).

Treatment depends on the stage and histology of the tumor (NSCLC or SCLC). Conventional therapy includes surgery, radiation, chemotherapy and sometimes a

combination of all three [1]. New approaches are made with targeted drugs, such as bevacizumab, erlotinib or crizotinib [1]. Unlike conventional chemotherapy, the above drugs exploit characteristics specific to the tumor, which makes them less toxic and initially more effective.

However, the 5-year survival rates of only 16% are dismal [1]. In the US, around 159,480 deaths are expected for the year 2013. Thus lung cancer accounts for 27% of all cancer deaths, killing more men and women than any other type of cancer (Figure 1C) [1]. In Germany, the situation is equally dire (Figure 1D). In women lung cancer is among the top 3 causes of cancer deaths. In men it is by far the leading cause, accounting for 26% of cancer related deaths [2].

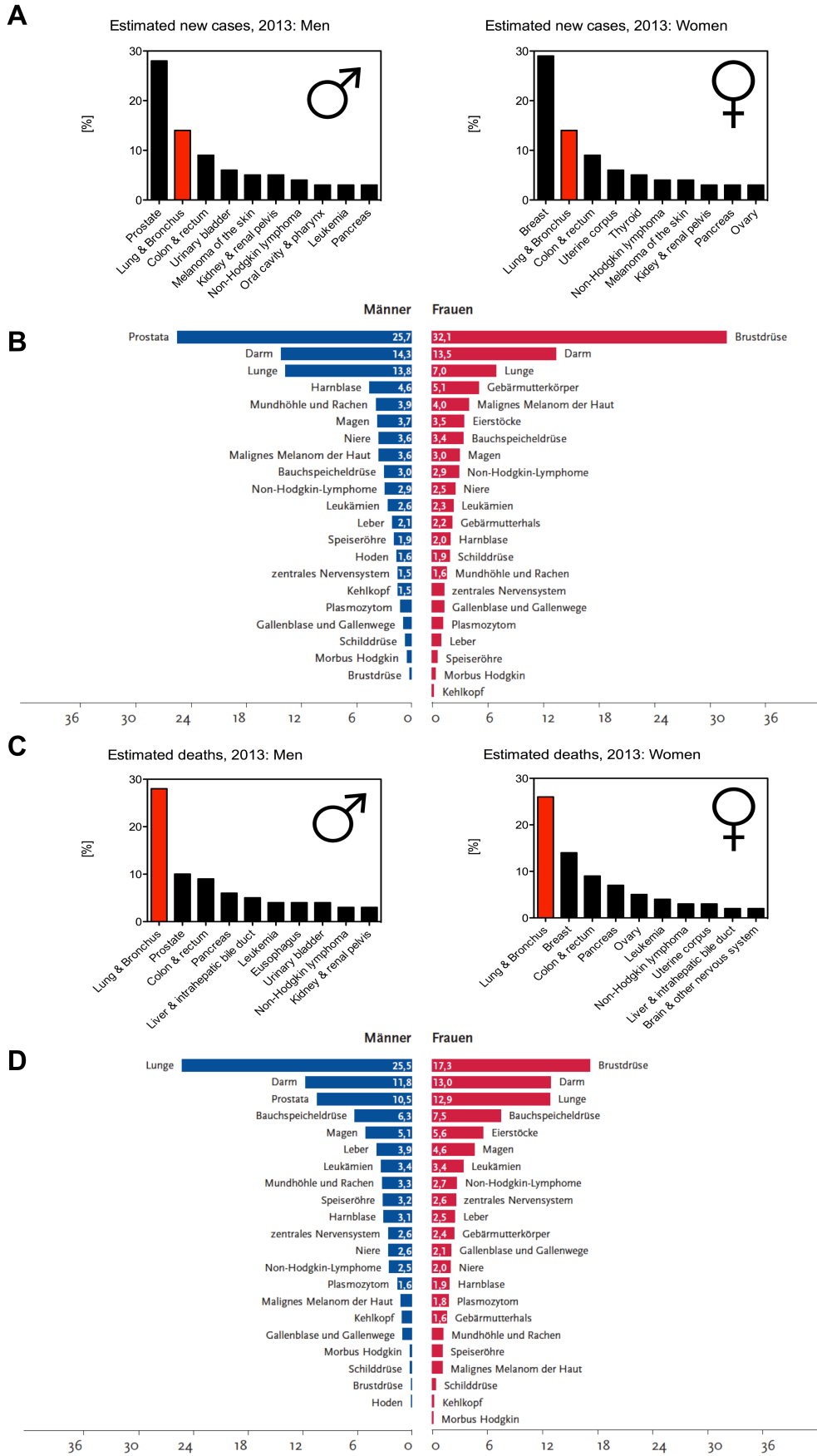


**Figure 1:** A) Estimated new cancer cases for American men and women expected in 2013. B) New cancer cases for German men and women in 2008. Graph adapted from Kaatsch et al, 2012. C) Estimated cancer related deaths for American men and women expected in 2013. D) Cancer related deaths for German men and women in 2008. Graph adapted from Kaatsch et al, 2012. [1] [2]

## 1.2.2. EGFR and lung cancer

### 1.2.2.1. EGFR function

Epidermal growth factor receptor (EGFR/ErbB2/HER-1) is a cell-surface tyrosine kinase receptor [15] [16]. It is a 170-kd transmembrane glycoprotein and a member of the ErbB family of receptors [15] [16] [5]. Other members include ErbB2/HER-2/neu, ErbB3/HER-3 and ErbB4/HER-4 [16] [5].

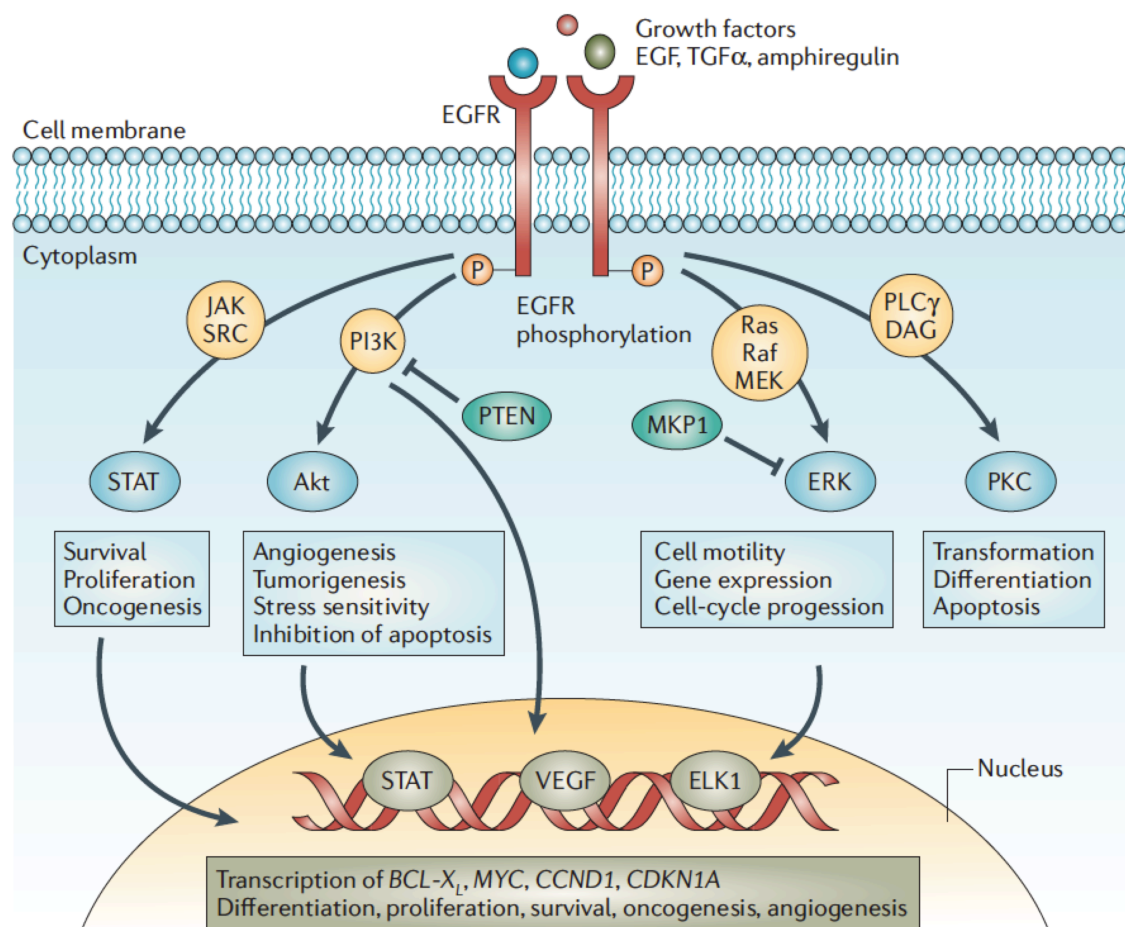
EGFR signaling leads to cellular proliferation, differentiation and anti-apoptotic survival signals [15] [16]. It is further associated with gene expression and angiogenesis [15] [16]. In tumor cells, EGFR stimulation promotes tumor cell motility, adhesion and metastasis [16] (Figure 2).

EGFR signaling is induced by extracellular ligands, mainly epidermal growth factor (EGF) and transforming-growth factor  $\alpha$  (TGF $\alpha$ ) [15] [16]. Upon ligand binding, EGFR transitions from an inactive monomeric form to an active homo- or heterodimer [15] [16]. EGFR heterodimerization occurs with HER2 [16]. After dimerization, EGFR is internalized into clathrin-coated pits [17] and EGFR tyrosine kinase is autophosphorylated [16]. Phosphorylated tyrosine kinase residues act as binding sites for signal transducers and activators of intracellular substrates [16]. Activated downstream pathways of EGFR include PI3K-Akt, RAS-RAF-MEK-ERK, JAK-SRC-STAT, and PLC-DAG-PKC [15] [16] (Figure 2).

Besides activating the aforementioned signaling pathways, EGFR has also been shown to be able to translocate to the nucleus [15] [18] [19] [17]. Nuclear translocation has been associated with transcription activation [17], binding of cyclins D and E [17], and serving as a chaperone for transcription factor STAT5 [17]. Furthermore, it has been suggested that nuclear EGFR may be able to influence DNA double strand break (DSB) repair [15] [20]. Others have shown that nuclear EGFR associates with and increases activity of DNA-PKcs, which plays

an important part in DNA DSB repair by non-homologous endjoining (NHEJ) [15] [20].

EGFR is overexpressed in many cancers such as breast cancer, head-and-neck cancer, NSCLC, renal, ovarian and colon cancer [16]. In fact EGFR is overexpressed in about 40-80% of NSCLC [16]. Overexpression of EGFR results in a high metastatic rate, poor tumor differentiation and increased rate of tumor growth [16]. Thus EGFR has long been a target for anti-cancer therapy.



*CCND1*, gene encoding cyclin D1; *CDKN1A*, gene encoding p21; JAK, Janus kinase; TGF $\alpha$ , transforming growth factor- $\alpha$ .

**Figure 2:** EGFR ligands (EGF, TGF $\alpha$ , amphiregulin) activate the receptor, leading to homo- or heterodimerization and phosphorylation of EGFR. Several downstream pathways can be activated by EGFR; some important ones are shown here. EGFR activates Akt via PI3K, which results in inhibition of apoptosis, cell proliferation and angiogenesis. By activating the Ras-MAPK pathway EGFR stimulates cell motility, gene expression and cell-cycle progression [15]. Graphic adapted from Nyati et al, 2006.

### 1.2.2.2. Mutant EGFR in lung cancer

Somatic activating mutations in EGFR can be found in 10% of NSCLC patients in North America/Europe [12]. In NSCLC patients of East-Asian descent this number increases to 30% [12]. Besides East-Asian ethnicity, there is a higher prevalence of these activating mutations in non smokers and adenocarcinoma histology [12] [13]. Female sex seemed to correlate with mutant EGFR as well, however this may be due to the fact that women are more likely to have never smoked [12]. As for East-Asian ethnicity it is unclear whether the genetic background or the environment promotes EGFR mutations [12]. A study comparing the prevalence of EGFR mutations in lung cancer patients with US citizenship and East Asian descent to East Asian lung cancer patients would clarify this issue [12].

Mutations in EGFR occur mainly in four exons (18-21). These exons encode the ATP-binding pocket of the tyrosine kinase catalytic domain [12] [5]. The most common mutations are in-frame deletions in exon 19, which account for 50% of EGFR mutations [5]. The second most frequent mutation is substitutions at L858 within exon 21, which alters the activation loop of EGFR [5]. The L858 mutation is responsible for 40% of mutations in EGFR [5]. With a frequency of only 5%, mutations found in exon 18 and 20 are less common [5]. All the above somatic mutations lead to very similar phenotypes except for mutations within exon 20 [5]. Most importantly all EGFR mutations mentioned, excluding mutations within exon 20, render tumors equally sensitive to EGFR tyrosine kinase inhibitors in the clinic [5] [21] [22] [23]. Henceforth, all EGFR mutations will be referred to as “mutant EGFR”.

Mutant EGFR contains oncogenic properties, driving tumor growth and survival [5]. Characteristic of mutant EGFR is its permanent active state independent of the presence of a ligand. As a consequence EGFR downstream pathways involved in cell growth and survival signaling, such as ERK1/2 and PI-3 kinase/AKT pathway, are hyperactive [5]. Mutant EGFR acts as an activated oncogene for tumor cell survival and proliferation, rendering tumor cells dependent on overactive EGFR signaling [5] [24]. This phenomenon is termed as “oncogene addiction”, which was first coined by Bernard Weinstein [25] [26] [27]

[24]. Interestingly mutant EGFR signaling as the driving force of the tumor is also its Achilles Heel. The dependency on survival signals emanated by hyperactive EGFR makes the cancer cell vulnerable to disruption of EGFR signaling. When EGFR is inhibited the cancer cell loses its most important source of growth and survival signals and thus undergoes apoptosis. Clinically this phenomenon can be exploited with targeted therapy using EGFR tyrosine kinase inhibitors (TKI), such as gefitinib or erlotinib [12] [5]. These small-molecule inhibitors bind to the intracellular tyrosine kinase domain of EGFR and prevent EGFR tyrosine kinase phosphorylation, thus disrupting activation of EGFR downstream pathways. When mutant EGFR signaling is disrupted in this manner it results in massive tumor cell death in pre-clinical models [5] [24]. The clinical response of NSCLC patients with activating EGFR mutations to treatment with EGFR TKI is quite impressive and significant tumor shrinkage can be achieved [4] (Figure 3). Despite this initial success most patients relapse within 6-12 months of treatment [5]. Only a few patients benefit from this treatment for up to 5 years [5]. Eventually all patients develop drug resistance to these EGFR TKI and experience disease progression [12] [5].

There are a number of ways by which EGFR-mutant cancer cells can acquire resistance to EGFR inhibitors [28] [12] [13] [5]. No matter which resistance mechanism is present the outcome is the same, in that cancer cells maintain growth signaling in the presence of EGFR TKI [28]. Here, I will present two mechanisms that are clinically validated [28].

In 50% of lung cancer patients, resistance is gained through the development of a “secondary” mutation within the EGFR catalytic domain [12] [5]. Moreover, 90 % of these secondary mutations are comprised of the T790M missense substitution, which restores ATP affinity to the catalytic domain and reduces susceptibility to TKI [12] [29] [5]. ATP outcompetes TKI for the catalytic domain and as a result EGFR autophosphorylation is restored and downstream signaling is maintained in the presence of TKI [5]. Second generation EGFR TKI may be able to circumvent this issue, by covalently binding to the receptor, thereby preventing ATP from accessing it irreversibly. So far two second-generation EGFR TKI showed promising results in advanced clinical trials (phase III) [12] [30]. One of these

second-generation drugs, afatinib, is currently under review for approval by the FDA [31] [32] [33].

An alternative form of resistance towards EGFR TKI has been shown to be through the amplification of the gene encoding MET receptor tyrosine kinase [28] [12] [5]. This alteration is seen in 5-10% of NSCLC patients with acquired TKI resistance [12] [5] [30]. Amplified MET is able to sustain survival signals through the PI-3 kinase/Akt pathway when mutant EGFR is inhibited [5]. Thus applying combined treatment with an EGFR TKI and MET kinase inhibitor counteracts this problem and result in cancer cell death [5]. However, it is yet to be validated, if this strategy works in patients.

Both resistance mechanisms, T790M and MET amplification, can be recapitulated in cell line models, reassuring the value of such preclinical studies [34, 35].

The overwhelming success of targeted therapy with EGFR inhibitors in mutant EGFR lung cancer justifies a targeted treatment approach. However given that all patients develop resistance to this treatment, there is a need to investigate new possible targets in this patient group. As the next section will explain, the DNA Damage Response (DDR) machinery is often defective in tumors, thus providing a pool of possible targets [36].

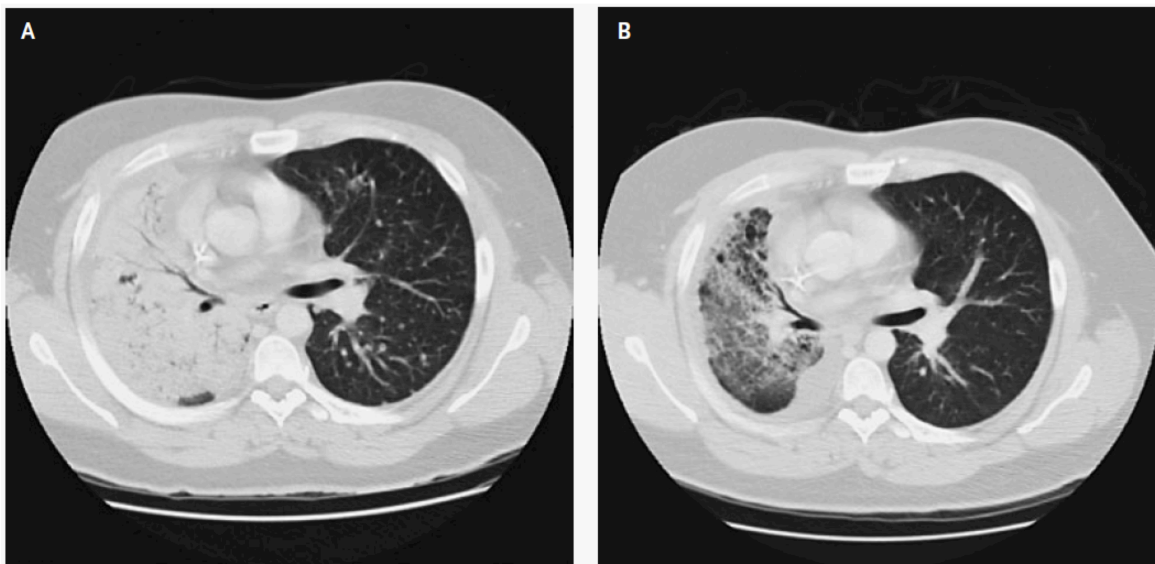


**Figure 3:** Pictures show a computer tomographic scan of the chest in a patient with refractory NSCLC before treatment with gefitinib (A) and 6 weeks after treatment with gefitinib was initiated (B) [4].

## 1.3. DNA repair

### 1.3.1. Defective DNA repair – Promoter and “Achilles Heel” of cancers

At the core of any replicating cell lies its genetic blueprint, the DNA. It stores all the necessary information for any cell to exist, develop and function. The integrity of this crucial component is therefore of utmost importance. Exposure to exogenous threats, such as ionizing radiation (IR), UV radiation, and chemicals as well as endogenously arising reactive oxygen species (ROS) pose a constant challenge to keeping the DNA intact.

When DNA damage occurs, the DNA damage response (DDR) is activated. This means, depending on the type of DNA damage, specific DNA repair pathways are activated to locate the damage, recruit other repair proteins and fulfill repair of the corrupted DNA. Alternatively, if the damage is too severe and cannot be repaired, cell death or senescence is initiated. However, if there are defects within the DDR, cells with faultily repaired DNA damage may be allowed to proliferate as well, which leads to DNA rearrangements and mutations in the subsequent generations. The presence of activated oncogenes, such as mutant EGFR, may exacerbate this phenomenon. Activated oncogenes often cause increased proliferation, which heightens replication stress, resulting in more DNA damage and increased need for the DDR. However not only cells with repaired damage continue to proliferate, those with defective DDR do so as well, which leads to mutations, genomic instability and eventually cancer development (Figure 4). Thus in tumorigenesis activated oncogenes may cause selection pressure for defects in the DDR. [36]

Defective DDR could be seen as a double-edged sword. On the one hand defective DDR promotes carcinogenesis, on the other hand it may weaken the tumor's ability to cope with DNA damage. Thus when challenged with DNA damaging agents, cancers with deficient DNA repair cannot cope with the overwhelming DNA damage and are therefore sensitized to such drugs. Many conventional chemotherapeutics are in fact DNA damaging agents and they may potentially exploit this phenomenon. In order to advance from toxic “one-size-fits

all” chemotherapy to more selective and better-tolerated targeted therapies, elucidating the precise DNA repair defect is of great interest.

There is clinical evidence that EGFR-mutant lung cancer patients respond better to platinum-based DNA damaging agents, such as cisplatin, than patients harboring the wild-type version [7] [8] [9]. Hence we hypothesized that EGFR-mutant tumors are defective in repairing the kind of DNA damage produced by platinum agents.

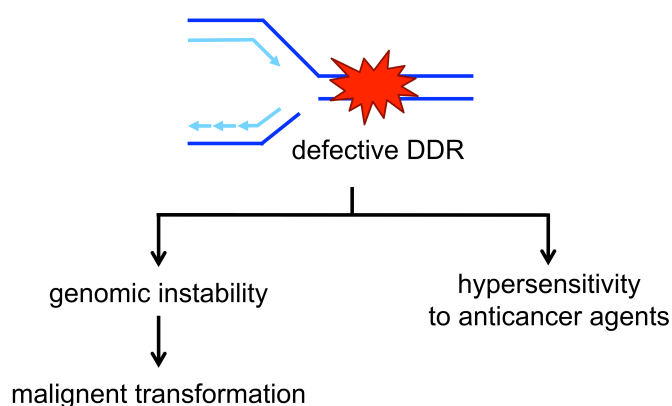


**Figure 4:** Defective DNA damage response (DDR) can lead to genomic instability and malignant transformation. Such cancers are susceptible to DNA damaging agents due to the underlying defect in the DDR [36].

## 1.3.2. DNA Interstrand Crosslink (ICL) Repair

### 1.3.2.1. DNA damaging agents: cisplatin and MMC

Cisplatin, cisplatinum, or cis-diamminedichloroplatinum(II) (CDDP) was first synthesized and described in 1845 as Peyrone’s chloride [37]. More than 100 years later, its biological activity was discovered by accident, yet it took only 3 years thereafter for the first cancer patients to be treated [37] [38]. In 1978 cisplatin gained FDA approval [37].

Mitomycin C (MMC) on the other hand is a naturally occurring product, which was originally derived from fungal sources [38]. It has been used clinically since 1956 [38].

The mode of action of both drugs is very similar. In principal, the compound is activated intracellular and two leaving groups are ejected (Figure 5). In place of

the ejected chemical groups the compound covalently binds to DNA or proteins [37] [38]. In the case of cisplatin this activation happens as follows: Due to the low intracellular chloride levels, cisplatin is aquated, which means the two chloride molecules leave the cisplatin compound sequentially as they get replaced by water molecules. In this activated form cisplatin can covalently bind to DNA or proteins. As for DNA adducts, cisplatin preferentially binds to the  $N^7$ -position of guanosine or adenosine, leading to monoadducts or in the case of two bases being bound leads to formation of crosslinks [38].

MMC is similarly activated intracellularly by cycloreduction. It preferentially crosslinks guanosine residues [38].

If the two crosslinked bases are located on the same DNA strand, they are called intrastrand crosslinks. If the bases are located on opposing DNA strands, it results in much more toxic structures termed interstrand crosslinks (ICL) (Figure 5C). [37] [38]. Even though the damage caused by MMC consists of only 5-10% of ICL and in the case of cisplatin this is even less than 5%, it is believed that the toxicity of both compounds can be attributed to these lesions [38]. This is due to the genotoxic effect of ICL, if left unrepaired. Protein adducts and DNA intrastrand crosslinks are less harmful than ICL, as damaged protein can be replaced and intrastrand crosslinks can be bypassed during transcription and replication [38]. ICL however, if left unrepaired, covalently bind opposing DNA strands together, thus preventing separation of the DNA double helix [38]. Separation of DNA strands is needed for transcription and replication [37] [38]. By inhibiting these most essential cellular processes, unrepaired ICL quickly lead to apoptosis [38].

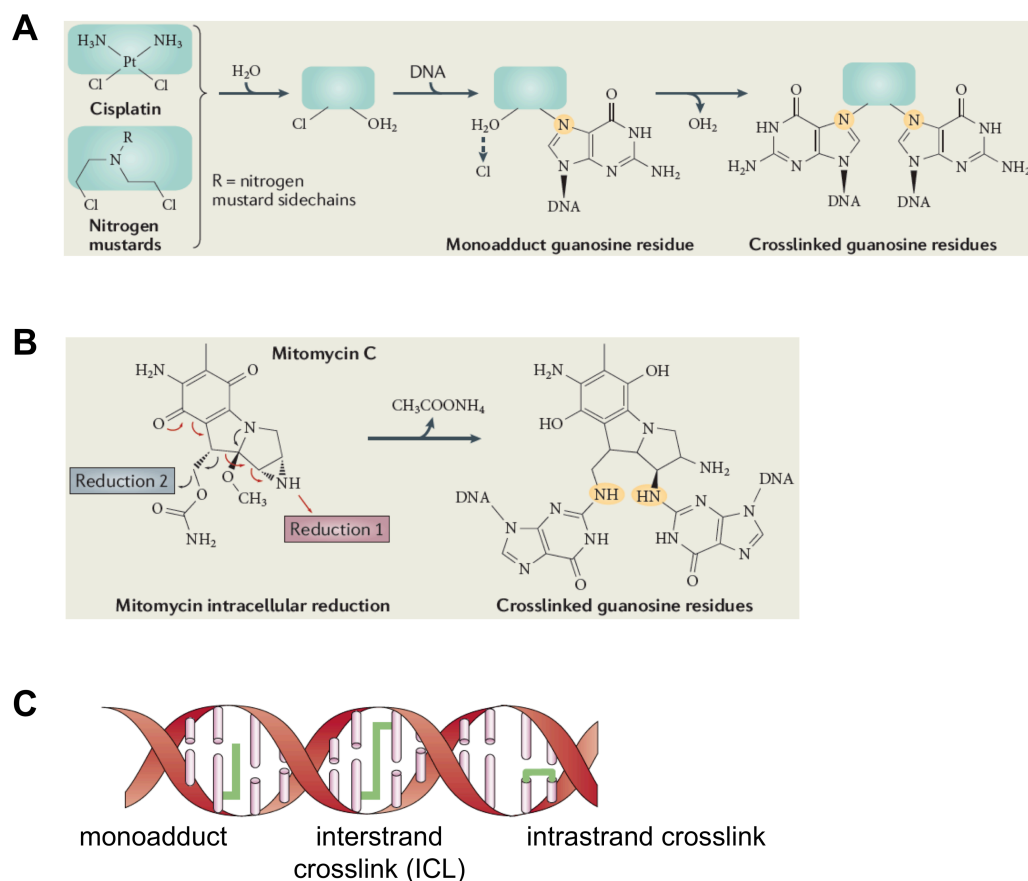


**Figure 5:** A) Mechanism of activation of cisplatin: The two chloride ions are displaced by water molecules, due to low intracellular chloride levels. The activated compound can then bind to bases on the DNA strand, most commonly the  $N^7$ -position of guanosine or adenosine [38]. B) Mechanism of activation of MMC: Through photon-mediated reduction of the molecule two moieties are ejected and the compound binds to DNA bases instead [38]. C) Cisplatin and MMC can either form monoadducts, interstrand crosslinks or intrastrand crosslinks when binding to DNA bases [39].

### 1.3.2.2. ICL repair by Fanconi Anemia (FA) pathway and Homologous Recombination Repair (HRR)

ICL interfere with transcription and DNA replication; thus their removal is necessary throughout the cell cycle [40]. ICL repair in G1 phase differs from repair in S and G2 phase [40]. ICL are especially toxic during S phase, as they impede proper DNA replication. Therefore we will be focusing on replication-dependent repair occurring during S/G2 phase.

During S-phase the replication fork will collide with unremoved ICL (Figure 6). Newer models suggest that a second replication fork might collide with the ICL from the other side [41]. However, these cell-free experiments were done studying replication of plasmids [41]. The likelihood of two replication forks converging at

the same ICL in a human cell is unknown [36]. Therefore, here we will describe the repair with just one fork colliding.

Unable to move forward, the replication fork stalls and may collapse. A stalled replication fork initiates the DNA damage response (DDR) [40]. This entails activation of the Fanconi Anemia pathway for removal of the ICL, leaving a DSB, which is then repaired by Homologous Recombination Repair (HRR). Removal of an ICL happens in 3 phases:

1. FA-proteins recognize the ICL and activate the FA-pathway
2. Recruitment and activation of the FA-core complex and the “ID-complex”
3. Incision and removal of ICL

The ensuing repair intermediate is a one-ended DSB, which is subsequently repaired by HRR. Repair occurs in two main steps:

1. The broken DNA end invades the sister chromatid, using it as a template for repair. This creates a Holliday junction where DNA strands cross over.
2. The Holliday junction is resolved by nucleases, re-establishing an intact replication fork.

In more detail ICL repair occurs as follows. The FANCM-FAAP24-MHF1/2 complex recognizes the stalled replication fork at the DNA lesion. It is responsible for FA-pathway activation and the recruitment of the FA core complex (reviewed in [42]). FANCM hereby forms a heterodimeric complex with FAAP24. Together they recognize the DNA lesion, stabilize the stalled replication fork and initiate ATR-CHK1-dependent signaling. ATR-CHK1 in turn phosphorylates and activates downstream FA proteins (FANCA/E/D2/I). MHF1 (Histone fold protein 1) and MHF2 help FANCM to maintain a stable association with chromatin. They further augment pathway activation and promote the recruitment of the Fanconi Anemia (FA) core complex to chromatin.

The FA core complex consists of 8 proteins. These are FANCA, FANCB, FANCC, FANCE, FANCF, FANCG, FANCL and FANCM. Accessory proteins to the FA core complex are FAAP20, FAAP24 and FAAP100 [40] [42]. FANCM recruits the FA core complex to the site of damage, where the complex is responsible for a key regulatory step in the FA-pathway: ubiquitination of the downstream FA-proteins FANCD2 and FANCI [40] [42]. FANCL serves as an ubiquitin E3 ligase, which monoubiquitinates FANCD2 at Lys561 and FANCI at Lys523 [40] [42]. Promoted by BRCA1, the monoubiquitinated FANCD2-I complex or “ID-complex”

then relocates to the DNA lesion [42], which can be visualized with immunofluorescent staining as sub nuclear foci [36]. Monoubiquitination of FANCD2 is necessary for localization of the ID-complex to the chromatin and lack of the monoubiquitination results in absence of FANCD2 foci [43] [44]. Except for FANCM, all members of the FA core complex are essential for monoubiquitination of the ID-complex [40]. Thus proficiency to form FANCD2 foci is not only a convenient biomarker to assess integrity of this key regulatory step, but also reveals if the FA core complex and upstream events in the FA-pathway are functioning.

Next, the activated and monoubiquitinated ID-complex coordinates unhooking of the ICL [40] [42]. ICL unhooking occurs through incisions on either side of the ICL on the same DNA strand, leaving the ICL tethered to the complementary strand [40]. On the complementary strand trans-lesion synthesis (TLS) facilitates bypass of the tethered ICL lesion [40] [42], which is then removed completely by nucleotide excision repair (NER) [42].

For ICL unhooking to occur, the ID-complex recruits and regulates the proteins involved in this step. ICL unhooking is an intricate interplay between several structure-specific endonucleases: XPF-ERCC1, MUS81-EME1, SLX1 and FAN1 [40] [42]. The distinct and potentially overlapping roles of these endonucleases are not well defined. In the current model, ubiquitinated ID-complex serves as a docking site for endonucleases FAN1 and SLX4/FANCP [42]. Both nucleases contain the ubiquitin-binding domain UBZ4 (ubiquitin-binding zinc finger 4), which specifically recognizes and binds to the ubiquitin moiety of FANCD2 [42] [45]. SLX4/FANCP in turn recruits the remaining nucleases (XPF-ERCC1, MUS81-EME1 and SLX1) [40] [42]. How exactly ICL unhooking occurs remains unclear. The nucleases differ in their preference to incise 5'- or 3'-flaps; thus responsibility to unhook the ICL 5' or 3' may be assigned among the different nucleases.

FAN1 (FANCD2-associated nuclease 1, KIAA1018) is an endonuclease which preferentially incises 5'-flaps [45] [42]. It is of opposite polarity to nucleases MUS81-EME1 and XPF-ERCC1, which prefer to cleave 3'-flaps [45] [46] [47]. FAN1 is known to be required for resistance to ICL inducing drugs [40]. Human cells depleted of FAN1 are thus highly sensitized to MMC and cisplatin and display increased chromosomal radials when exposed to MMC [46] [45] [48]. FAN1 recruitment to ICL is dependent on the ubiquitinated ID-complex [40]. FAN1

is further epistatic to FANCD2, since knockdown of either or both yields similar levels of sensitivity to MMC treatment [45].

SLX4/FANCP in turn serves as a scaffold, modulator and cofactor for the remaining nucleases XPF-ERCC1, MUS81-EME1 and SLX1, thus providing a “tool belt” for ICL unhooking [40] [42]. SLX4/FANCP in complex with SLX1 functions as an endonuclease cleaving 5'-flaps and 3'-flaps at replication fork structures [42]. Depletion of SLX4/FANCP leads to hypersensitivity to MMC and cisplatin, but not UV or IR [42].

ICL unhooking results in a one-ended DSB, which is further repaired by HRR [40] [42] [49]. In a nutshell HRR uses the sister chromatid as a template to elongate the broken DNA strand. Using a template for repair makes HRR particularly faithful [42]. In more detail, for HRR to occur first the DSB needs to be resected by the MRN complex, creating 3' overhangs coated with RPA [40] [42] [49] [50]. Then RAD51 is loaded onto 3'-overhangs, replacing RPA [42]. RAD51 is the key player in HRR, thus the ability to form RAD51 foci can be used as a biomarker for HRR integrity [51] [52] [53] [36] [6]. RAD51 loading is directly or indirectly promoted by many proteins including several FA-proteins, most importantly BRCA2/FANCD1 and its partner PALB2/FANCN, which directly interacts with RAD51 protein to facilitate RAD51 loading. Other promoting proteins are FANCI, RAD51C/FANCO, as well as BRCA1 [42]. RAD51 is responsible for homology search on the sister chromatid. Where homology is found the RAD51 coated DNA strand invades the sister chromatid. DNA polymerases use the sister chromatid as a template to elongate the invading DNA strand. This creates a D-loop and a Holliday junction (HJ) where DNA strands cross over [54] [55]. Finally the Holliday junctions are resolved to restore an intact replication fork [56]. How resolution occurs in detail remains elusive. However, it is known that FAN1 is implicated in late stage HRR and may be involved in the resolution of HRR intermediates [57] [58] [59] [60]. Interestingly FAN1's binding partner FANCD2, as well as FANCI, showed high binding affinity to Holliday junctions [57]. Furthermore, FAN1-depleted cells sustain RAD51 foci, further supporting a role of FAN1 in late stage HRR [59] [57]. Besides FAN1 several other candidates have also been identified to play a role in the process, including BLM, MUS81-EME1, ID-complex, SLX4/FANCP-SLX1 complex, GEN1, and RAD51C/FANCO [56] [40] [42].

The last step of repair includes the USP1-UAF1 DUB complex deubiquitinating FANCD2, which results in deactivation of the FA pathway and completion of DNA repair [40] [42].

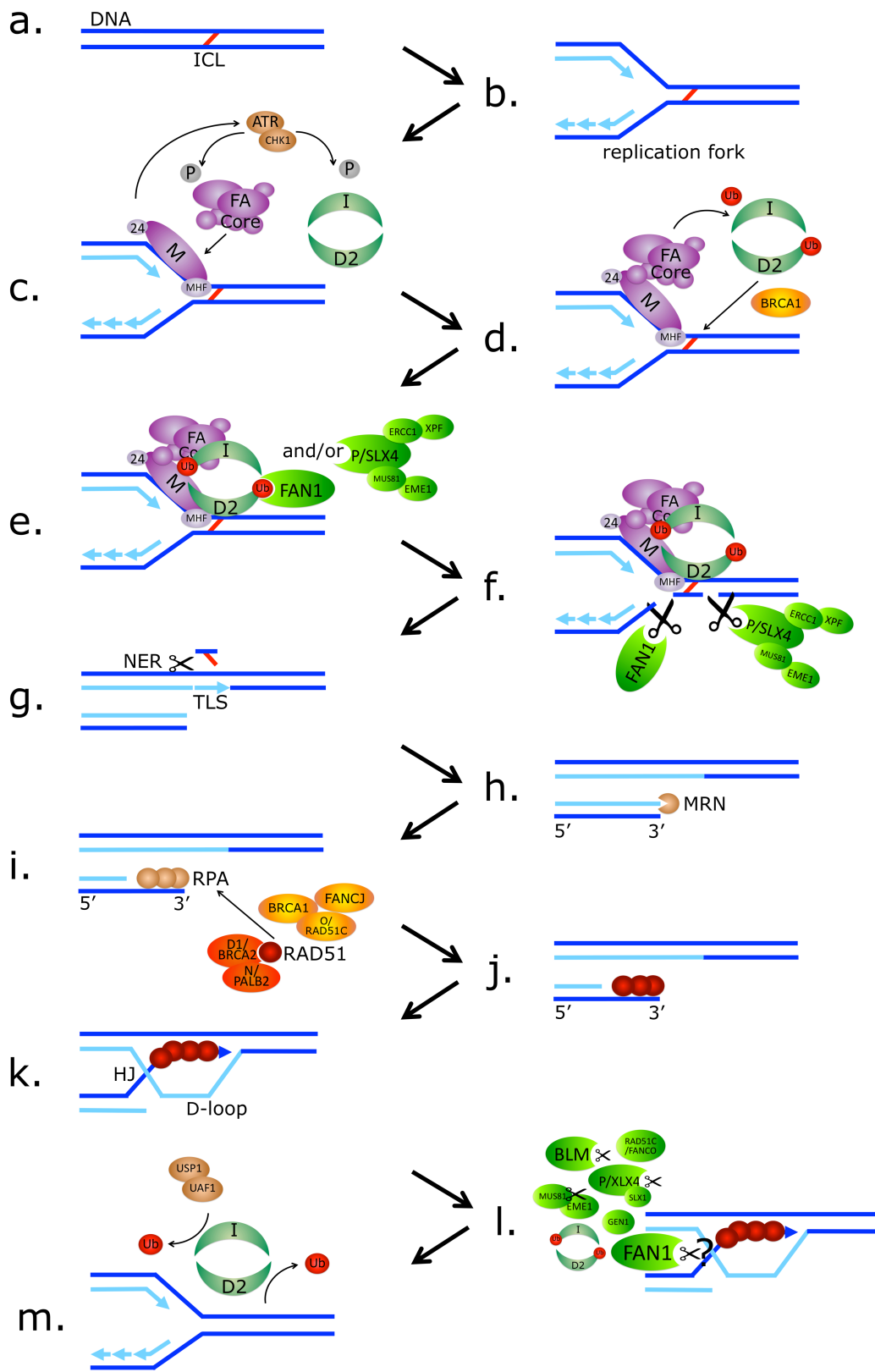


**Figure 6: Repair of ICL by FA pathway and HRR.** a. Unrepaired interstrand crosslink (ICL). b. During S-phase the replication fork collides and stalls at ICL. c. The FANCM-FAAP24-MHF1/2 complex detects the lesion, recruits the FA core complex and initiates ATR-CHK1-dependent checkpoint response. ATR/CHK1 activates several FA proteins by phosphorylation. d. Activated FA core complex ubiquitinates the ID-complex and, promoted by BRCA1, recruits it to the lesion. e. Ubiquitinated FANCD2 recruits the nucleases involved in ICL incision f. Nucleases cut on either side of the ICL, thus “unhooking” it. g. TLS bypasses the unhooked ICL and NER finally removes it. h. MRN complex resects the one-ended DSB to create 3'-overhangs. i. RPA covers 3' overhangs to protect them from degradation. RAD51 replaces RPA. RAD51 loading onto ssDNA is directly promoted by BRCA2 and PALB2, and indirectly by many other proteins. j. RAD51 filaments are responsible for homology search on the sister chromatid. k. Where homology is found RAD51 mediates strand invasion, which leads to D-loop formation and a Holliday junction (HJ). The broken end is elongated by polymerases using the sister chromatid as a template. l. Several players are involved in HJ resolution m. An intact replication fork is recovered. USP1/UAF1 shuts down the repair response by de-ubiquitinating the ID-complex [42] [40] [45] [49] [46].

### 1.3.3. Targeting defects in DNA repair

#### 1.3.3.1. Concept of targeted therapies

In general targeted therapies exploit characteristics which are specific to the tumor but absent in normal cells. With this approach the therapy is harmful to the cancer cell, while normal tissue is not affected. The NCI (National Cancer Institute) Dictionary of Cancer Terms defines targeted therapies as follows: “A type of treatment that uses drugs or other substances, such as monoclonal antibodies, to identify and attack specific cancer cells. Targeted therapy may have fewer side effects than other types of cancer treatments.”

In contrast to this new treatment approach, conventional chemotherapy affects all rapidly dividing cells, thus leading to toxic side effects commonly seen in standard anticancer therapies.

#### 1.3.3.2. Targeted therapy with PARP inhibitors

While there are many different approaches for targeted therapies, we were most interested in exploiting defects in the DNA repair machinery. PARP inhibitors are a promising group of new drugs, which target such repair defects.

### 1.3.3.2.1. PARP1 function

PARP1 is a poly(ADP-ribose) polymerase and one of 17 members of the PARP protein family [61] [3]. PARP1 plays an important role in the repair of DNA single-strand breaks (SSB) [3]. It is responsible for the detection of such lesions and the initiation of the SSB repair (SSBR) pathway [3]. When PARP1 detects a break in the DNA, it binds to it through its zinc finger domain [3]. PARP1 then catalyses the polymerization of ADP-ribose moieties, or PARsylation, onto target proteins. NAD<sup>+</sup> is used as a substrate and nicotinamide is released in the process [3]. PARsylation of a protein changes its conformation, stability and activity. At SSB PARP1 catalyzes PARsylation mostly onto itself (automodification), but also onto histones (heteromodification) [3] [61]. “PAR-chains” attached to PARP1 serve like a beacon to direct and recruit DNA repair enzymes to the site of damage [61]. Furthermore, PARsylated histones are released from the DNA, the chromatin is relaxed and access of DNA repair proteins to the site of damage is facilitated [61]. Thus this shows that if PARP1 is inhibited, SSBR is compromised [3].

### 1.3.3.2.2. PARP inhibitors

Nicotinamide, which is a side product of PARsylation, is a weak PARP1 inhibitor [3]. In order to develop potent PARP inhibitors, nicotinamide analogues were synthesized and further refined [3]. Currently the third generation of PARP inhibitors are being tested in the clinic [3]. Olaparib (AZD2281), which we used in this study, belongs to this promising group of new drugs [3].

In 2005 PARP inhibitors caused great excitement, when it was shown that they could selectively inhibit growth of cells with defective BRCA1 or BRCA2 [3]. The selectivity of PARP inhibitors can be explained with the concept of “synthetic lethality” (Figure 7) [62] [3]. This phenomenon was first described in fruit flies (*Drosophila melanogaster*) by the geneticist Calvin Bridges in 1922 [62]. The term “synthetic lethality” was later coined by his colleague Theodore Dobzhansky [63]. Synthetic lethality occurs when cells with mutations in gene A or gene B are viable, but those with mutations in both genes A and B are not [3] [61] [64] [62] [63]. While mutant BRCA cells are viable, defective BRCA and loss of PARP

function leads to cell death. Yet instead of an additional endogenous mutation, loss of viability is achieved by inhibiting PARP pharmacologically [3].

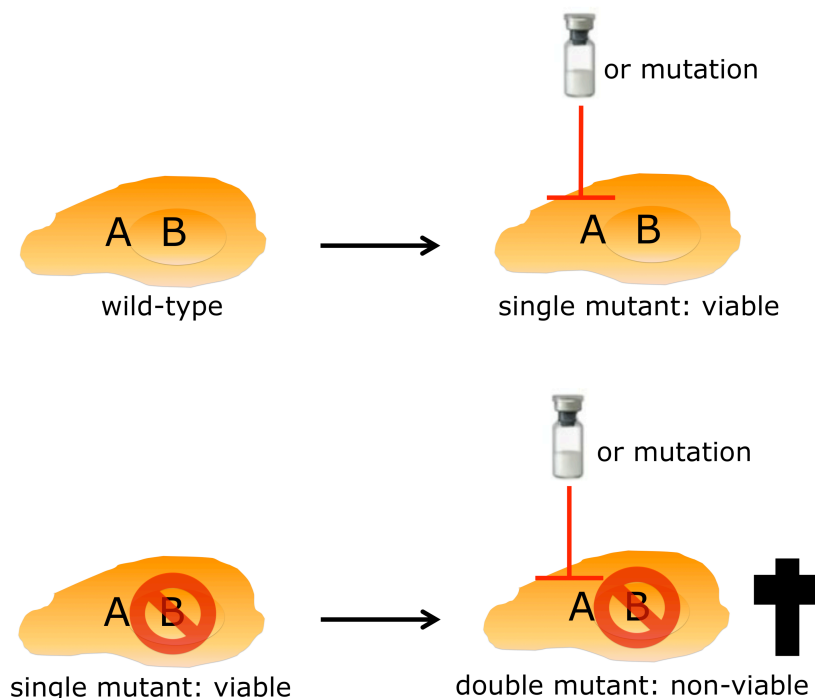


**Figure 7: Concept of Synthetic Lethality.** Two genes are synthetic lethal to each other, if a defect in either leaves the cell viable, but a defect in both leads to cell death [3] [61] [64] [62] [63].

Mechanistically synthetic lethality between BRCA and PARP can be explained as follows (Figure 8):

It is known that PARP inhibitors impair SSB repair, however the precise consequence of PARP inhibition is a matter of debate. The original model argues that PARP inhibitors cause spontaneously occurring SSB to persist. Another model suggests PARP inhibitors trap PARP at SSB, thus hindering repair [65] [66]. Either way during DNA replication the replication fork runs into an unrepaired SSB, collapses, and the result is a toxic one-ended DSB. Normal cells can deploy HRR to repair the DSB and restore DNA integrity [3] [65]. BRCA1 and BRCA2 play important roles in HRR. Cells defective in one of the BRCA genes are deficient in HRR, thus they are impaired in their ability to repair DSB resulting from PARP inhibition. The persisting DSB lead to cell death [3]. Therefore defects in HRR are associated with hypersensitivity to PARP inhibitors [67] [68] [52].

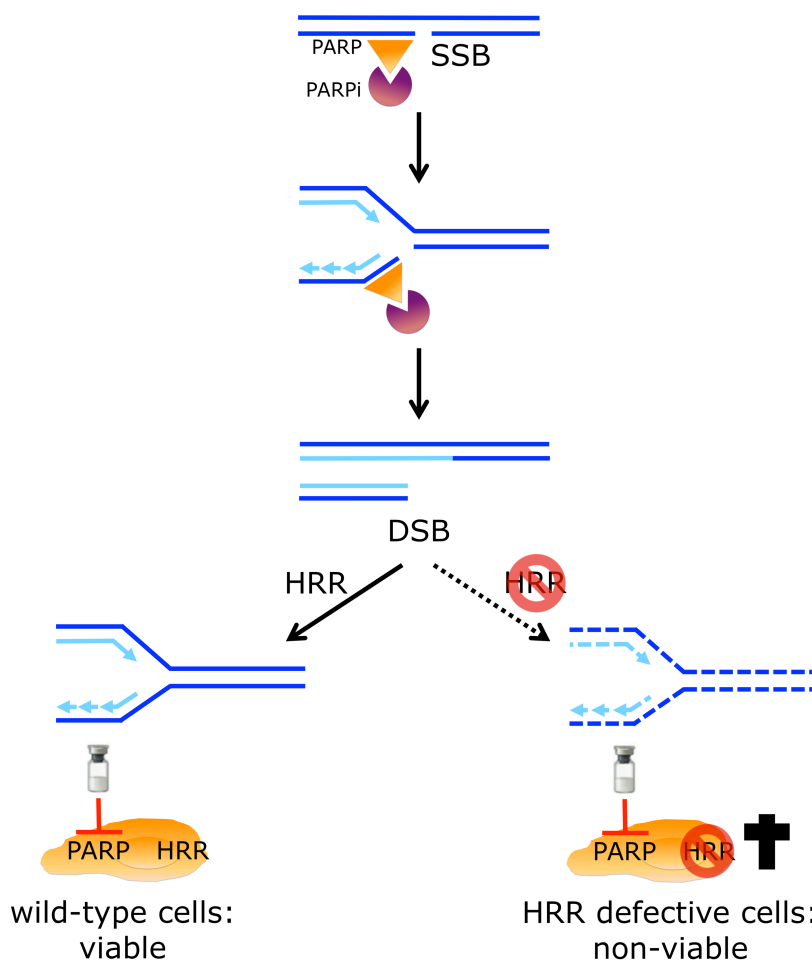


**Figure 8: Synthetic lethality between PARP inhibitors and HRR defects.** PARP inhibitors impair SSB repair. Unrepaired SSB become DSB during DNA replication. Those DSB can be repaired by HRR in a wild-type cell, but remain unrepaired in cells defective in HRR. Unrepaired DSB are lethal.

Several clinical studies are ongoing to prove this model in patients. Exciting results confirm a benefit for patients with BRCA1/2 mutated cancers from treatment with PARP inhibitors (reviewed in [3]). PARP inhibitors were further shown to be effective in BRCA1/2 mutated breast, ovarian and prostate cancer patients, leading to significant and durable antitumor responses [3]. A phase II trial yielded promising results for the treatment of breast or ovarian cancer patients with germline BRCA mutations [3]. PARP inhibitors are selectively lethal to the BRCA-mutated cancer cell. It is therefore not surprising, that many of the typical toxic side effects associated with standard chemotherapy are absent with PARP inhibitor treatment [3].

The efficacy and low toxicity of PARP inhibitors encourages efforts to identify more patient groups who may benefit from this treatment, beyond those with BRCA-deficient cancers. PARP inhibitors may be synthetic lethal with defects in other proteins involved in HRR, as well as FA proteins [3] [65]. In this study we will suggest a new patient group, which may benefit from treatment with PARP inhibitors: EGFR-mutant lung cancer patients.

## **2. MATERIALS AND METHODS**

## 2.1. Materials

### 2.1.1. Drugs, chemicals, antibodies

Table 2.1: Drugs

Drug	Company
Cisplatin (cp)	Sigma-Aldrich
Mitomycin C (MMC)	Sigma-Aldrich
Hydroxyurea (HU)	Sigma-Aldrich
LY 294002	LC laboratories
Olaparib (AZ-2281)	LC laboratories
KU-55933	Chemdea
Erlotinib	LC laboratories
Gefitinib	LC laboratories
puromycin	Sigma-Aldrich
NU7026	Sigma-Aldrich
Ampicillin	Stratagene

Table 2.2: Antibodies

Antibody		Company/Brand	Assay
<b>Primary Antibodies:</b>			
Rad51	Ms mAb [14B4] (GTX70230)	GeneTex	Immunofluorescent staining, Western Blot
$\gamma$ H2AX	Phospho S139, Ms mAb [3F2] (ab22551)	Abcam	Immunofluorescent staining
pATM	Phospho S1981, Ms mAb	Rockland	Immunofluorescent staining
RPA	p34 Ab-1 (9H8), Ms mAb (MS-691-B0)	Neo Markers	Immunofluorescent staining
BRCA1	Anti-BRCA1 Mouse mAb Ab-1 (OP92)	Calbiochem	Immunofluorescent staining
FANCD2	Rb pAb (NB 100-182)	Novus Biologicals	Immunofluorescent staining
PCNA	Rb pAb (ab2426)	Abcam	Immunofluorescent staining
EGFR	Ms mAb [1F4], specific for human EGFR (#2239)	Cell Signaling	Western Blot
EGFR	Rb pAb (sc-03)	Santa cruz	Western Blot
pEGFR	pY992, Rb pAb (44-786G)	Biosource	Western Blot
Akt	Rb Ab	Cell signaling	Western Blot
pAKT	(S473) rabbit mAb	Cell signaling	Western Blot
ERK	p44/42 MAPK Erk1/2 Rabbit Ab	Cell signaling	Western Blot

pERK	P-p44/42 MAPK Erk1/2 Rb Ab	Cell signaling	Western Blot
FAN1	Rb pAb (ab95171)	Abcam	Western Blot
Caspase 3	Anti-Caspase-3 Rabbit pAb (235412)	Calbiochem	Western Blot
$\beta$ -actin	Ms mAb	Sigma-Aldrich	Western Blot
<b>Secondary Antibodies:</b>			
Goat anti-rabbit Alexa 488		Invitrogen	Immunofluorescent staining
Goat anti-mouse Alexa 488 (A- 11029)		Invitrogen	Immunofluorescent staining
Chicken anti-rabbit Alexa 488		Invitrogen	Immunofluorescent staining
Goat anti-rabbit Alexa 555 (A21429)		Invitrogen	Immunofluorescent staining
Goat anti-mouse Alexa 568 (A11004)		Invitrogen	Immunofluorescent staining
Goat anti-rabbit HRP (sc-2030)		Santa cruz	Western Blot
Goat anti-mouse HRP (sc-2031)		Santa cruz	Western Blot

Table 2.3: Kits

<b>Kit</b>	<b>Company</b>	<b>Assay</b>
MycoAlert® Mycoplasma Detection Kit	Lonza	Mycoplasma detection
CometAssay® (#4250-050-K)	Trevigen	Comet Assay
PureLink™ Quick Plasmid Miniprep Kit (#K2100-10)	Invitrogen	Plasmid purification

Table 2.4: Biochemicals, chemicals, cell culture material and other material

<b>(Bio)Chemicals, cell culture material and others</b>	<b>Company</b>	<b>Assay/Usage</b>
TripLE™ Express (12604-013)	Invitrogen	Cell culture
DMSO (Dimethyl Sulfoxide)	Sigma-Aldrich	Cell culture, drug solvent
SYTO® 60	Life technologies™	Cell survival
Formaldehyde	Sigma-Aldrich	
4% Paraformaldehyde	Boston BioProducts	Foci
PBS, 10X (Phosphate Buffered Saline), PH 7.4 NaCl (800g), KCl (20g), Na <sub>2</sub> HPO <sub>4</sub> (144g), KH <sub>2</sub> PO <sub>4</sub> (24g) dissolved in 10l dH <sub>2</sub> O	Fisher Scientific (NaCl) Sigma-Aldrich (all others)	
Ethanol, 200 proof (absolute), #E7023	Sigma-Aldrich	
Methanol	Fisher Scientific	
Isopropanol (for molecular biology, ≥99%)	Sigma-Aldrich	

#I9516		
Vectashield mounting medium (H-1000)	Vector laboratories	Foci
Nailpolish – clear #271	New York Color	Foci
TritonX	Sigma-Aldrich	Foci
Dulbecco's modified Eagle's medium (DMEM)	Sigma-Aldrich	Cell culture
RPMI-1640	Sigma-Aldrich	Cell culture
DMEM/F12	Sigma-Aldrich	Cell culture
$\alpha$ -MEM (#M8042)	Sigma-Aldrich	Cell culture
FBS (fetal bovine serum)	Gibco, Life Technologies	
BGS (bovine growth serum)	HyClone	Cell culture
BSA (bovine serum albumin)	Sigma-Aldrich	
DAPI (4',6-diamidino-2-phenylindole)	Sigma-Aldrich	Foci
Propidium iodide	Sigma-Aldrich	Flow Cytometry
RNase A (20mg/ml)	Invitrogen	Flow cytometry
Igepal	Sigma-Aldrich	Flow Cytometry
Lysis Buffer	BioSource	Western Blot
PMSF	Sigma-Aldrich	Western Blot
Protease inhibitor	Sigma-Aldrich	Western Blot
Bio-Rad Protein Assay dye reagent concentrate	Bio-Rad	Western Blot
UltraPure 10% SDS	GIBCO	Western Blot
Blotting-Grad Blocker, Nonfat dry milk (#170-6404)	Bio-Rad	Western Blot
Novex® ECL HRP Chemiluminescent Substrate Reagent Kit	invitrogen	Western Blot
Orange-G DNA loading dye (6X) (BM-102G)	Boston Bioproducts	Plasmid identification
Ethidium Bromide (E1510)	Sigma	Plasmid identification
Restriction Enzymes: Sal1 (20U/ul) (#R0138S) – red buffer 3 Apa1 (50U/ul) (#R0114S) – green buffer 4	New England Biolabs	Plasmid identification
Buffers for restriction enzymes: NEBuffer 3 (#B7003S) NEBuffer 4 (#B7004S)	New England Biolabs	Plasmid identification
BSA for restriction digest: BSA, #B9001S	New England Biolabs	Plasmid identification
High DNA Mass™ Ladder (#10496-016)	Invitrogen	Plasmid identification
Standard Low -mr Agarose (#162-0102)	Bio-Rad	Plasmid identification
TAE-Buffer 50X (Tris-acetate-EDTA Buffer)	Boston BioProducts	Plasmid identification

Metafectene®Pro	Bionttx	Plasmid transfection
Luria Broth (LB)	Sigma-Aldrich	Plasmid amplification
Bacteriological Agar	Sigma-Aldrich	Plasmid amplification

## 2.1.2. Equipment

Table 2.5: Disposable Equipment

Disposable equipment	Company	Assay
Flasks: T25/75/175 cell culture flask (#353109/#353136/#353118)	BD Biosciences	Cell culture, Cell survival (colony formation)
CryoTube™ vials 1.8ml	Thermo Scientific	Cell culture (freezing cells)
Dishes: 60mm (#430166)	Corning	
Dishes: 100mm	Fisherbrand	
Plates: 12-well, 24-well (#3513/#3524)	Costar	Cell survival (Syto60)
Chamber slides: 4-well, 8-well	BD falcon	Foci
Premium Cover Glass (#12-548-5E)	Fisher Scientific	Foci
Microcentrifuge Tubes 1.5ml (#02-682-556)	Fisher Scientific	
Tubes: 15ml, 50ml	BD falcon	
Glass pipettes: 1ml, 2ml	BD falcon	
Glass pipettes: 5ml, 10ml	Fisher Scientific	
Glass pipettes: 25ml, 50ml	Costar corning	
Pipettips: 10µl, 1000µl	Corning	
Pipettips: 200µl	Fisher Scientific	
Round bottom tube with cell strainer, 5ml	BD falcon	Flow Cytometry
Parafilm "M", PM-999	Pechiney Plastic Packaging	
Gloves: Purple Nitrile, #55081	Kimberly clark	
Disposable Cell Scraper #08-100-241	Fisher Scientific	Western Blot (Lysates)
Disposable plastic cuvette #14-955-127	Fisher Scientific	Western Blot
Invitrolon PVDF Filter paper sandwich 0.45µm pore size	invitrogen	Western Blot
Amersham Hyperfilm ECL	GE Healthcare	Western Blot
Tissue-Tek® OCT™ Compound #4583	Sakura	Tissue freezing

Cryomold	Fisher	Tissue freezing
S.O.C. Medium	Invitrogen	Plasmid amplification
Polypropylene Round-Bottom Tubes, 14ml #352059	Becton Dickinson	Plasmid amplification
Polystyrene Petri Dish 100mm x 15mm	Fisherbrand (Fisher Scientific)	Plasmid amplification
Disposable Inoculating Loops/Needles #22-363-609	Fisher Scientific	Plasmid amplification

Table 2.6: Technical Equipment

Technical equipment	Company	Assay
CL2 Centrifuge	Thermo Scientific	
Hemocytometer	Reichert	Cell culture
Pipetman	Gilson	
Microscope eclipse TS100	Nikon	
Odyssey Li Cor Infrared Fluorescence Detection Imager	Li-Cor Biosciences	Cell survival (Syto60)
Odyssey v1.2 imaging software	Li-Cor Biosciences	Cell survival (Syto60)
Shaker	Thomas Scientific	
BD LSR II Flow Cytometer	BD Bioscience	Flow Cytometry
FACSDiva 6.1.2	BD Bioscience	Flow Cytometry
FlowJo Software	Tree Star	Flow Cytometry
Gene Quant Pro	Amersham Biosciences	
Select Heatblock	VWR	Western Blot
Xcell SureLock™ Mini-Cell	Invitrogen	Western Blot (electrophoresis)
Mini-PROTEAN® 3 Cell	Bio-Rad	Western Blot (transfer)
Micropulser	Bio-Rad	Plasmid amplification
Electroporation Cuvette, 1mm Gap	Fisher Biotech	Plasmid amplification
ElectroMAX DH10B™ Cells #18290-015	Invitrogen	Plasmid amplification
37°C Bacterial Shaker	Lab-Line	Plasmid amplification
Sorvall RC 5C Plus Centrifuge	Thermo Scientific	Plasmid amplification
Sorvall SLA-1500 Rotor	Thermo Scientific	Plasmid amplification
GeneFlash Syngene Bio Imaging	Syngene	DNA gel imaging
Microfuge 18 Centrifuge	Beckman Coulter	
Microfuge R Centrifuge	Beckman Coulter	
GeneQuant	Amersham Biosciences	DNA/Protein concentration
Quartz and Glass Micro Cells for	Fisherbrand	DNA concentration

Spectrophotometers, 500 $\mu$ L #14-385-928A		
Olympus BX51 fluorescence microscope	Olympus	
OWL A4 electrophoresis tank + OSP-105 (power supply)	Thermo Scientific	Comet Assay

### 2.1.3. Company Addresses

Table 2.7: Company addresses

<b>Company</b>	<b>Address</b>
Abcam	Cambridge, MA, USA
Ambion (Life technologies)	Carlsbad, CA, USA
Amersham Biosciences (GE Healthcare)	Pittsburgh, PA, USA
Beckman Coulter	Danvers, MA, USA
Becton Dickinson (BD) - Biosciences	San Jose, CA, USA
Bethyl Laboratories	Montgomery, TX, USA
Bio-Rad Laboratories	Hercules, CA, USA
Biontex-USA	San Diego, CA, USA
Biosource (invitrogen, Life Technologies)	Medford, MA, USA
Boston Bioproducts	Ashland, MA, USA
Calbiochem (EMD Millipore)	Billerica, MA, USA
Cell Signaling	Danvers, MA, USA
Chemdea	Ridgewood, NJ, USA
Corning	Tewksbury, MA, USA
Costar (Corning)	Tewksbury, MA, USA
Falcon (Corning)	Tewksbury, MA, USA
Fisher biotech (Thermo Fisher Scientific)	Cambridge, MA, USA
Fisher Scientific (Thermo Fisher Scientific)	Fair Lawn, NJ, USA
Fisherbrand (Thermo Fisher Scientific)	Cambridge, MA, USA
GE Healthcare	Boston, MA, USA
GeneTex	Irvine, CA, USA
Gibco (invitrogen, Life technologies)	Carlsbad, CA, USA
Gilson	Middleton, WI, USA
Hyclone (Thermo Fisher Scientific)	Cambridge, MA, USA
Invitrogen (Life technologies)	Carlsbad, CA, USA
Kimberly Clark	Franklin, MA, USA
Lab-Line	Melrose Park, IL, USA
LC laboratories	Woburn, MA, USA
Li-Cor Biosciences	Lincoln, NE, USA
Life technologies	Carlsbad, CA, USA
Lonza	Walkersville, MD, USA
Neo Markers (Thermo Fisher Scientific)	Fremont, CA, USA

New England Biolabs	Ipswich, MA, USA
New York Color	Boston, MA, USA
Nikon	Melville, NY, USA
Novus Biologicals	Littleton, CO, USA
Olympus	Center Valley, PA, USA
Pechiney Plastic Packaging	Chicago, IL, USA
Reichert	Depew, NY, USA
Roche	Indianapolis, IN, USA
Rockland Immunochemicals	Gilbertsville, PA, USA
Sakura	Torrance, CA, USA
Santa Cruz	Dallas, TX, USA
Sigma-Aldrich	St. Louis, MO, USA
Stratagene	La Jolla, CA, USA
Syngene	Frederick, MD, USA
Thermo Scientific (Thermo Fisher Scientific)	West Palm Beach, FL, USA
Thomas Scientific	Swedesboro, NJ, USA
Tree Star	Ashland, OR, USA
Trevigen	Gaithersburg, MD, USA
Vector laboratories	Burlingame, CA, USA
VWR	Radnor, PA, USA

## 2.2. Methods

### 2.2.1. Cell lines

Cell lines were selected from a previously published panel located in the Center for Molecular Therapeutics (CMT) at Massachusetts General Hospital, except for A549, H1650, and HCC4006, which were purchased directly from ATCC. Mouse embryonic fibroblasts (MEF) were kindly provided by Matt Meyerson. SV40-transformed fibroblasts derived from patients with FA group D2 (PD20-D2) and their retrovirally complemented counterparts expressing wild-type protein (PD20+D2) were obtained from the OHSU Fanconi anemia cell repository [69]. The identity of each of the cell lines in the panel was tested as described previously [70].

All media was supplemented with 10% Bovine Growth Serum (HyClone), 20 mM HEPES, 2 mM L-glutamine (Sigma–Aldrich), and 1% Penicillin-Streptomycin (Sigma-Aldrich).

Table 2.8: Cell lines

Name	Description	Media
<b>1. Human NSCLC cell lines</b>		
<b>1.1 EGFR wild-type:</b>		
A549		DMEM
NCI-H1703		RPMI1640
NCI-H1792		RPMI1640
ABC1		DMEM/F12
H1299		RPMI
H2126		DMEM/F12
H23		RPMI
<b>1.1 EGFR-mutant:</b>		
PC3	EGFR mutation: del E746_A750	DMEM/F12
PC9	EGFR mutation: del E746_A750	RPMI1640
PC9sc	Subclone of PC9	RPMI1640
IR7	EGFR mutation: del E746_A750 (single gefitinib-resistant clone)	RPMI + 2 $\mu$ M gefitinib
GR7	EGFR mutation: del E746_A750 (single gefitinib-resistant clone)	RPMI + 2 $\mu$ M gefitinib
gt-PC9 #4	EGFR mutation: del E746_A750 (single gefitinib-resistant clone)	RPMI + 2 $\mu$ M gefitinib
gtpPC9, gtPC9-p	EGFR mutation: del E746_A750 (pooled gefitinib-resistant population)	RPMI + 2 $\mu$ M gefitinib
etPC9	EGFR mutation: del E746_A750 (single erlotinib-resistant clone)	RPMI + 2.5 $\mu$ M erlotinib
etmPC9	EGFR mutation: del E746_A750 (pooled erlotinib-resistant population)	RPMI + 2.5 $\mu$ M erlotinib
PC14	EGFR mutation: exon 19, del E746_A750	RPMI1640
HCC827	EGFR mutation: exon 19, del E746_A750	RPMI1640
HCC GR6	EGFR mutation: exon 19, del E746_A750	RPMI + gefitinib
NCI-H3255	EGFR mutation: L858R	RPMI1640
KHM-3S	EGFR mutation: exon 19, del E746_A750	RPMI1640
H1650	EGFR mutation: exon 19, del E746_A750	RPMI1640
H4006	EGFR mutation: exon 19, del E746_A750	RPMI1640
<b>2. Mouse embryonic fibroblasts (MEF):</b>		
NIH-3T3 wt	transfected with pBabe puro expression vector containing human EGFRwt	DMEM
NIH-3T3 L/R	transfected with pBabe puro expression vector containing human EGFRmut (L858R)	DMEM
NIH-3T3 del	transfected with pBabe puro expression vector containing human EGFRmut (del E746_A750)	DMEM
<b>3. Human Fibroblasts:</b>		
PD20-D2	Fibroblasts, FANCD2 null	$\alpha$ -MEM
PD20+D2	Fibroblasts complemented with wild-type FANCD2	$\alpha$ -MEM + 1 $\mu$ g/ml puromycin

### 2.2.2. Cell culture

Cells were cultured as adherent monolayers at 37° C and 5% CO<sub>2</sub> in a humidified incubator. Cells were grown in tissue culture flasks up to 80-90% confluency. To split cells, media was removed and remainders washed off with PBS. Cells were detached by using TripLE™ Express and replated at a minimum of 8x10<sup>5</sup> cells/75cm<sup>2</sup>. Cells were kept in culture for up to 20 passages.

All cell lines were tested for mycoplasma and found negative. Tests were performed with the MycoAlert® Mycoplasma Detection Kit.

Materials	Company
TripLE™ Express (12604-013)	Invitrogen
MycoAlert® Mycoplasma Detection Kit	Lonza

### 2.2.3. Freezing, thawing, storage

Cell lines were frozen at the lowest passage number possible. Cells were detached using TripLE and pelleted at 1,500 rpm for 5min. The cell pellet was resuspended in freezing media (10% DMSO in respective cell line media) at 10<sup>6</sup> cells/ml and aliquots of 1ml were distributed in cryogenic vials. Vials were kept on ice for 20min, before freezing at -20°C for 24h and subsequent transfer to -80°C for short term storage. For long term storage, vials were kept in liquid nitrogen tanks.

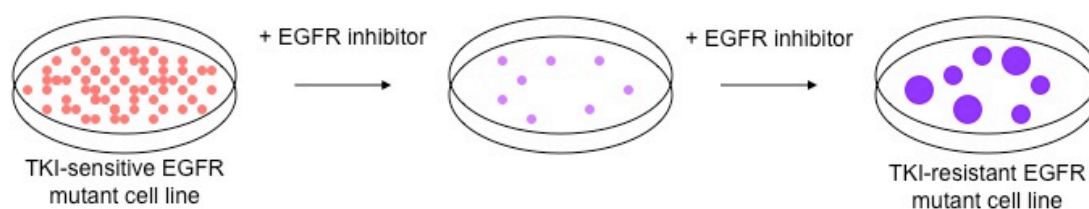
To thaw cells, vials were defrosted in a water bath at 37°C. Cell suspension was diluted in 10ml of warm media and cells were pelleted at 1,500 rpm for 5min. Cells were resuspended in 5ml media and transferred to a T25 flask. 24 hours later media was exchanged. Cells were passaged at least once before conducting experiments with them.

Materials	Company
CryoTube™ vials 1.8ml	Thermo Scientific

### 2.2.4. Creating EGFR TKI resistant cell lines

We kindly received EGFR TKI resistant cell pairs from Dr. Settleman and Dr. Engelman [71] [34]. Additionally we created our own TKI-sensitive/-resistant cell

pairs according to Sharma et al [71]. Briefly  $10^5$  cells were plated in 10 cm plates and allowed to adhere for 24 hours. Cells were then treated with 2  $\mu$ M gefitinib or 2.5  $\mu$ M erlotinib. Fresh media-containing drug was replaced every 3 days until clones of drug-resistant cells appeared. Approximately fifty clones per dish appeared after 30 days of drug selection. Isolated clones were individually expanded in drug-containing media. Alternatively drug resistant populations were pooled for further propagation.



### 2.2.5. Long-term cell survival: Colony formation assay

Cells were seeded in T25 flasks and left to adhere over night for a maximum of 18 hours before treatment. For survival after IR, cells were irradiated using a Siemens Stabilipan 2 X-ray generator operated at 250 kVp and 12 mA, at a dose rate of 1.98 Gy/min. For survival after drug, media was exchanged with media containing the drug. Cells were incubated for 1 hour. For olaparib incubation was increased to 72 hours. After incubation, drug-containing media was aspirated, cells were washed once with PBS and fresh media was added. Cells were left in the incubator to form colonies for 2-3 weeks. Colonies were fixed with methanol and stained with methylene blue. All colonies consisting of at least 50 cells were counted.

Plating efficiency (PE) was determined as:  $PE = \frac{\text{\#colonies}}{\text{\#cells seeded}}$

Survival fraction (SF) was calculated as:  $SF = \frac{PE \text{ treated cells}}{PE \text{ untreated cells}}$

#### Methylene Blue solution:

Methylene blue (Sigma) 2g

Ethanol (190 proof, Fisher Scientific) 600ml

Methylene blue was dissolved in ethanol by stirring with a magnet for 24 hours.

Solution was stored in the dark for 1 month before use.

### **2.2.6. Short-term cell survival: Syto60 staining**

Cells were seeded in 12- or 24-well dishes and allowed to adhere over night. 3 wells were filled with media only to assess background fluorescence. Cells were treated in triplicates for 72 hours. Media was removed, cells were washed once with PBS and fixed with 3.7% formaldehyde for 15 min. Formaldehyde was discarded and remainders washed off three times with PBS. Cells were stained with Syto60 diluted 1:8000 in PBS for 15min. Syto60 is a cell-permeant red fluorescent stain, which binds to nucleic acids. Staining solution was removed and cells were washed 3x with PBS. Plates were scanned with the Odyssey Li Cor Infrared Fluorescence Detection Imager. The integrated intensity per well was calculated using the corresponding software. Intensity readings were averaged for each triplicate treatment and the background intensity was subtracted. Survival was calculated as survival fraction (SF).

SF [%] = average intensity (treatment) / average intensity (untreated)

### **2.2.7. Foci formation assay**

#### **2.2.7.1. Immunofluorescent staining in cell lines**

Cells were seeded in 4- or 8-well chamber slides and left to adhere over night. Cells were then irradiated or treated with drug. At specific time points after treatment cells were fixed. For fixation media was removed. Cells were washed once with PBS and fixed with 4% Paraformaldehyde for 10min. Three washes with PBS followed, before cells were subjected to permeabilization buffer or to 0.25% TritonX/PBS (for Rad51 foci) for 10min. Three washes with PBS stopped permeabilization, and blocking buffer was applied for at least 1h or over night. Alternatively, for 53BPI foci staining the blocking solution consisted of 5% goat serum, 0.2% milk, 0.1% TritonX in PBS. For Rad51 foci staining, 5% FBS in PBS was used for blocking. Cells were rinsed once with PBS and incubated with the primary antibody dilutions according to the table below. After incubation with the primary, residues of the antibody are washed off with PBS for 3x 5min. Incubation with the secondary followed. After incubating for 1h, the antibody was washed off

in the same fashion. Then cell nuclei were stained with DAPI-solution (1:1000 in dH<sub>2</sub>O) for 2min. DAPI-solution was washed off with PBS twice. Chamber walls were detached from slide and excess liquid was aspirated. Vectashield mounting medium was dropped on each well and cover slips were placed onto each slide. Excess mounting medium was removed using a filter paper. Slides were sealed using translucent nail polish. Foci were visualized using an Olympus BX51 fluorescence microscope. Foci per nuclei were counted for at least 100 cells for each condition. Slides were stored in the dark at 4°C for up to 2 weeks.

<b>Permeabilization Buffer</b>
0.5% Triton-X
20mM HEPES, pH 7.9
50mM NaCl
3mM KCl
300mM Sucrose
1X PBS

<b>Blocking Buffer</b>
0.5% NP40
10% BGS
0.3% NaN <sub>3</sub> (sodium azide)
1X PBS

<b>Antibodies</b>	<b>Dilution</b>	<b>Diluent</b>	<b>Incubation</b>
1 <sup>st</sup> Ab: Rad51 2 <sup>nd</sup> Ab: goat anti-mouse	1:500 1:200	5% FBS/PBS	1 <sup>st</sup> Ab: Over night, 4°C, shaker 2 <sup>nd</sup> Ab: 1h, RT, shaker
1 <sup>st</sup> Ab: gH2AX 2 <sup>nd</sup> Ab: goat anti-mouse	1:200 1:1000	2% BSA/PBS	1 <sup>st</sup> Ab: 2h, RT, shaker 2 <sup>nd</sup> Ab: 1h, RT, shaker
1 <sup>st</sup> Ab: 53BP1 2 <sup>nd</sup> Ab: goat anti-rabbit	1:200 1:1000	3% GS/0.1% TritonX/PBS	1 <sup>st</sup> Ab: 1h, RT, shaker 2 <sup>nd</sup> Ab: 1h, RT, shaker
1 <sup>st</sup> Ab: pATM 2 <sup>nd</sup> Ab: goat anti-mouse	1:200 1:1000	2% BSA/PBS	1 <sup>st</sup> Ab: 1h, RT, shaker 2 <sup>nd</sup> Ab: 1h, RT, shaker
1 <sup>st</sup> Ab: RPA 2 <sup>nd</sup> Ab: goat anti-mouse	1:200 1:1000	2% BSA/PBS	1 <sup>st</sup> Ab: 3h, 37°C, humidified chamber 2 <sup>nd</sup> Ab: 1h, RT, shaker
1 <sup>st</sup> Ab: pRPA 32 2 <sup>nd</sup> Ab: Chicken anti-rabbit	1:400	2% BSA/PBS	1 <sup>st</sup> Ab: 4h, RT, shaker 2 <sup>nd</sup> Ab: 1h, RT, shaker
1 <sup>st</sup> Ab: FANCD2 2 <sup>nd</sup> Ab: Chicken anti-rabbit	1:500 1:1000	2% BSA/PBS	1 <sup>st</sup> Ab: 3h, 37°C, humidified chamber 2 <sup>nd</sup> Ab: 1h, RT, shaker

### 2.2.7.2. Immunofluorescent staining in tissue

Fresh tumor tissue was collected on protocols approved by Institutional Review Boards. The tumor biopsy was immediately placed into a 50ml Falcon tube containing 10ml of RPMI (same as for cell culture minus L-glutamine and Pen-Strep). Tumor tissue was cut into three equal pieces, submerged in RPMI and

incubated at 37°C and 5% CO<sub>2</sub>. The samples were treated with 10Gy, 10µM olaparib for 24 hours or left untreated. 24 hours after starting treatment, tumor pieces were each transferred into a 15ml falcon tube and washed once with PBS. A container was filled with liquid nitrogen and the bottom of a 100mm Petri dish was positioned to float in it. One drop of OCT Compound was placed in a Cryomold, the tumor piece put on top of it and covered with more OCT compound. The cryomold was set on the floating Petri dish for a few minutes until the OCT compound was frozen. Frozen tissue blocks were sliced, placed on slides and stored at -80°C.

For staining, a slide with a tissue slice was retrieved from the freezer and thawed at RT for 20min. The tissue was fixed with 2% PFA for 15min, followed by 2 washes with PBS, each 10min. Next the tissue was permeabilized with 0.5% TritonX for 5min at RT. Then the slide was washed 3 times with PBS for 10min each wash. Blocking ensued by covering the tissue with 8% BSA/PBS for 1h at RT in a humidified chamber. A 5min wash with PBS followed. Incubation with the primary antibody was done at 4°C over night. The antibody was washed off 3 times for 5min using PBS. Incubation with the secondary antibody lasted for 1h at RT in a humid chamber covered from light. Again the antibody was washed off 3x for 5min using PBS. Nuclei were stained for 2min using a DAPI-solution (1µg/ml in dH<sub>2</sub>O followed by 2 quick washes in PBS. Tissue was covered with vectashield and coverslip. The slides were sealed with translucent nail polish and stored at 4°C for up to 6 months.

Additionally, control slides were stained with H&E (Hematoxylin and eosin).

### **2.2.8. Flow Cytometry**

Cells were seeded in a T75 tissue culture flask at an appropriate density to yield ~70% confluency at the time of harvest. Cells were treated with MMC (25ng/ml for 24h) the day after seeding. After treatment, cells were detached by incubating with TripLE. To avoid cell clumping, TripLE-cell suspension was thoroughly mixed, using a 2ml glass pipette with a 10µl pipette tip attached to the former. The cell suspension was diluted with complete media and transferred to a 15ml BD Falcon tube. Cells were pelleted for 5 min at 1500rpm. Media was aspirated, and the cell

pellet was washed with 5ml PBS. Cells were pelleted, washed with PBS and pelleted again to be dissolved in 0.5ml PBS. 2ml of ice cold Ethanol (100%) was slowly added drop-wise, while vortexing on low speed. Samples were left at 4°C over night. The next day cells were spun down and supernatant discarded. The pellet was washed with 1ml 1% BSA/PBS and centrifuged. Washing and centrifuging was repeated. The cleaned cell pellet was resuspended in 0.2ml 1% BSA/PBS and pushed through cell strainer caps into round bottom Flow tubes. To ensure degradation of RNA, 10µl of RNase A solution (20mg/ml) was added to the cell suspension and incubated at 37°C for 30min. 490µl of freshly prepared fixative was added (4% propidium iodide/0.1% Igepal/PBS). Samples were kept protected from light. Cell cycle data collection was done using a 3 Laser LSRII running FACSDiva 6.1.2, and FlowJo Software was used for analysis.

## **2.2.9. Western Blot**

### **2.2.9.1. Isolation of proteins**

Cells were grown in 100mm dishes and, if required, treated before harvesting. Media was removed and cells were washed twice with ice cold PBS. 50µl of lysis buffer (0.5% PMSF/1% Protease inhibitor/Biosource Buffer) was distributed on each dish. While incubating for 30min on ice, dishes were rocked to spread the lysis buffer. Lysates were collected by scraping cells from the dish using a cell scraper and transferred into ice cold 1.5ml Eppendorf tubes. Lysates were mixed 3x by pipetting up and down before spinning them at 14,000rpm for 10 min at 4°C. The supernatant was collected in fresh ice cold Eppendorf tubes. Lysates were stored at -20°C.

### **2.2.9.2. Protein quantification: The Bio-Rad protein assay**

The Bio-Rad protein assay is based on the method of Bradford [72]. In a disposable plastic cuvette, 2µl of the lysate was diluted with 798µl dH<sub>2</sub>O. 200µl Bio-Rad dye reagent concentrate was added and incubated for 5min before measuring the absorbance with a GeneQuant spectrophotometer at 596nm. To generate the standard calibration curve, the absorbance of samples with defined concentrations of BSA diluted in dH<sub>2</sub>O (0-5µg/ml) was measured.

### 2.2.9.3. SDS-PAGE

#### 2.2.9.3.1. Sample preparation

Samples were denatured and reduced before loading. To do so lysates containing 40µg-100µg of protein were mixed with LDS Sample Buffer, Sample Reducing Agent and dH<sub>2</sub>O was added to a final volume of 25µl or 37µl depending on the well-size of the gel. Samples were heated at 70°C in a heatblock for 10min before loading.

Materials	Company
NuPAGE® LDS Sample Buffer (4X)	Invitrogen
NuPAGE® Sample Reducing Agent (10X)	Invitrogen

#### 2.2.9.3.2. Electrophoresis

The Xcell SureLock™ Mini-Cell was assembled, the appropriate gel inserted and submerged in adequate running buffer. Samples were loaded into the wells. To monitor electrophoresis, transfer and approximate protein size, pre-stained protein standards were added in one well. Electrophoresis was performed at 100-200V until the dye molecule reached the bottom of the gel.

Electrophoresis Buffer	Company
NuPAGE® MOPS SDS Running Buffer (20X)	Invitrogen
NuPAGE® MES SDS Running Buffer (20X)	Invitrogen
NuPAGE® Tris-Acetate SDS Running Buffer (20X)	Invitrogen

Gel	Company
NuPAGE® 3-8% Tris-Acetate Gel	Invitrogen
NuPAGE® 4-12% Bis-Tris Gel	Invitrogen
NuPAGE® 10% Bis-Tris Gel	Invitrogen

Protein Standard	Company
Novex® Sharp Pre-stained Protein Standard	Invitrogen
HiMark™ Pre-stained Protein Standard	Invitrogen

#### 2.2.9.4. Transfer

A wet transfer was performed using the Bio-Rad Protean 3 Cell System. Sponges and filter were soaked in transfer buffer. The membrane (PVDF) was immersed in methanol for 2min and subsequently incubated with transfer buffer. The gel was equilibrated with transfer buffer as well. A “sandwich” was assembled consisting of: sponge – filter paper – gel – membrane – filter paper – sponge. The sandwich

was tightly clamped together and inserted into the tank with the membrane facing the anode, the gel facing the cathode. Pre-chilled transfer buffer was added and an ice pack was placed next to the sandwich for additional cooling. The chamber was placed on ice, and the transfer was performed at 100V for about 1h.

<b>Transfer buffer</b>	
NuPAGE® Transfer Buffer (20x)	
Methanol (10%)	
SDS (1%)	

### 2.2.9.5. Detection

After transfer the membrane was briefly washed with TBST and blocked with 5% milk/TBST for 1h. Membrane was washed once with TBST and incubated with primary antibody solution (diluted 1:1,000 in 5% BSA/TBST) at 4°C on a shaker over night. The next day the membrane was washed 3x with TBST for 10min each before incubating with secondary antibody solution (diluted 1:10,000 in 5% BSA/TBST) for 1h at RT on shaker. Membrane was washed 3x with TBST for 10min each. Excess TBST was drained from membrane and the membrane was covered with a chemiluminescent enhancer mix (Novex® ECL HRP Chemiluminescent Substrate Reagent Kit) for 2min. The chemiluminescence emanating from the membrane was detected by manual exposure of X-ray films.

TBST (Tris-Buffered Saline and Tween20) Solution, pH 7.6:

Tris Base (Sigma-Aldrich)	242 g
Sodium Chloride (Sigma-Aldrich)	800 g
Tween20 (Sigma-Aldrich)	50 ml
dH <sub>2</sub> O	q.s. 10 l

### 2.2.10. Chromatid aberrations

Exponential growing cells were treated with 0.5µM MMC for 1 hour, collected in the first metaphase after treatment by adding colcemid (0.2 µg/ml) (Gibco) for 4 h and prepared for analysis by standard protocols. Slides were coded and 25–75 metaphases were scored for the fraction of cells with tri- and quadriradials and expressed as average radials per cell. The assay was kindly performed by K.

Borgmann (Center for Oncology, University Medical Center Hamburg-Eppendorf, University of Hamburg, Germany) according to previously described protocol [73] [74].

## 2.2.11. Transfections

### 2.2.11.1. Plasmids

Full-length human EGFR expression constructs encoding wild-type, L858R, or delL747-P753insS proteins were described previously [75]. A lentiviral expression vector encoding GFP-flagged FAN1 (PHAGE CMV N-EGFP-FL\_FAN1) was a gift from Stephen Elledge [76]. Plasmid pEGFP-N1 was obtained from Invitrogen.

### 2.2.11.2. Plasmid amplification

#### 2.2.11.2.1. Transformation

##### Day 1

Electroporation Cuvettes were chilled at  $-20^{\circ}\text{C}$ , while thawing DH10B electrocompetent cells on ice. SOC media was pre-warmed at  $37^{\circ}\text{C}$ . For each plasmid,  $10\mu\text{l}$  of electrocompetent cells were added in an Eppendorf tube and chilled on ice.  $1\mu\text{l}$  pUC control plasmid ( $10\text{pg}/\mu\text{l}$ ) or  $1\mu\text{l}$  of plasmid of interest ( $100\text{ng}/\mu\text{l}$ ) was added to  $10\mu\text{l}$  cells on ice. Plasmid-DNA mix was resuspended and inserted into chilled cuvettes. Cuvettes were wiped off to remove condensation water and placed into electroporeser. Program was set to bacteria "Ec1" and time at "ms". Transformation of DNA into Ecoli was performed by pressing "pulse" once.  $1\text{ml}$  of pre-warmed SOC media was added into the cuvette to suspend bacteria. Bacterial suspension was then transferred to a  $14\text{ml}$  bacterial tube. The tubes were incubated in a shaker at  $37^{\circ}\text{C}$  for 0.5-1h at 250rpm. In the meantime Luria Broth-Ampicillin plates ( $0.1\text{mg}/\text{ml}$  ampicillin) were placed into incubator at  $37^{\circ}\text{C}$  to warm up. For each plasmid, 3 plates were streaked with different volumes of the respective bacterial suspension ( $5\text{-}100\mu\text{l}$ ). For the control plasmid just 1 plate was streaked with  $5\mu\text{l}$ . Plates were placed into an incubator and left uncovered to dry for 10min. Plates were covered and overturned to incubate at  $37^{\circ}\text{C}$  over night, but not longer than 16 hours.

**Day2**

For each plasmid, a single colony was picked from the plates, using a 10 $\mu$ l pipette. The entire tip was ejected into a 14ml BD falcon tube containing 5ml LB with antibiotic (0.1mg/ml ampicillin). Tubes were incubated in a bacteria shaker at 37°C for 6-8h. 1ml of bacteria suspension was transferred to a fresh tube containing 5ml Ampicillin/Luria Broth (LB). Tubes were incubated in the bacteria shaker at 37°C over night (12-16h).

Preparation of Luria Broth (LB) Solution:

25g Luria Broth was dissolved in 1l dH<sub>2</sub>O, solution was autoclaved and stored at 4°C.

Preparation of Luria Broth-Ampicillin plates:

15g Bacteriological Agar was dissolved in 1l LB Solution. Mixture was microwaved on high and boiled for about 1min. Solution was left to cool down until warm to the touch, then ampicillin (100mg/l) was added and dissolved. 20ml of Ampicillin LB Solution was poured into polystyrene Petri dishes (100mmx15mm). Plates were left to cool down further, covered and stored at 4°C.

**2.2.11.2.2. DNA Purification**

DNA was purified using PureLink™ HQ Mini Plasmid Purification Kit. In a microcentrifuge tube, 1-3ml (1-2 x 10<sup>9</sup>) of E. coli from overnight culture was pelleted at 1,500 x g for 15min. Pellet was resuspended in 240 $\mu$ l of Resuspension Solution containing RNase A (0.1mg/ml). 240 $\mu$ l of Lysis Buffer was added and mixed gently by inverting 4-8 times. Mix was incubated for 3-5 min at room temperature. 340 $\mu$ l of Neutralization/Binding Buffer was added and mixed gently by inverting 4-8 times. Mix was centrifuged at max. speed to clarify cell lysate. Supernatant was decanted into a PureLink™ spin column sitting inside a 2ml collection tube. Supernatant was pushed through column by centrifuging at RT at 14,000 x g for 1 min. Flowthrough was discarded and column placed back into the collection tube. 650 $\mu$ l of Wash Buffer containing ethanol was pipetted into the column and pushed through by centrifuging at RT at 14,000 x g for 1min. Flowthrough was discarded and column placed back into the collection tube.

Column was centrifuged again at maximum speed for 3 min to remove the residual wash buffer. Column was placed into a clean 1.7ml elution tube. 20-50µl of Elution Buffer was added to the center of the column, incubated for 1min at RT and centrifuged at max. speed for 1min. The collection tube containing the eluted plasmid was stored at -20°C.

GeneQuant was used for assessing the concentration and 260/280 ratio of the eluted plasmid.

### 2.2.11.3. Plasmid identification

Identity of amplified plasmid was confirmed by DNA restriction digest and subsequent analyses of fragment sizes on an agarose gel. Restriction digest was mixed in 1.7ml Eppendorf tubes as follows:

Restriction Reaction:

Ingredient	Volume
10X NEBuffer (enzyme specific)	2 µl
100X (1mg/ml) BSA	0.2 µl
Restriction enzyme	10U/µg DNA
DNA	0.5 µg
dH <sub>2</sub> O	up to 20µl

Restriction enzymes:

Sal1 (20U/ul) – red buffer 3

Apa1 (50U/ul) – green buffer 4

Tubes were incubated for 1-3h at 37°C. In the meantime 500ml TAE Buffer was prepared by diluting 50X TAE with dH<sub>2</sub>O. The DNA gel was prepared by suspending 0.8g agarose in 100ml TAE and microwaving it until liquid was clear. 5µl Ethidium bromide (10mg/ml) was mixed into liquid and poured into mold containing comb. Gel was let to set until solid, comb was removed, gel was placed in electrophoresis box and submerged in TAE buffer until completely covered. First well was filled with 10µl DNA ladder mixed with 2.5µl orange loading dye. 0.25µg uncut plasmid mixed with 1µl loading dye and 4.5µl dH<sub>2</sub>O was run as a control in the second well. 4µl of loading dye was added to the 20µl of restriction

reaction and loaded into the third well. Gel was run at 80V for about 1h. DNA fragments in the gel were visualized using UV light and photographed in a GeneFlash chamber.

#### **2.2.11.4. Plasmid transfection**

A day prior to transfection, cells were seeded in 60mm dishes for western blot lysates or 4-well chamber slides for foci assays. Using antibiotic- and serum-free media, two Eppendorf tubes were prepared as follows:

Tube A:

For 60mm dish: 6 µg plasmid in 200µl media

For 4-well chamber: 1.5µg plasmid in 50µl media

Tube B:

For 60mm dish: 18 µl Metafectene®Pro in 200µl media

For 4-well chamber: 3µl Metafectene®Pro in 50µl media

Content of tube A was added into tube B, pipetted up and down once and incubated for 15min at RT. Media on cells was replaced with fresh complete media. Transfection mix was added drop wise to cells and mixed by swirling dish or rocking chambers gently. Cells were incubated at 37°C and 5% CO<sub>2</sub> and assayed at 48 hours after transfection.

#### **2.2.12. Gene silencing**

For siRNA transfections, exponentially growing A549 cells were mock-transfected or transfected with validated siEGFR or a scrambled control siRNA (Ambion). Transfections were carried out using the X-tremeGENE transfection kit according to the manufacturer's instructions (Roche). Western blotting and subsequent experiments were performed 48 hours after transfection. The assay was kindly performed by Meng Wang.

### 2.2.13. Modified alkaline comet assay

Cells were seeded in a 60mm dish and left to adhere over night. Cells were treated with 50 $\mu$ M cisplatin for 1h, washed once with PBS, and fresh media was replaced. Cells were left to repair for up to 24h. For harvesting, cells were irradiated with 12.5 Gy to introduce a fixed amount of DSB, immediately put on ice and protected from light throughout the assay. Two control samples were prepared in parallel: irradiated with 12.5 Gy and untreated cells. Dishes were rinsed once with ice cold PBS (Ca<sup>2+</sup> and Mg<sup>2+</sup> free), then cells were scraped off using a cell scraper and suspended in PBS at 1.5x10<sup>5</sup> cells/ml. Lysis Solution was prepared and chilled at 4°C for at least 20min before use. LMAgarose was melted in a beaker of boiling water for 5min and kept in a 37°C water bath for at least 20min to cool down. Cell suspension and molten LMAgarose was combined at a ratio of 1:10 (v/v), and 50 $\mu$ l was immediately pipetted onto CometSlide™. The side of the pipette was used to spread agarose/cells over the sample area. Slides were left at 4°C in the dark for 10min. Next, slides were immersed in prechilled Lysis Solution at 4°C for 30min. Excess buffer was drained from slides, and the slides were submerged in Alkaline Unwinding Solution for 40min at RT. Slides were placed in an electrophoresis slide tray at equidistance from electrodes. The tank was filled with Alkaline Electrophoresis Solution until slides were just fully covered. The tank was covered with the Slide Tray Overlay. Based on the distance between electrodes, the power supply was set to 22V (1V/cm) and run for 30min. Excess electrophoresis buffer was drained from slides, and slides were washed twice in dH<sub>2</sub>O for 5min each, then in 70% ethanol for 5min. Samples were dried for 15min. 100 $\mu$ l of diluted SYBR® Green I was placed on each sample and incubated for 5min at 4°. Excess SYBR solution was removed, and samples were dried completely at RT. Samples were covered with Vectashield mounting medium and a cover slip. Slides were sealed with translucent nail polish. Pictures were taken using Olympus BX51 microscope and attached camera. Tail moment was analysed using TriTek CometScore™ software.

<b>Lysis solution</b> Provided by CometAssay® Reagent Kit from Trevigen®
<b>Comet LMAgarose</b> Provided by CometAssay® Reagent Kit from Trevigen®
<b>Alkaline Unwinding Solution:</b> NaOH Pellets      0.4g 200mM EDTA      250µl (provided with the kit) dH <sub>2</sub> O              49.75ml
<b>Alkaline Electrophoresis Solution:</b> NaOH pellets                              8g 500mM EDTA, pH8                      2ml dH <sub>2</sub> O (after NaOH is dissolved) q.s. to: 1l
<b>SYBR® Green I dilution</b> SYBR® Green I      1µl (provided with the kit) TE Buffer, pH 7.5   10ml Storage: in the dark at 4°C for several weeks
<b>TE Buffer:</b> 10mM Tris-HCl pH 7.5 1mM EDTA

To quantify the amount of ICL remaining unhooked in the cell, we employed the following formula as previously described [20]:

$$\text{ICL remaining [\%]} = \left( 1 - \frac{\text{Cp.IR} - \emptyset}{\text{IR} - \emptyset} \right) \times 100 \%$$

Cp.IR = Tailmoment of cisplatin treated and irradiated cells

∅ = Tailmoment of untreated cells

IR = Tailmoment of irradiated cells

Cells are irradiated to introduce a fixed amount of DSB. ICL retain the DNA, shortening the tailmoment. Complete unhooking would therefore result in the same tailmoment as irradiated only controls. The smaller the tail of cisplatin/IR treated cells, the less unhooking occurred and vice versa.

### 2.2.14. Alkaline comet assay

The assay was conducted as described for the modified version, with the only difference that samples were not irradiated prior to harvesting.

### **2.2.15. Gene expression analysis**

Microarray expression data were obtained from the publicly available Cancer Cell Line Encyclopedia (CCLE) at <http://www.broadinstitute.org/ccle/home>.

### **2.2.16. Statistical Analysis**

Statistical comparisons of data points were carried out by use of the t-test, either paired or one-sample on normalized data, as appropriate (GraphPad Prism 4.03, GraphPad Software, San Diego, CA, USA). Statistical significance was defined at the level of  $p = 0.05$  or less.

# **3. RESULTS**

### **3.1. EGFR-mutant cell lines are impaired in repairing DNA damage resulting in a Fanconi Anemia like cellular phenotype**

#### **3.1.1. EGFR-mutant cell lines exhibit increased sensitivity to ICL inducing agents**

In a first step we aimed to confirm the clinical observation of increased sensitivity to cisplatin of EGFR-mutant NSCLC in a panel of human lung cancer cell lines in vitro [7] [8] [9].

We examined clonogenic survival of various EGFR-mutant lung cancer cell lines compared to EGFR-wild-type ones when treated with interstrand crosslinking agent cisplatin (Figure 1 A+B). As the clinical observation suggested, we found EGFR-mutant lung cancer cell lines to be more sensitive to cisplatin, with 3/6 EGFR-mutant cell lines (PC9, PC14, KHM-3S) exhibiting survival fractions of only 3.9-28.3% (at 8  $\mu$ M) compared to >40% for the rest.

To confirm increased sensitivity of EGFR-mutant cell lines to DNA ICL we tested another crosslinking agent mitomycin C (MMC). Similarly we found EGFR-mutant cell lines to be more sensitive to the drug than EGFR-wild-type ones (Figure 1 C).

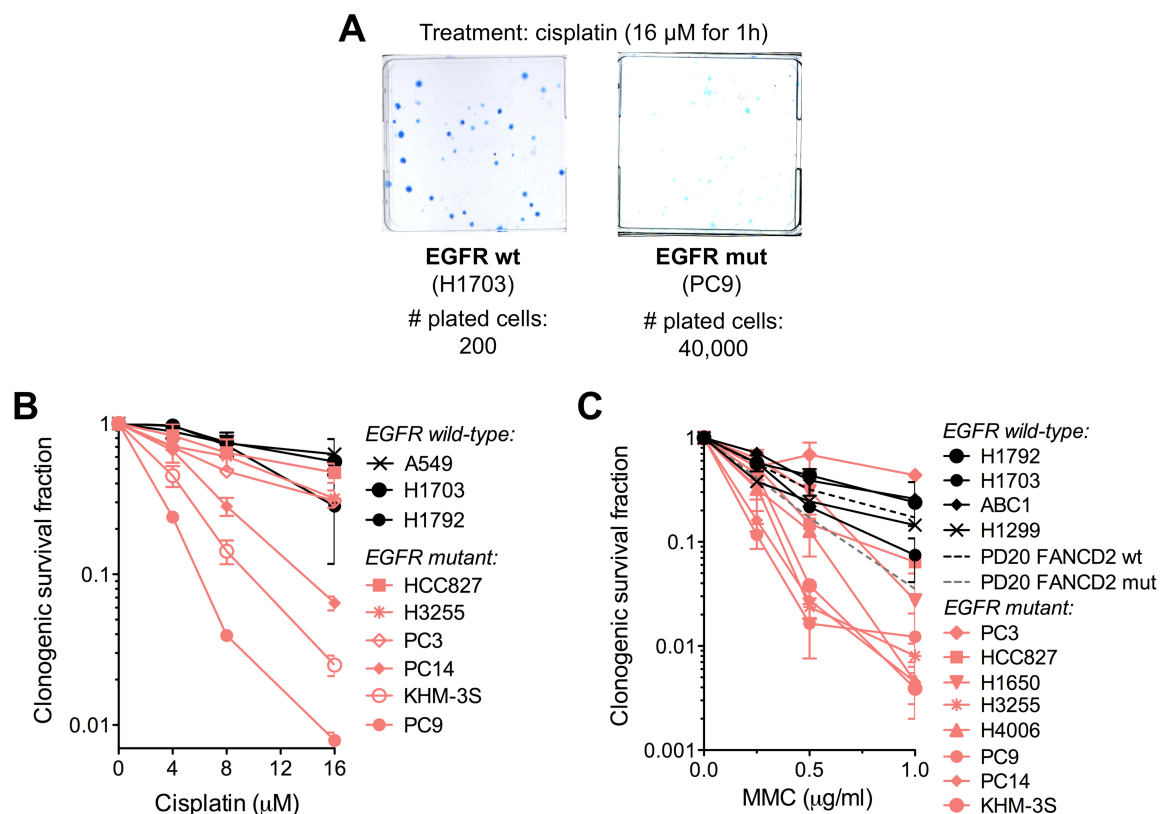


**Figure 1:** A) Colony formation assay: pictures show colonies of an EGFR wild-type lung cancer cell line (left) versus an EGFR-mutant one (right). Cells were seeded, left to adhere over night, and treated with 16  $\mu$ M cisplatin for 1h. About 2 weeks later colonies were fixed and stained with Methylene Blue. B) Clonogenic survival fractions of a panel of 9 human lung cancer cell lines with wild-type versus mutant EGFR. Data points represent log mean  $\pm$  standard error based on 2 or 3 biological repeats. C) Clonogenic survival of lung cancer cell lines. The previously published survival of isogenic PD20 fibroblasts with wild-type (wt) or mutant (mut) FANCD2 is indicated as dotted lines [44]. Clonogenic survival assays for HCC4006 and H1650 were kindly performed by Chake Tokadjian. Data points represent log mean  $\pm$  standard error based on 2 or 3 biological repeats.

### 3.1.2. EGFR mutation sensitizes to ICL inducing agents

Next we wanted to assess the influence of EGFR mutation status on clonogenic survival. We obtained isogenic mouse embryonic fibroblasts stably transfected with plasmid containing either human EGFR-wild-type or EGFR-mutant. We confirmed equal expression levels of transfected human EGFR by Western Blot (Figure 2A) and evaluated clonogenic survival when treated with cisplatin or MMC (Figure 2B+C). Again the cell line expressing EGFR-mutant was more sensitive to both crosslinking agents, cisplatin and MMC, than the one expressing human EGFR-wild-type.

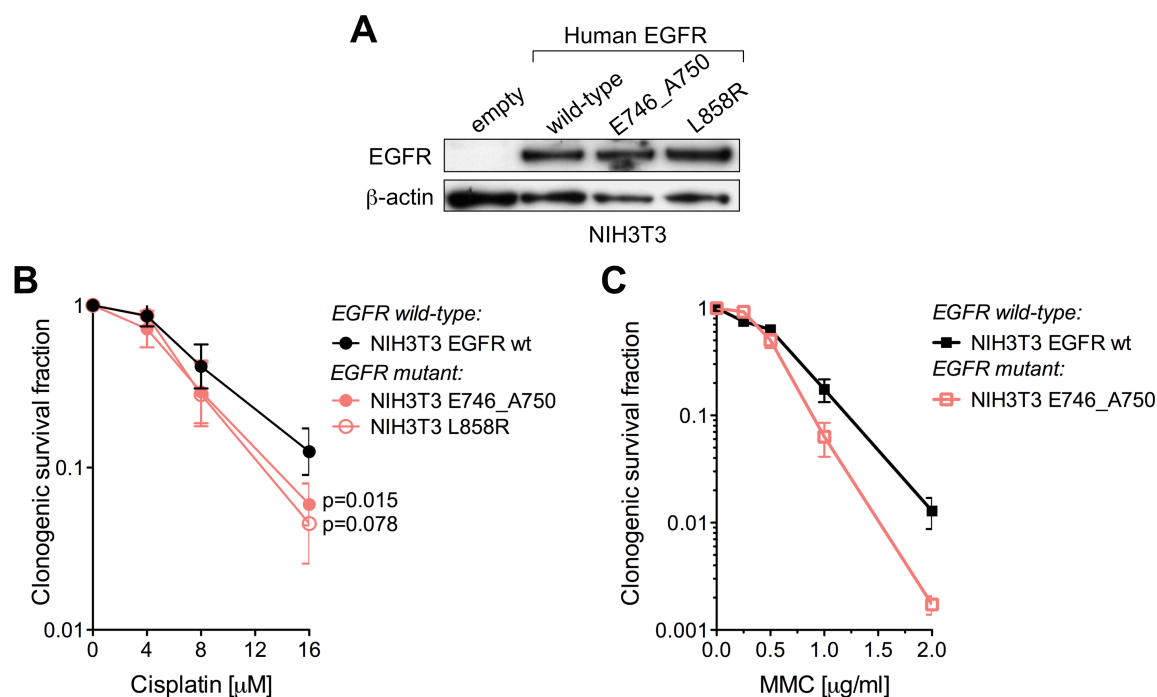


**Figure 2:** A) Western blot demonstrating expression of human EGFR in NIH3T3 MEFs stably transfected with plasmids containing human wild-type or mutant EGFR: E746\_A750 (del19) or L858R EGFR. B) Clonogenic survival of isogenic MEF clones expressing human wild-type or mutant EGFR after 1 hour treatment with increasing concentrations of cisplatin. Data points represent log mean  $\pm$  standard error based on 3 (cisplatin) or 6 (MMC) biological repeats. C) Analogous to B, clonogenic survival of isogenic MEF clones expressing wild-type or mutant EGFR after 1 hour treatment with MMC.

### 3.1.3. EGFR-mutant cell lines show increased unrepaired DNA damage upon treatment with cisplatin

In addition to clonogenic survival we measured sensitivity to cisplatin by evaluating DNA damage levels. H2AX is a histone variant, which becomes phosphorylated if there is DNA damage in close proximity. Therefore phosphorylated H2AX, called  $\gamma$ H2AX, is commonly used as a DNA damage marker [77].  $\gamma$ H2AX can be visualized as foci by employing immunofluorescence microscopy [77] [6]. We quantified  $\gamma$ H2AX foci levels 24h after treatment with cisplatin. 5/6 EGFR-mutant cell lines showed increases of  $\gamma$ H2AX foci of 1.1-1.7-fold relative to EGFR wild-type cells (Figure 3). This indicates more unrepaired DNA damage remains in EGFR-mutant cell lines 24h after treating with cisplatin.

$\gamma$ H2AX foci levels further correlated with cisplatin sensitivity,  $r^2=0.85$ ,  $p=0.003$  (Figure 3D).

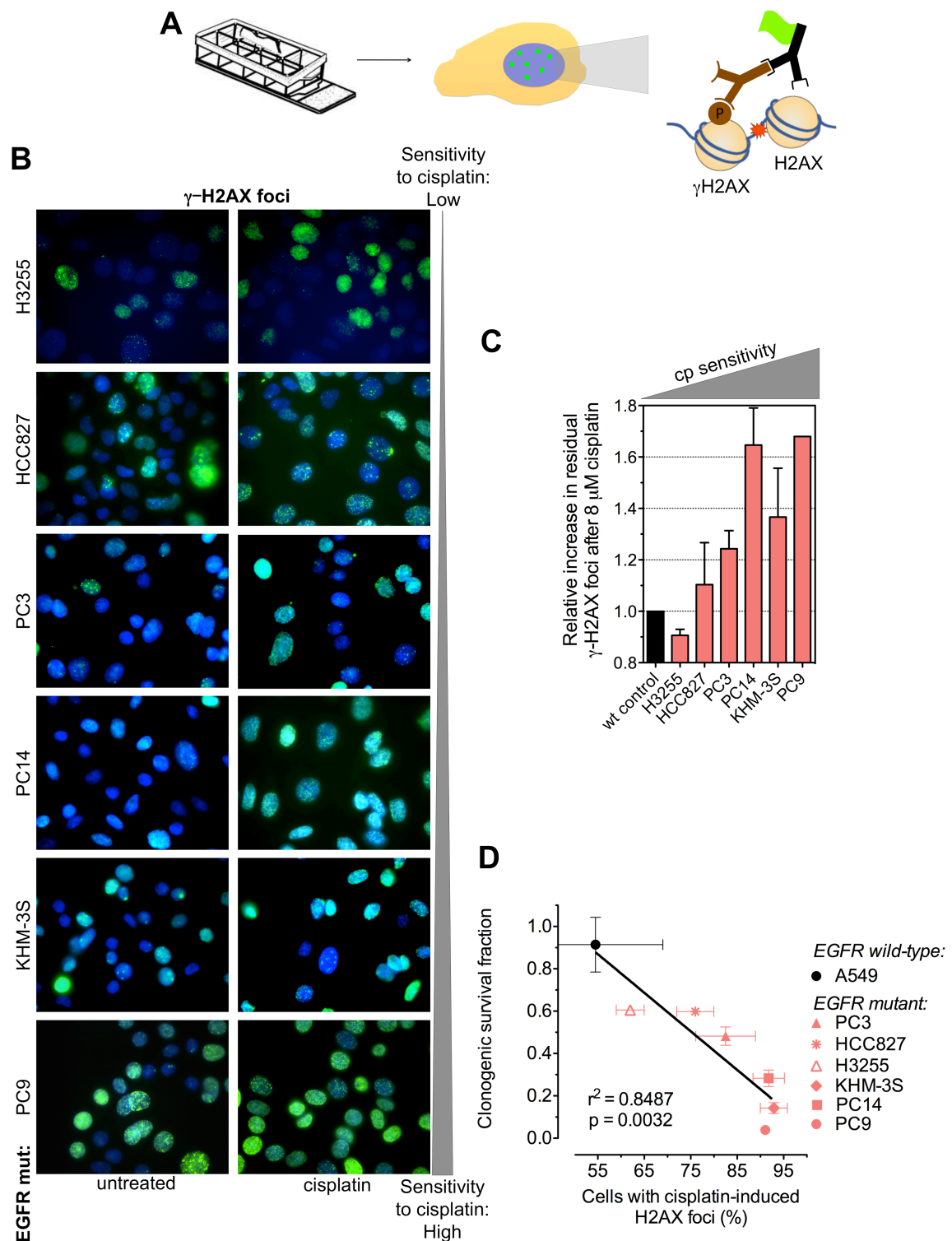


**Figure 3:** A) Immunofluorescent staining of foci: cells are seeded, treated, fixed and stained in chamber slides. Proteins of interest accumulate at DNA damage. These protein clusters or “foci” can be visualized by incubating with primary antibody against the protein of interest and subsequent incubation with immunofluorescent secondary antibody

directed against the primary. Nuclei are stained with DAPI (blue). B) Fraction of cells with residual  $\gamma$ H2AX foci correlates with clonogenic survival after cisplatin treatment. Shown are representative images of  $\gamma$ H2AX foci in EGFR-mutant lung cancer cell lines. 24 hours after treatment with 8  $\mu$ M cisplatin, cells were fixed and stained with anti- $\gamma$ H2AX antibody (green) and nuclei visualized with DAPI (blue). Cell lines are ranked according to decreasing clonogenic survival after treatment with 8  $\mu$ M cisplatin based on data in Figure 1 and illustrated by grey triangle on the left-hand side. C) Relative increase in the fraction of cells with  $\geq 20$   $\gamma$ H2AX foci/nucleus 24 hours after cisplatin treatment (8  $\mu$ M for 1 hour), with number of foci in untreated cells subtracted. EGFR-mutant cell lines are ranked according to their relative cisplatin sensitivity. Bars show mean  $\pm$  standard error based on 2-3 biological repeats. wt, wild-type EGFR cisplatin-resistant A549 as control. D) Clonogenic survival fractions at 8  $\mu$ M cisplatin correlates with residual  $\gamma$ H2AX foci with  $r^2=0.85$  and  $p = 0.003$ .

### 3.1.4. EGFR-mutant cells arrest in G2 phase when challenged with MMC

ICL are repaired by the FA/HRR pathways during S-phase [40] [42]. Cells deficient in the FA pathway are unable to repair ICL and, due to the lingering DNA damage, arrest in G2 phase. In order to establish whether EGFR-mutant lung cancer cells display a similar phenotype, we set out to assess alterations in the cell cycle distribution after MMC treatment. We performed Flow Cytometry after exposure to 25ng/ml MMC for 24h and found pronounced G2/M cell cycle arrest of 46%-50% in the EGFR-mutant human lung cancer cell lines compared to only 18% in the EGFR wild-type cell line (Figure 4A+C). As controls we measured cell cycle distribution of an isogenic cell pair, proficient or deficient in the FA pathway, after MMC and as expected found massive G2/M arrest in the FA-deficient cell line (41% versus 25%) (Figure 4B). In terms of cell cycle distribution after MMC treatment, we noticed striking resemblance of the EGFR-mutant human lung cancer cell line with the FA-deficient cell line, whereas the EGFR wild-type human lung cancer cells mirrored the FA-wild-type ones (Figure 4C). These results are the first indicator of a possible defect in the FA/HRR pathway in EGFR-mutant cell lines.

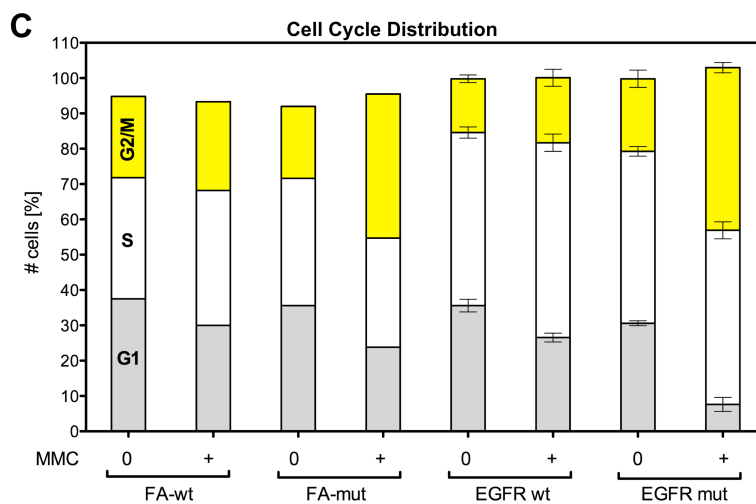
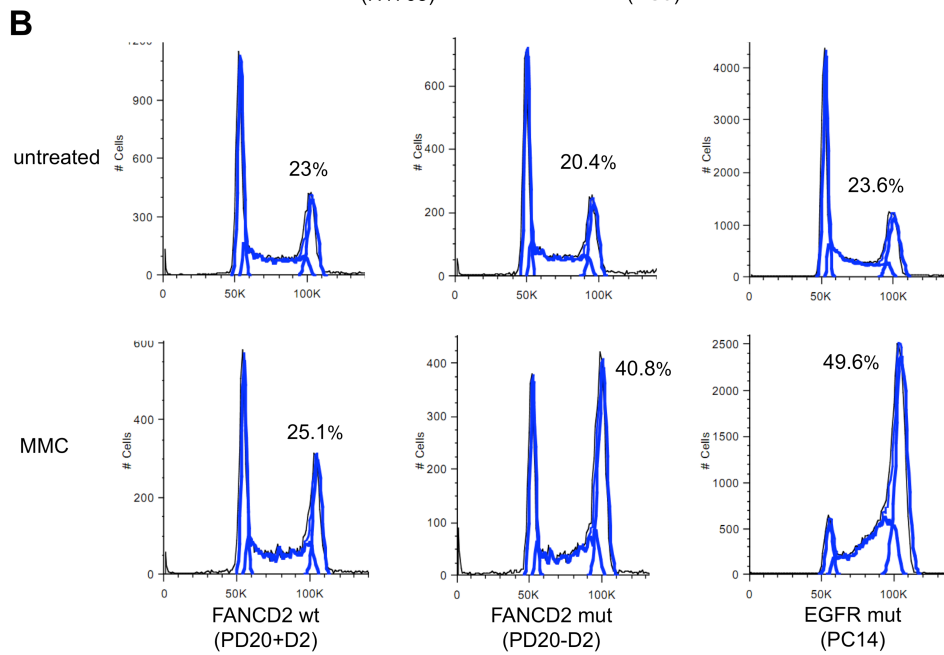
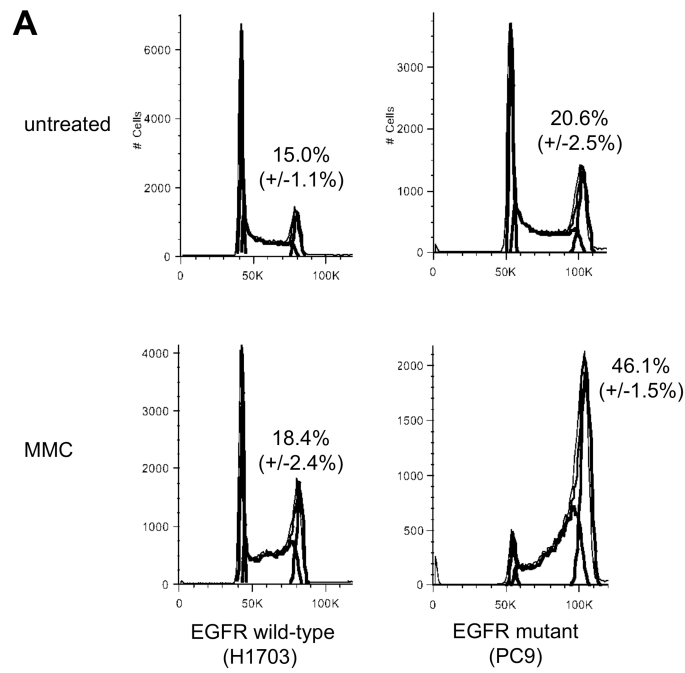


**Figure 4:** A) Flow cytometry demonstrating crosslinker-induced G2/M arrest: Cell cycle distribution measured by Flow cytometry with and without MMC treatment (25 ng/ml for 24 hours). For EGFR wt/mut samples the fraction of cells in G2/M is given as mean  $\pm$  standard error based on 2 biological repeats. B) Cell cycle distribution measured by flow cytometry analogous to A. The G2/M arrest seen in FANCD2-mutant PD20 fibroblasts treated with mitomycin C (MMC) at 25 ng/ml for 24 hours is comparable to the cell cycle profile obtained with the EGFR-mutant cell line PC14. C) Cell cycle distribution as measured in A+B depicted as bar graph.

### **3.1.5. Increased chromosomal radials can be found in EGFR-mutant cells treated with MMC**

Cells deficient in the FA/HRR-pathway arrest in G2/M phase after treatment with crosslinking agents, because of an inability to repair ICL. During DNA replication, replication forks stall and collapse at ICL, which creates DNA breaks. Broken non-homologous chromatids may erroneously fuse together, which can be visualized in metaphase spreads as chromosomal radials. Chromosomal radials disturb normal distribution of chromosomes to daughter cells. The cell cannot perform proper cell division and therefore arrests in G2/M phase. To establish whether EGFR-mutant cells display another hallmark of FA/HRR-defective cells, we quantified chromosomal radials after MMC treatment. MMC elicited 3-6x more chromosomal radials per cell in EGFR-mutant cell lines (PC9, PC14) compared to the EGFR wild-type cell line (H1703) (Figure 5 A+B). In this setting EGFR-mutant cells behaved similar to the FA-deficient cell line (PD20-D2), which exhibited 2.3x more radials/cell than the EGFR wild-type cell line (H1703) (Figure 5B).

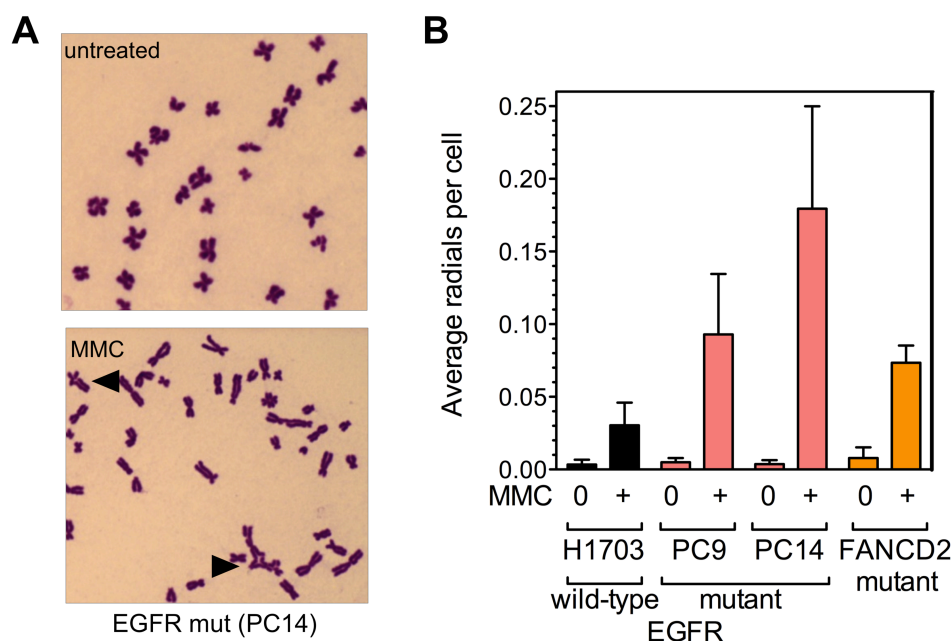


**Figure 5:** A) Panel shows representative metaphase spread with MMC-induced chromosomal radials indicated by triangles. B) Graph shows the average number of radials per cell. Bars represent mean  $\pm$  standard error based on 2-3 biological repeats. FANCD2-mutant PD20 fibroblasts are included as a control. These data were kindly obtained for us by Kerstin Borgmann at Center for Oncology, University Medical Center Hamburg-Eppendorf, Germany.

### 3.1.6. EGFR mutation is associated with increased ATM activity

FA-deficient cells have been reported to show elevated levels of phosphorylated and thus activated ataxia telangiectasia mutated (ATM) [78] [79]. Phosphorylated ATM (pATM) can be visualized as foci by immunofluorescence microscopy. We measured ATM activity in EGFR wild-type and mutant cell lines by quantifying pATM foci after treatment with cisplatin (Figure 6). 50-62% of cells scored positive for pATM foci in cisplatin sensitive EGFR-mutant cell lines (PC9, PC14). In comparison only 2-26% of cells were found positive in EGFR wild-type cells. Again cisplatin sensitive EGFR-mutant cell lines resembled a FA-deficient phenotype.

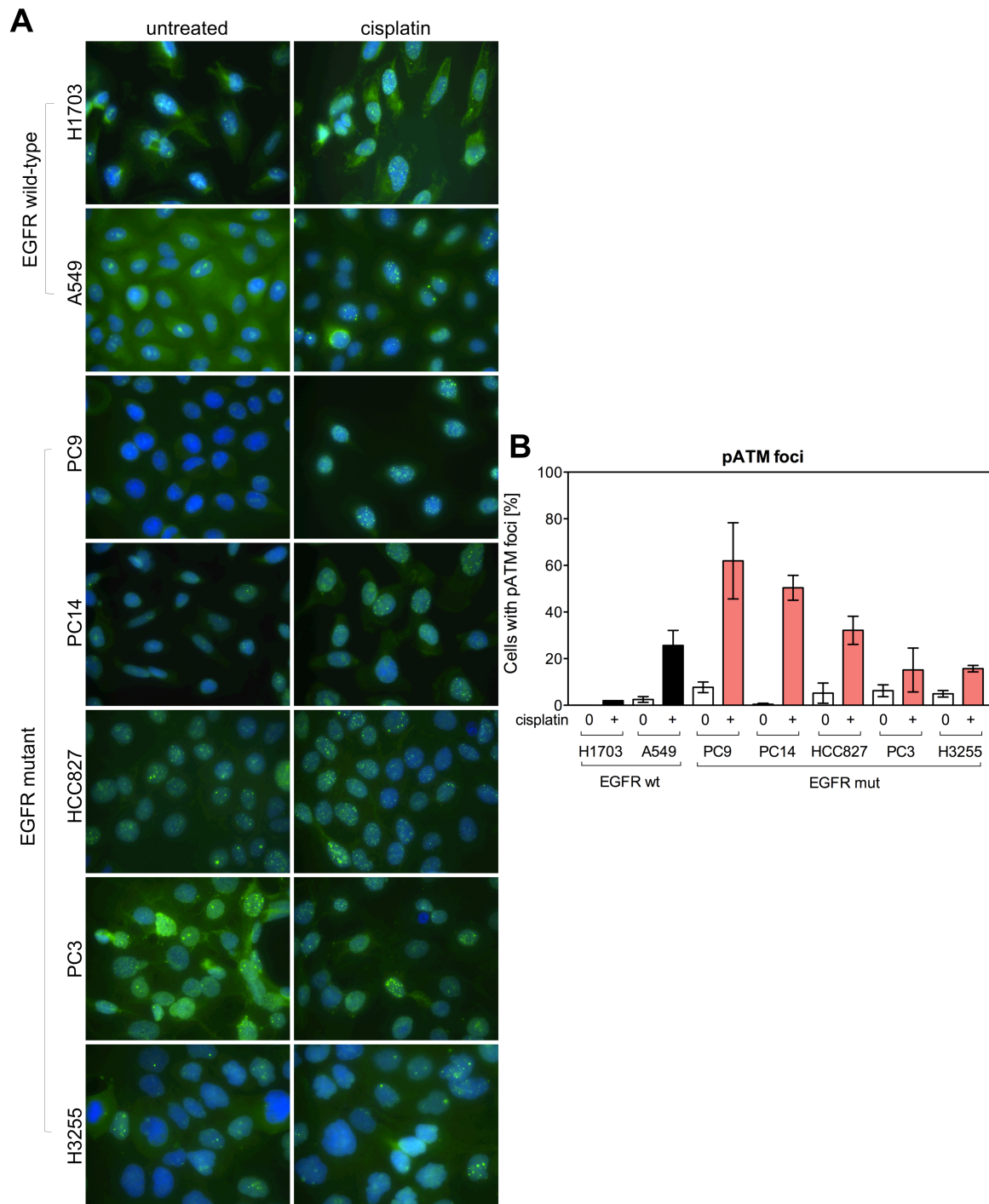


**Figure 6:** A) Representative pictures of pATM foci in EGFR wild-type and mutant lung cancer cell lines at 24 hours after treatment with 8  $\mu$ M cisplatin for 1 hour. B) Corresponding graph to A. Fraction of cells with at least 10 subnuclear phospho-ATM foci were scored. Bars depict means  $\pm$  standard error based on two biological repeats. Increased levels of pATM foci in mutant EGFR cell lines PC9 and PC14 correlate with cellular FA phenotype.

## **3.2. Mutated EGFR impairs FA/HRR pathway resulting in lack of repair protein RAD51 in response to ICL**

### **3.2.1. EGFR-mutant cells, like FA-deficient ones, do not form RAD51 repair foci in response to ICL**

We established that EGFR-mutant cell lines exhibit a FA-like phenotype upon treatment with crosslinking agents. We then set out to explore the underlying cause of this phenotype. Based on the results up to this point, we hypothesized the presence of a defect in the FA/HRR pathway in EGFR-mutant cell lines. RAD51 is a key repair protein within the HRR pathway. After removal or unhooking of the ICL, RAD51 assembles as filaments on processed DNA ends and mediates crucial subsequent steps of HRR [42]. RAD51 filaments can be visualized as RAD51 foci. The ability to form these foci is used as a marker for proficient HRR [6]. We treated EGFR-wild-type and –mutant lung cancer cell lines with cisplatin and assessed HRR proficiency by quantifying RAD51 foci. We found a pronounced reduction of RAD51 foci induction in the cisplatin-sensitive EGFR-mutant cell lines (PC9, PC14, KHM-3S): only 1.7-2.8% of these mutant cells scored positive for RAD51 foci compared to 31-36% in EGFR wild-type cell lines (Figure 7 A+B). Lack of RAD51 foci correlated with cisplatin sensitivity:  $r^2=0.69$ ,  $p=0.01$  (Figure 7C). Furthermore, we confirmed that disruption of the FA-pathway leads to reduced RAD51 foci levels, as FA-deficient cells form fewer RAD51 foci (PD20-D2, 16%) than FA-proficient ones (PD20+D2, 38%) upon treatment with MMC (Figure 7D). Birkelbach et al showed similar results using cisplatin for treatment [6].

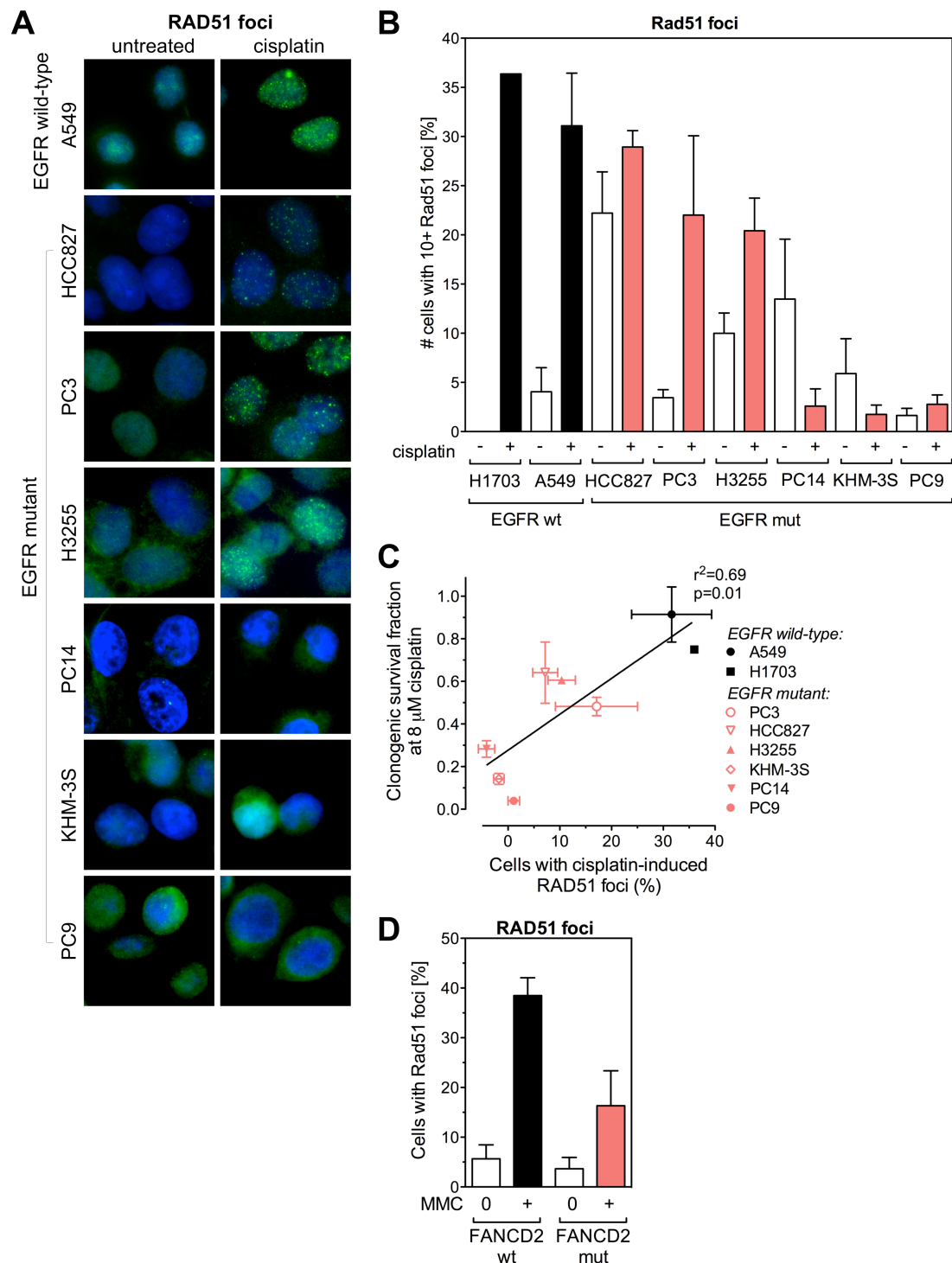


**Figure 7:** A) Representative pictures of RAD51 foci formation (green) in EGFR wild-type and mutant lung cancer cell lines overlaid with DAPI staining. Cells were treated with 8  $\mu$ M cisplatin for 1h and evaluated 5h afterwards. B) Corresponding graph to A. Fraction of cells with at least 10 subnuclear RAD51 foci were scored positive. Bars depict means  $\pm$  standard error based on 2-3 biological repeats. C) Correlation of clonogenic survival at 8  $\mu$ M cisplatin with fraction of cells containing  $\geq 10$  RAD51 foci. Line represents result of linear regression analysis. D) Crosslinker-induced RAD51 foci formation is impaired in FANCD2 mutant cells, comparable to our previously published findings [69]. PD20 cells were treated with 1 mg/ml MMC for 1 hour and analyzed for RAD51 foci at 5 hours after starting treatment with MMC. Bars represent means  $\pm$  standard error based on 3 biological repeats.

### 3.2.2. EGFR-mutant cells contain normal levels of RAD51 protein

The inability of EGFR-mutant cells to form RAD51 foci upon treatment with crosslinking agents indicates a defect in HRR or further upstream in the FA-pathway. We aimed to understand why EGFR-mutants cannot form RAD51 foci. First we wished to confirm that EGFR-mutants express RAD51 protein. Thus we measured RAD51 protein levels by western blotting and found levels to be normal in EGFR-mutants compared to –wild-type cells (Figure 8).

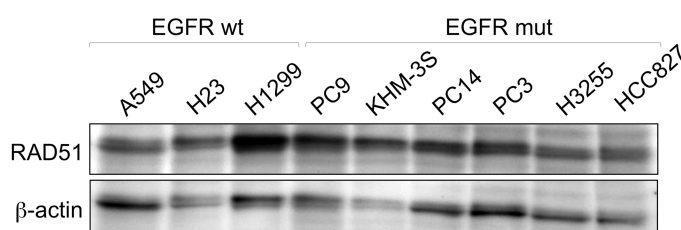


**Figure 8:** RAD51 protein is expressed similarly across all cell lines analyzed regardless of EGFR mutation status. Whole cell lysates were obtained and RAD51 protein levels were detected using anti-RAD51 antibody.

### 3.2.3. RAD51 foci defect in EGFR-mutant cells is specific for ICL damage

We asked ourselves whether EGFR-mutant cells are generally defective in forming RAD51 foci or whether lack of RAD51 is specific for ICL damage. Unlike the FA-pathway, HRR is not only involved in ICL repair. HRR is deployed for DNA DSB repair during S/G2-phase. These DSB can be intermediate structures during ICL repair or may be caused directly, for example by DNA damaging agents such as IR. Interestingly we found EGFR-mutant cells to be proficient in forming RAD51 foci when treated with IR. 33% of EGFR-mutant cells scored RAD51 positive, which is higher compared to just 5% when treated with cisplatin (Figure 9). In fact when treated with IR, EGFR-mutant cells contained almost as many RAD51 positive cells as the EGFR wild-type cell line (49%). We therefore concluded the

defect must be upstream of RAD51 foci formation and within the FA-pathway as it is specific for ICL damage.

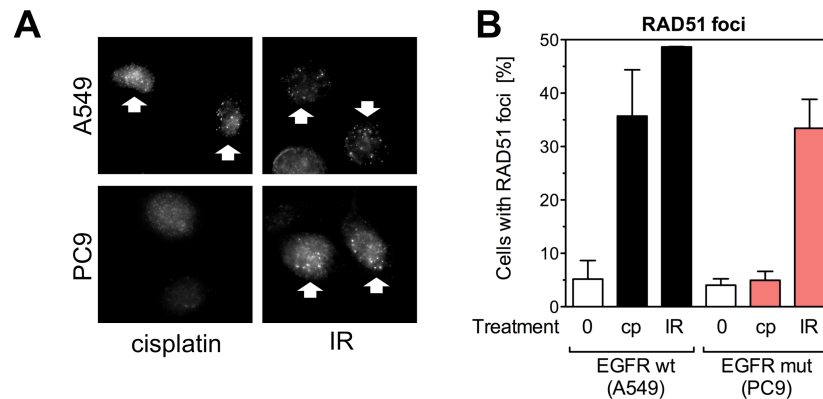


**Figure 9:** A) Representative images are shown of nuclei with RAD51 foci induced 5 hours after treatment with cisplatin (cp, 8  $\mu$ M for 1 hour) or ionizing radiation (IR, 8 Gy). B) Corresponding graph to A. Fractions of cells with  $\geq 10$  RAD51 foci are displayed. Bars represent mean  $\pm$  standard error based on 2-3 biological repeats.

### 3.2.4. EGFR nuclear translocation does not correlate with the observed FA/HRR defect

We further aimed to elucidate how EGFR may influence the FA/HRR pathway. It has been shown that upon treatment with cisplatin wild-type but not mutant EGFR translocates into the nucleus where it may promote DNA repair by stimulating activity of DNA-PKcs [20]. We did indeed observe translocation of wild-type but not mutant EGFR into the nucleus upon cisplatin treatment, albeit to a very low degree (Figure 10). Only 6% of cells contained EGFR wild-type in the nucleus after treatment, which seems unlikely to be able to account for the pronounced RAD51 foci defect and cisplatin sensitivity seen in mutant EGFR cell lines.

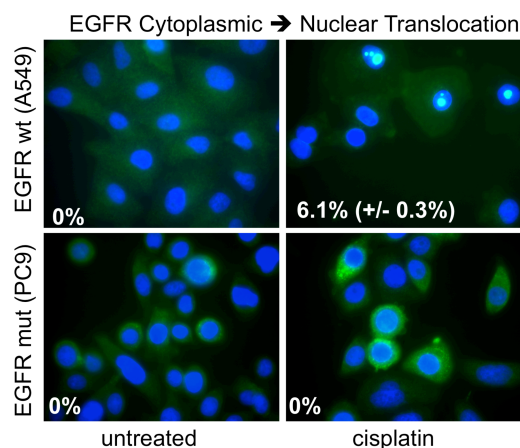


**Figure 10:** Nuclear translocation of wild-type EGFR was induced by treatment with 8 $\mu$ M cisplatin for 1h in EGFR wild-type (A549) and EGFR-mutant (PC9) cells. EGFR staining was performed at 5h after starting treatment. Translocation of wild-type EGFR did not correlate with the magnitude of the repair defect seen in mutant cell lines. Images are overlays of DAPI and anti-EGFR stain (green) and illustrate nuclear translocation of EGFR. EGFR staining was kindly performed by Meng Wang. Percentages indicate mean  $\pm$  standard error based on two biological repeats.

### 3.2.5. DNA-PKcs activity does not affect sensitivity to cisplatin

To address the possibility that wild-type EGFR may promote DNA repair through increasing DNA-PKcs activity as others have claimed, we analyzed whether inhibition of DNA-PKcs has any sensitizing effect to cisplatin in EGFR wild-type, but not mutant cells [20]. However, pharmacological inhibition of DNA-PKcs with NU7026 in isogenic EGFR-wt and -mutant MEFs did not result in any significant changes in clonogenic survival upon cisplatin treatment (Figure 11). At 8 $\mu$ M cisplatin survival fractions of EGFR-wild-type MEFs were 28% compared to 32% when DNA-PK inhibitor was added. EGFR-mutant MEFs exhibited 12% survival when treated with 8 $\mu$ M cisplatin compared to 18% when DNA-PK inhibitor was added. Thus, we ruled out DNA-PK activity as a candidate through which mutant EGFR could sensitize to ICL damage.

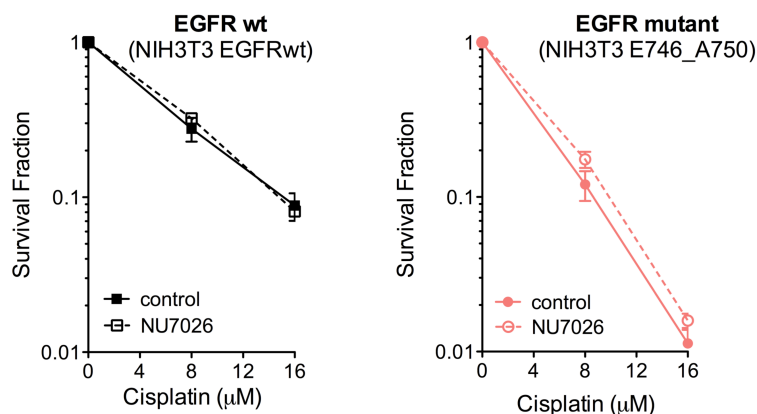


**Figure 11: Pharmacological DNA-PKcs inhibition has no influence on cellular sensitivity to cisplatin.** The isogenic NIH-3T3 cell pair with wild-type (wt) or mutant (mut) EGFR was treated with increasing doses of cisplatin for 1 hour and clonogenic survival was determined. For combination treatment with a DNA-PKcs inhibitor, cells were treated with 10  $\mu$ M of NU7026 for a total of 25 hours in addition to 1 hour of cisplatin treatment starting after 1 hour pre-incubation of NU7026. Following wash-off of NU7026 at 25 hours, cells were allowed to form colonies for 2 weeks. Data points represent means  $\pm$  standard error based on 2-3 biological repeats.

### 3.2.6. Overactive EGFR signaling in mutant cells does not account for lack of RAD51 foci

Unlike the wild-type version, mutant EGFR is constantly phosphorylated and therefore downstream signaling is continually activated independent of the presence of EGF ligand [5]. EGFR signaling involves AKT activation and AKT has been shown to suppress HRR [80]. Thus, we hypothesized that the overactive downstream signaling of mutant EGFR might impair FA/HRR resulting in lack of RAD51 foci. We therefore tested whether we could revert this impairment by reducing EGFR signaling in a mutant EGFR lung cancer cell line (PC9) with an EGFR inhibitor (erlotinib) or disrupt the pathway further downstream with a PI3K/AKT inhibitor (LY294002) before treating with cisplatin (Figure 12). Panels A and C show that the respective inhibitors were active in the cells. However, no matter whether we incubate with inhibitor for 2h or increased incubation to 19h or increased inhibitor concentrations, neither inhibitor led to rescue of RAD51 foci upon subsequent treatment with cisplatin. In all cases RAD51 foci positive cells remained well below 10%.

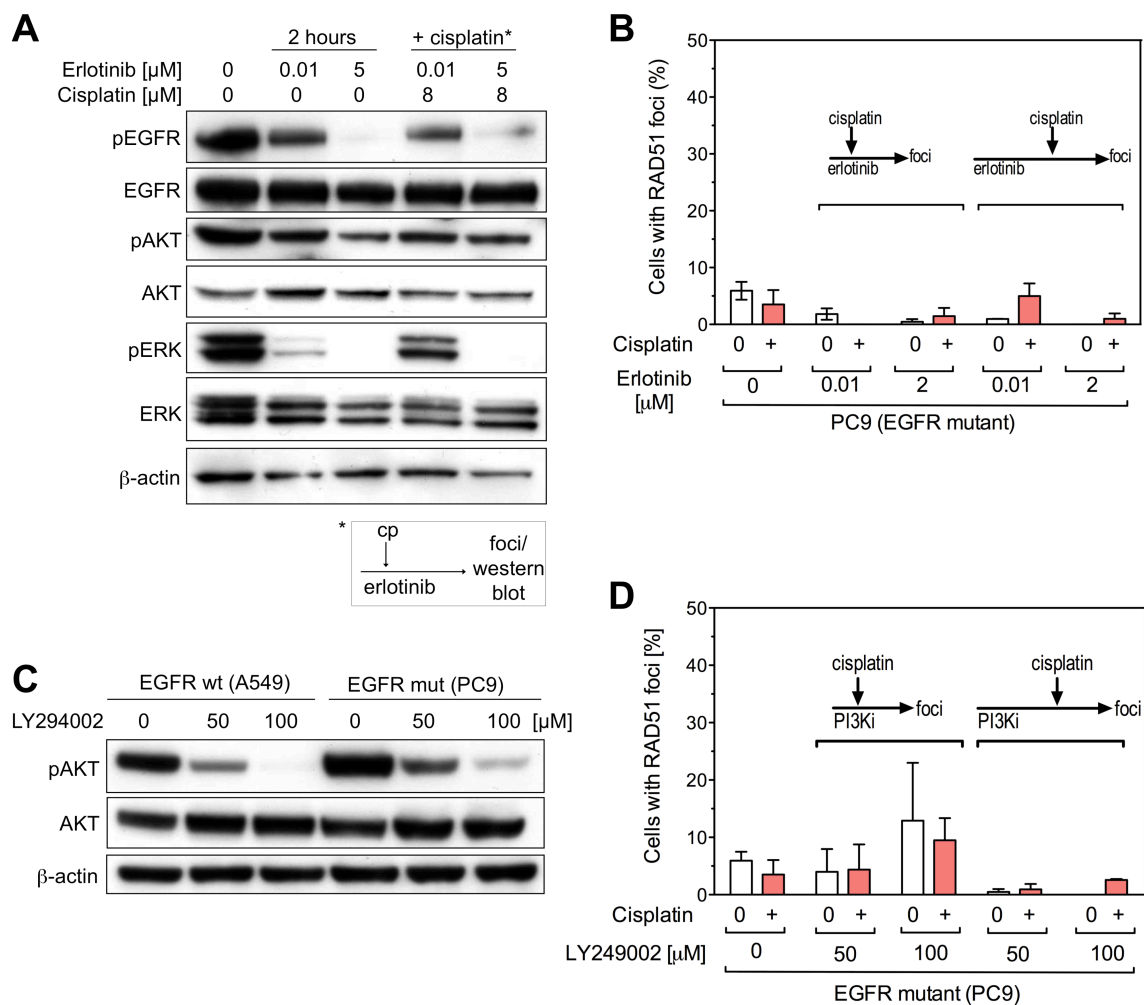


**Figure 12: Kinase-independent regulation of DNA repair by EGFR.** A) Inhibition of EGFR phosphorylation and downstream signaling in EGFR-mutant PC9 cells, complementing B. Western blot demonstrates that erlotinib concentrations between 0.01-5  $\mu\text{M}$  decrease phospho-EGFR levels to varying degrees as expected. The effect on p-ERK was more pronounced than on p-Akt. B) RAD51 foci formation in erlotinib-treated EGFR-mutant PC9 cells. Cells were exposed to erlotinib for 2 hours (illustrated by arrows in the left figure insert) or 19 hours (right insert) prior to adding cisplatin (8  $\mu\text{M}$ ). Bars represent mean  $\pm$  standard error based on 2 biological repeats. C) Inhibition of EGFR downstream signaling with the PI3K inhibitor LY294002. In order to assess effective inhibition of EGFR downstream signaling, a wild-type (wt) EGFR cell line (A549) and a mutant (mut) cell line (PC9) were treated with two different doses of the PI3K inhibitor. Phosphorylation of AKT decreased markedly in cells treated with 50  $\mu\text{M}$  LY294002 for 2 hours and almost vanished with 100  $\mu\text{M}$ . D) Disrupting PI3K-Akt axis does not rescue RAD51 foci formation, analogous to B. Control samples (first two bars) were untreated or treated with 8  $\mu\text{M}$  cisplatin for 1 hour and RAD51 foci were analyzed at 5 hours. Alternatively, cells were pretreated with 50 or 100  $\mu\text{M}$  PI3K inhibitor for either 2 or 19 hours prior to adding cisplatin. Cells were maintained in PI3K inhibitor until fixation at 5 hours after cisplatin treatment. Bars represent means  $\pm$  standard error based on two biological repeats.

### 3.2.7. EGFR impairs FANCD2/RAD51 pathway kinase-independently

We dismissed overactive mutant EGFR signaling as a likely candidate to be responsible for impaired FA/HRR. Next we sought to elucidate the effect of wild-type EGFR on RAD51 foci formation. Therefore we transfected human wild-type EGFR into a mutant EGFR lung cancer cell line (PC9), treated with cisplatin and quantified RAD51 foci (Figure 13). Interestingly we observed a pronounced increase in RAD51 foci from 7.5% in the EGFR-mutant control cell line compared to 17.9% in the EGFR-mutant cell line transfected with EGFR wild-type.

Inhibiting EGFR in a wild-type cell line (A549) had no effect on cisplatin-induced RAD51 foci levels (Figure 13D). However, silencing wild-type EGFR triggers an “EGFR-mutant phenotype” (Figure 13 C+D), resulting in decreased cisplatin-induced RAD51 foci levels.

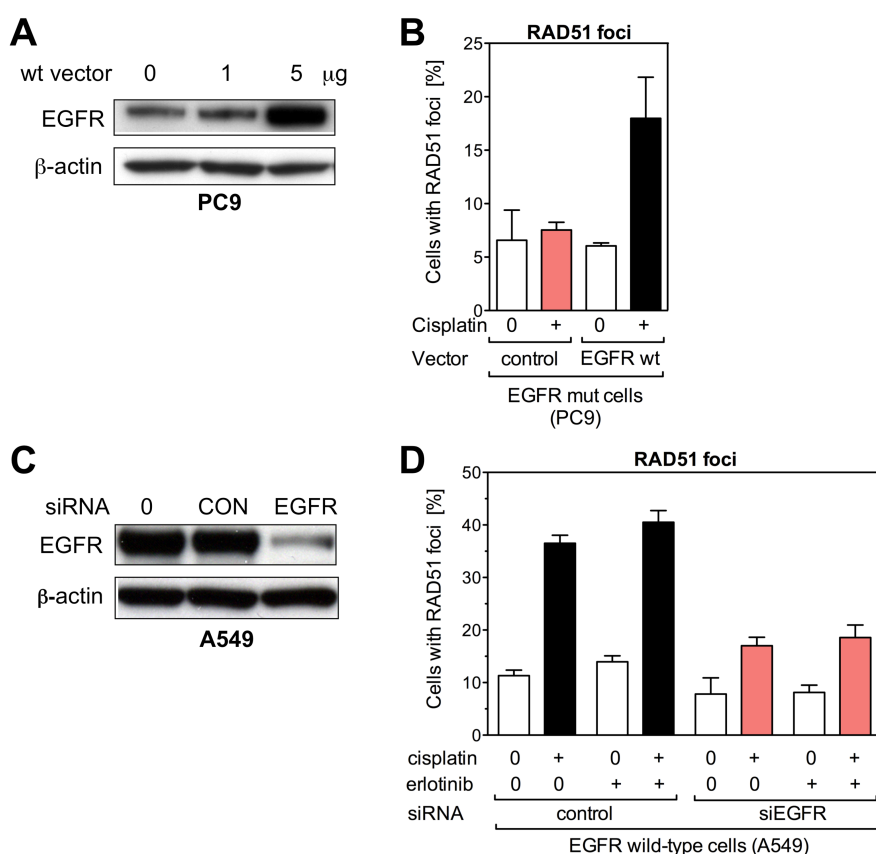


**Figure 13:** A) The western blot shows protein levels of EGFR in a mutant EGFR cell line (PC9) following transient transfection of 1 or 5  $\mu$ g of an expression vector encoding wild-type (wt) EGFR. B) Graph displays fraction of cells with  $\geq 10$  RAD51 foci 5 hours after cisplatin treatment (8  $\mu$ M for 1 hour) and 48 hours after transfection with either 5  $\mu$ g of the wild-type EGFR vector or an empty control. Bars represent mean  $\pm$  standard error based

on 2 biological repeats. C) Western blot shows A549 cells transfected with scrambled control (CON) siRNA or siRNA against EGFR. These data were kindly provided by Meng Wang. D) Graph indicates fraction of cells with RAD51 foci analogous to panel B. These data were kindly provided by Meng Wang.

### **3.3. Repair defect is downstream of FANCD2 at the stage of ICL unhooking involving failed recruitment of FAN1**

#### **3.3.1. EGFR mutation is epistatic to FANCD2**

To further elucidate the repair defect in mutant EGFR cell lines, we sought to establish if the impairment lies within the FA/HRR pathway or parallel to it. Therefore, we tested for epistasis between EGFR-mutation and disruption of the FA/HRR pathway by FANCD2 mutation. If EGFR mutation sensitizes to cisplatin by impairing the FA/HRR pathway, then the EGFR mutation should have no increased sensitization effect to ICL-inducing agents in a cell with already impaired FA/HRR pathway. In fact cells with EGFR-mutation alone or impaired FA/HRR alone or EGFR-mutation in addition to impaired FA/HRR should all show similar sensitization to crosslinking agents (Figure 14C). To test this we transfected FA/HRR-proficient (PD20+D2) and –deficient (PD20-D2) isogenic cell lines with EGFR-wild-type or EGFR-mutant, treated with MMC and evaluated unrepaired DNA damage by quantifying  $\gamma$ H2AX foci. To ensure that only cells are considered that contained transfected EGFR,, we performed co-transfection with a GFP encoding plasmid in a ratio 5:1 (EGFR-plasmid to GFP-plasmid). Thus cells that incorporated GFP-plasmid should contain EGFR-plasmid as well. These cells could easily be recognized due to their green hue and only these cells were included in the evaluation. Indeed, we observed similarly elevated  $\gamma$ H2AX foci levels of 60-65% in all cell lines containing one or both mutations compared to the double wild-type cell line. In an EGFR and FANCD2 wild-type context, there were only about half as many  $\gamma$ H2AX positive cells (35%).

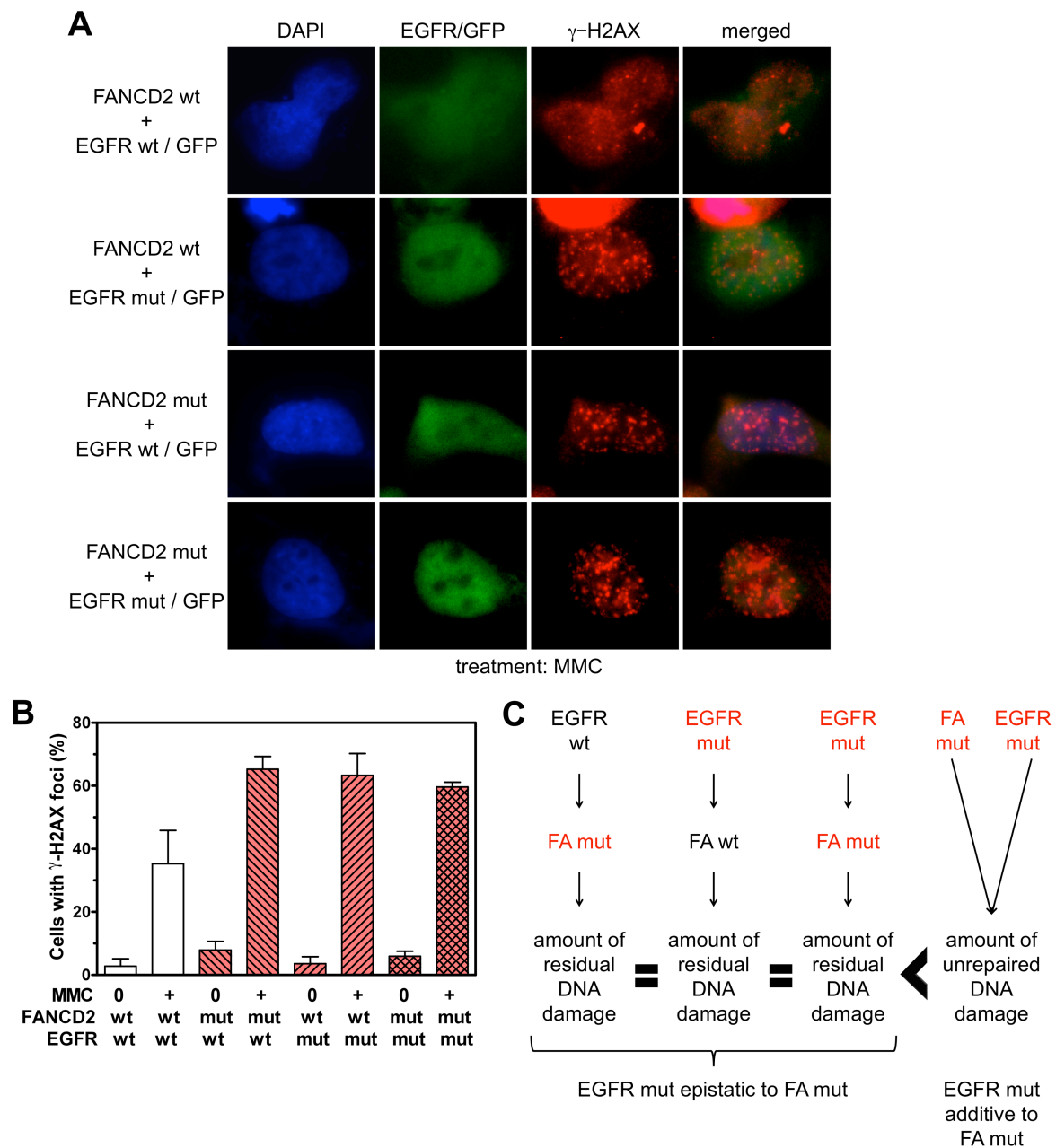


**Figure 14: DNA repair defect caused by EGFR mutation is epistatic with FANCD2.**

A) Mutant EGFR increases the number of  $\gamma$ H2AX foci in FANCD2 wild-type but not mutant cells after treatment with mitomycin C (MMC). The isogenic PD20 cell pair either mutant (mut) for FANCD2 or complemented with wild-type (wt) FANCD2 was transfected with expression vectors coding for wild-type or mutant EGFR together with GFP at a 5:1 molar ratio. Forty-eight hours after transfection, cells were treated with 1  $\mu$ g/ml MMC for 1 hour. At 24 hours, cells were stained for  $\gamma$ H2AX foci. Only successfully transfected cells expressing GFP were scored. Representative pictures are shown. B) Graph shows quantification of A. Bars represent mean  $\pm$  standard error based on 3 biological repeats. C) Principle of epistasis: mutant EGFR is epistatic to mutant FANCD2, if either or both mutations lead to the same level of DNA damage. Mutations would be additive if an increase in DNA damage levels was seen.

### 3.3.2. Increased replication fork stalling in EGFR-mutant cells

So far we have shown that EGFR-mutant cells harbor a defect within the FA/HRR pathway, which results in failure to form RAD51 foci. Furthermore EGFR-mutants are able to form RAD51 foci except when treated with ICL inducing agents, for which FA/HRR is needed. Thus we hypothesized the impairment to be within the FA/HRR pathway upstream of RAD51 foci formation. In order to unravel the precise defect within EGFR-mutant cell lines, we evaluated events within the FA/HRR pathway upstream of RAD51 foci formation.

RPA accumulates on exposed single-stranded DNA at stalled replication forks, which can be visualized as foci [81] [82] [83]. With some additional repair steps in between, RPA is later replaced by RAD51. We found EGFR-mutant cell lines to be capable in forming RPA foci when challenged with cisplatin. In fact we noticed elevated levels of RPA foci in EGFR-mutant cell lines (9-17%) compared to the EGFR wild-type one (3%), indicating increased replication fork stalling in the former.

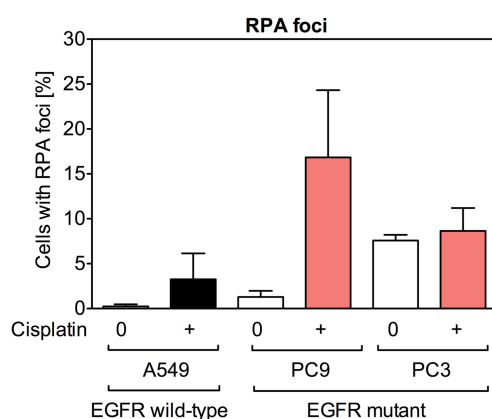


**Figure 15:** Illustration of increased replication fork stalling in EGFR-mutant PC9 cells. Shown is the fraction of cells with  $\geq 10$  replication protein A (RPA) foci 5 hours after treatment with 8  $\mu\text{M}$  cisplatin for 1 hour. Bars represent means  $\pm$  standard error based on 2-3 biological repeats.

### 3.3.3. Defect downstream of BRCA1

Next we evaluated the ability of EGFR-mutant cells to form BRCA1 foci, meaning the accumulation of BRCA1 at ICL. BRCA1 foci formation is an early step in the FA/HRR pathway. It is necessary for FANCD2 foci formation [42] [84]. FANCD2 foci formation is a crucial step within FA/HRR [42] [40]. BRCA1 foci formed normally in EGFR-mutant cell lines (PC9) upon treatment with cisplatin (Figure 16).

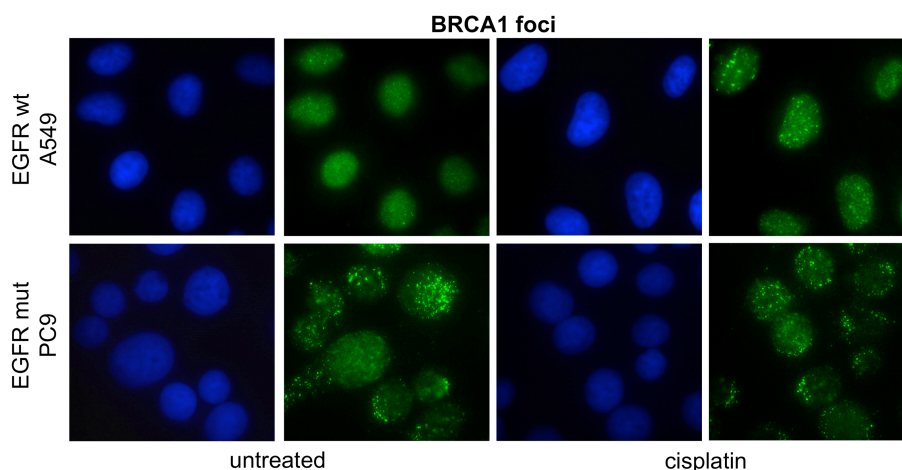


**Figure 16:** Representative images of subnuclear BRCA1 foci formation, which is upstream of FANCD2 foci, with and without treatment with 8  $\mu$ M cisplatin for 1 hour. These data were kindly provided by Natalie Ferraiolo.

### 3.3.4. Defect downstream of core complex, FANCD2

Within the FA-pathway several upstream events are necessary for FANCD2 foci to be able to form. One important upstream event is the assembly of several FA-proteins, forming the core complex at the ICL, which then mono-ubiquitinates FANCD2. This step is necessary for FANCD2 foci formation [43] [44]. Thus FANCD2 foci are a good marker for the integrity of such upstream events. EGFR-mutant cell lines (PC9, PC14) were proficient in forming FANCD2 foci after treatment with MMC. In fact levels were slightly elevated at 65-78% of FANCD2 foci positive cells in the EGFR-mutant cell lines compared to 53% in the EGFR wild-type one (Figure 17). We concluded from these data that the repair defect must lie downstream of FANCD2 foci formation, but upstream of RAD51 foci formation.

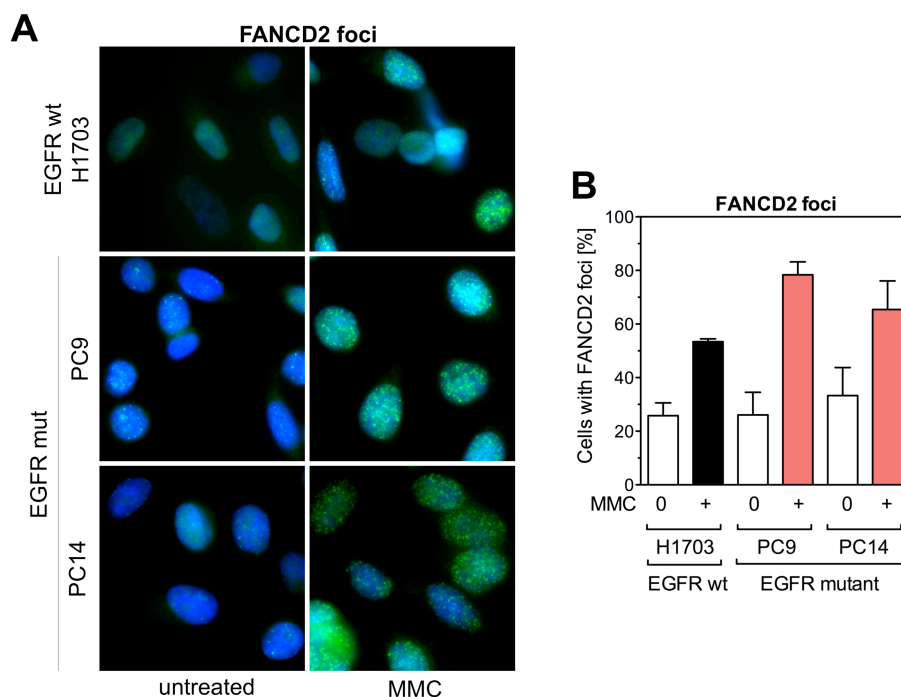


**Figure 17: Intact FANCD2 foci formation in EGFR-mutant cells.** A) Representative immunofluorescence microscopy images of intact subnuclear FANCD2 foci formation corresponding to graph in B. B) Fraction of nuclei with  $\geq 10$  FANCD2 foci in wild-type (wt) and mutant EGFR cell lines 24 hours after treatment with 0.5  $\mu\text{g/ml}$  MMC for 1 hour. Bars represent mean  $\pm$  standard error based on 2 biological repeats.

### 3.3.5. Impaired ICL unhooking

Incision or unhooking of the ICL occurs downstream of FANCD2 foci formation and upstream of RAD51 foci formation [40] [42]. This crucial step within ICL repair can be measured with a modified alkaline comet assay [20] [85] [86]. ICL keep DNA strands tied together and hinder DNA from migrating during electrophoresis. Therefore the more ICL, the less DNA migration and the shorter the comet tail. We treated an EGFR-mutant cell line (PC9), as well as an EGFR wild-type one (H1703) with cisplatin and evaluated unhooking of ICL at several time points after treatment by measuring the tail moment. We found the EGFR-mutant cell line to be strikingly deficient in unhooking ICL. At 24h after treatment, 55% of maximum detectable ICL remained compared to just 3% in EGFR wild-type cells. In an isogenic cell pair we detected similar results. ICL unhooking occurred much more slowly in the EGFR-mutant cells. Thus EGFR mutation correlates with defective ICL unhooking.

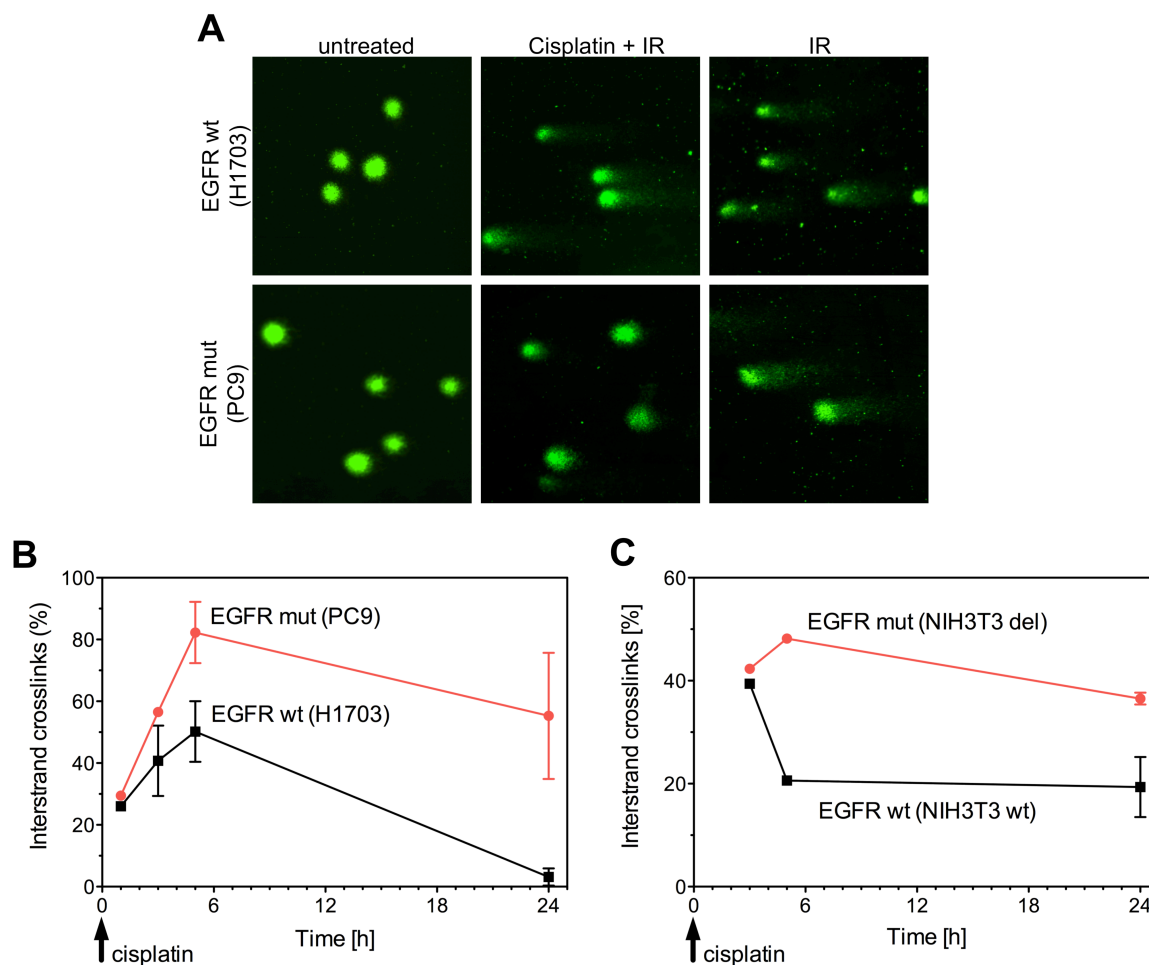


**Figure 18: Determining ICL repair using a modified alkaline Comet assay.** A) Representative images show comets 5 hours after treating cells with 50  $\mu$ M cisplatin for 1 hour and/or irradiating with 12.5 Gy ionizing radiation (IR) just before harvesting. Cells were irradiated to introduce a fixed number of random DNA DSB. ICL retain the double-stranded DNA, thereby shortening the tail moment. Complete unhooking would, therefore, result in the same tail moment as for irradiated only controls. The smaller the tail of cisplatin/IR-treated cells, the less unhooking occurred. Tails of mutant EGFR cells treated with cisplatin/IR are shorter than those in wild-type EGFR cells, indicating reduced unhooking of ICL.

B) Corresponding graph to A. Comparison of ICL repair in wild-type (wt) (H1703) and mutant (mut) (PC9) EGFR cell lines. Results are expressed as a percentage decrease in tail moment, so that 100% represents ICL saturation directly after irradiation resulting in complete restriction of DNA migration and 0% corresponds to maximum unhooking of induced ICL. Black arrow indicates time point when treatment with cisplatin was initiated. Data points represent mean  $\pm$  standard error based on 2-3 biological repeats. C) Quantification of remaining ICL in % in the isogenic NIH-3T3 cell pair with or without stable expression of mutant EGFR. Cells were treated and assay performed analogous A+B. The largest difference of unhooked ICL can be seen at 5 hours after starting treatment, with significant delay of unhooking in the mutant line even after 24 hours. Data points represent means  $\pm$  standard error based on 2 biological repeats

### 3.3.6. EGFR-mutant cells have low FAN1 gene expression

In order to elucidate why ICL unhooking is impaired in EGFR-mutant cell lines, we first analyzed gene expression levels of several nucleases involved in this step in a panel of 174 lung cancer cell lines (Figure 19). We found gene expression of one nuclease, FAN1, to be significantly lower ( $p=0.009$ ) in EGFR-mutant cell lines compared to EGFR wild-type ones.

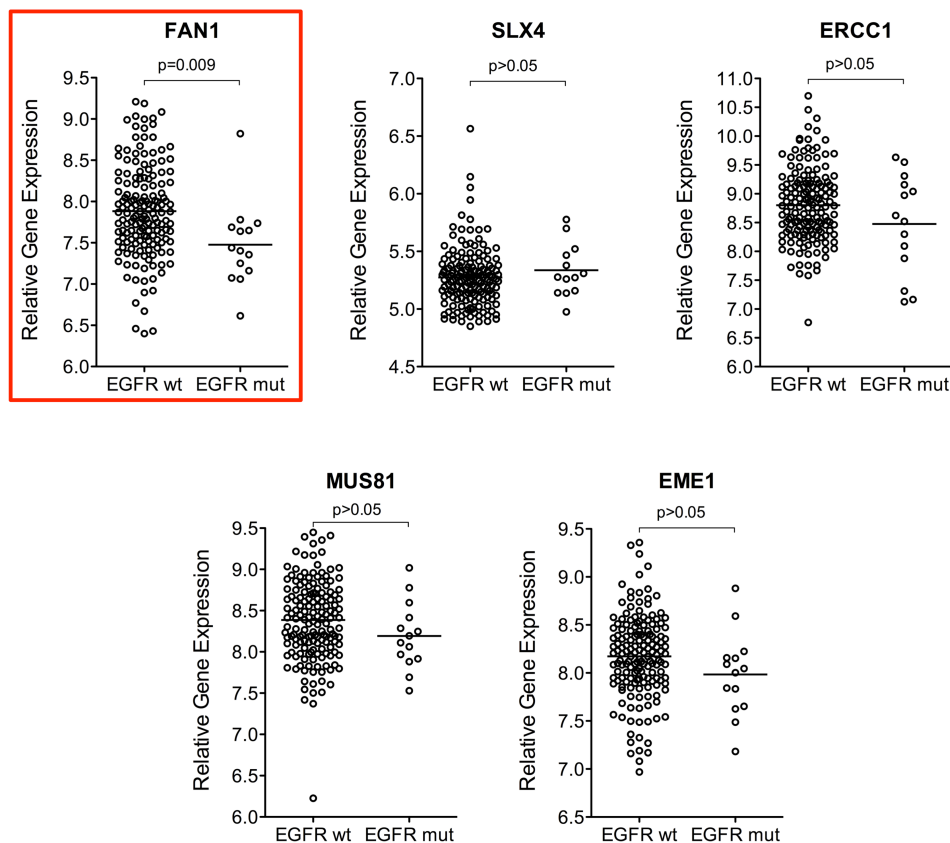


**Figure 19: Gene expression of factors involved in ICL unhooking.** The relative gene expression is shown on the y-axis. Cell lines are grouped into EGFR wild-type versus mutant based on the information in the data base. Horizontal lines represent the mean gene expression in each group. P-values are based on a two-tailed T-test. With a  $p=0.009$ , FAN1 nuclease expression was the only factor that was significantly lower in expression in the EGFR-mutant group compared to wild-type.

### 3.3.7. FAN1 protein levels tend to be reduced in EGFR-mutant cells

Next we examined whether low FAN1 gene expression translates into low protein expression, which could account for impaired ICL unhooking in EGFR-mutant

cells. Using western blotting we could not find striking differences in FAN1 protein levels between EGFR wild-type and mutant cell lines, however we did observe a tendency for low FAN1 protein expression in the mutant lines (Figure 20).

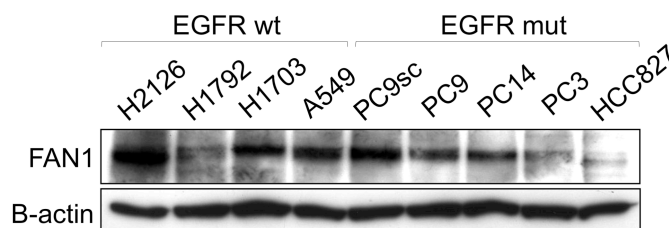


**Figure 20:** Western blot of FAN1 protein expression in wild-type and mutant EGFR lung cancer cell lines. FAN1 protein is expressed in all cell lines to varying degree, with a trend towards lower expression in the cell lines with known EGFR mutation.

### 3.3.8. EGFR-mutant cells fail to recruit FAN1 to ICL

We next wished to investigate FAN1 function. FAN1 is recruited by ubiquitinated FANCD2 to ICL. Accumulation of FAN1 at ICL can be visualized as foci. Since FAN1 primary antibodies currently on the market yielded unsatisfactory staining qualities, we circumvented this problem by transfecting GFP-tagged FAN1 into isogenic cell lines expressing either EGFR wild-type or EGFR-mutant. We treated with MMC and quantified FAN1 foci in transfected cells. Indeed, we found EGFR-mutant cells were impaired in FAN1 foci formation, with only 14% FAN1 positive cells compared to 35% positive cells in the EGFR wild-type one.

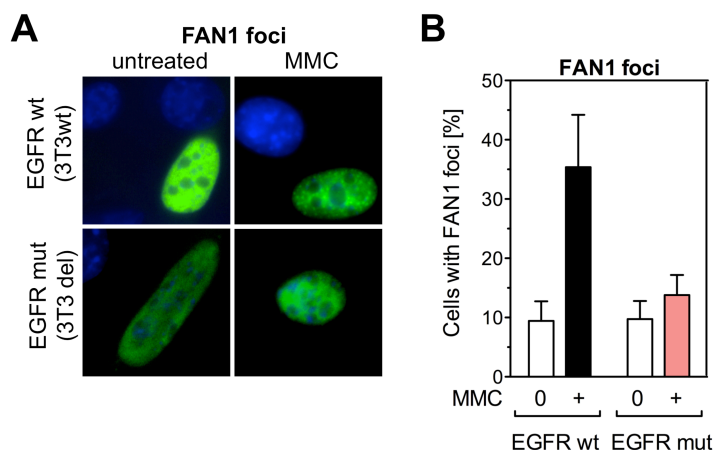


**Figure 21:** A) Representative immunofluorescence microscopy images are shown for an isogenic MEF cell pair with wild-type (wt) or E746\_A750 (mut) EGFR transiently transfected with GFP-tagged FAN1. Cells were treated with 80 ng/ml MMC for 24 hours. B) Corresponding graph to A. It shows fraction of cells with  $\geq 5$  foci FAN1. Bars represent mean  $\pm$  standard error based on 3 biological repeats.

### **3.4. Impaired FAN1 recruitment and HRR sensitizes EGFR-mutant cells to PARP inhibitors**

The data gathered so far indicates a new DNA repair defect specific to EGFR-mutant lung cancers: EGFR mutation correlates with impaired FAN1 function, reduced unhooking of ICL and increased sensitivity to ICL inducing agents. As we aimed to find new, targeted treatment approaches for this specific group of lung cancer patients, we scrutinized FAN1 function and found it to be involved not only in ICL unhooking, but also in late stages of HRR (Figure 23A) [58] [59] [60]. We hypothesized FAN1 recruitment to be reduced in EGFR-mutant cells independent of the type of damage inflicted. This should not only lead to impaired ICL repair, but also result in inefficient late stage HRR. Defects in HRR can be exploited with PARP inhibitors, as success in HRR-deficient (BRCA1/2 mutant) breast cancers shows [3]. Thus, we hypothesized targeted therapy with PARP inhibitors to be effective in EGFR-mutant cancers.

#### **3.4.1. EGFR-mutant cells fail to form FAN1 foci in response to PARP inhibitor olaparib**

First, we aimed to validate the notion of EGFR-mutant cells being impaired in recruiting FAN1 in response to PARP inhibitors. We treated an EGFR wild-type and mutant isogenic cell pair with the PARP inhibitor olaparib and evaluated FAN1 recruitment to DNA damage by quantifying FAN1 foci. Indeed, the EGFR-mutant cell line was unable to form FAN1 foci efficiently, resulting in less than half the amount of cells with foci compared to the EGFR wild-type cell line: 13% versus 29% in EGFR wild-type cells (Figure 22).

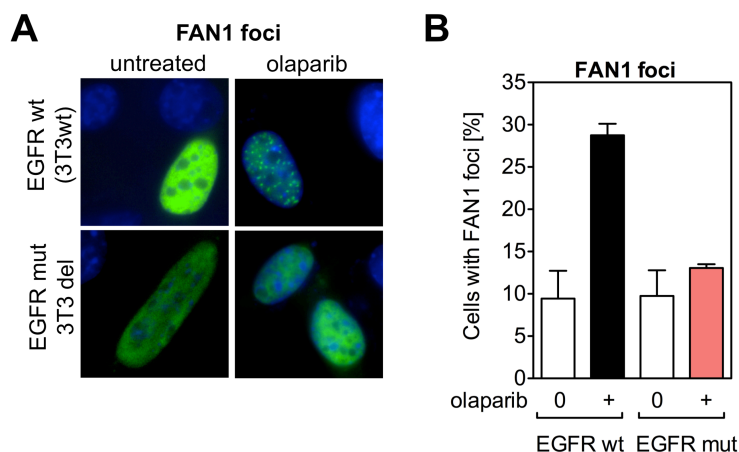


**Figure 22:** A) Representative images of subnuclear GFP signal (green) overlaid with DAPI (blue) in an isogenic MEF pair with wild-type (wt) or mutant (mut) EGFR transiently transfected with GFP-tagged FAN1. Cells were treated with 10  $\mu$ M olaparib for 24 hours. B) Corresponding graph to A. Fraction of cells with  $\geq 5$  FAN1 foci. Bars represent mean  $\pm$  standard error based on 3 biological repeats.

### 3.4.2. EGFR-mutant cells are impaired in RAD51 foci resolution after PARP inhibitor treatment

Next we wished to determine whether reduced recruitment of FAN1 results in impaired HRR by evaluating the induction and resolution of RAD51 foci. PARP inhibitors cause DNA damage indirectly by inhibiting the repair of existing SSB, which then become DSB during S-phase. Thus, we chose 24h after treatment as the first time point to allow the creation of DSB in cells entering S-phase. For the later time point we aimed to give cells enough time for RAD51 resolution to occur, yet we wanted to avoid evaluating any apoptotic cells. Apoptosis can occur as early as 24h after lethal DSB are inflicted. We reasoned 34h after olaparib treatment, which is equivalent to about 10h after DSB creation should be an adequate time point to evaluate RAD51 resolution.

We quantified RAD51 foci in an EGFR wild-type (A549) and EGFR-mutant lung cancer cell line (PC9) at 24h and 34h after treatment with olaparib (Figure 23). At the early time point after treatment we observed normal RAD51 foci formation in EGFR-mutants (33% versus 31% in EGFR wild-type cells). However, while RAD51 foci amounts drop to background levels in EGFR wild-type cells at 34h (84% reduction), foci levels remained high in EGFR-mutant ones (only 22% reduction). Interestingly a similar phenomenon is observed in an FANCD2

proficient/deficient isogenic cell pair. While RAD51 foci levels drop to background levels in the wild-type cell line at 34h, levels remain high in the mutant one.

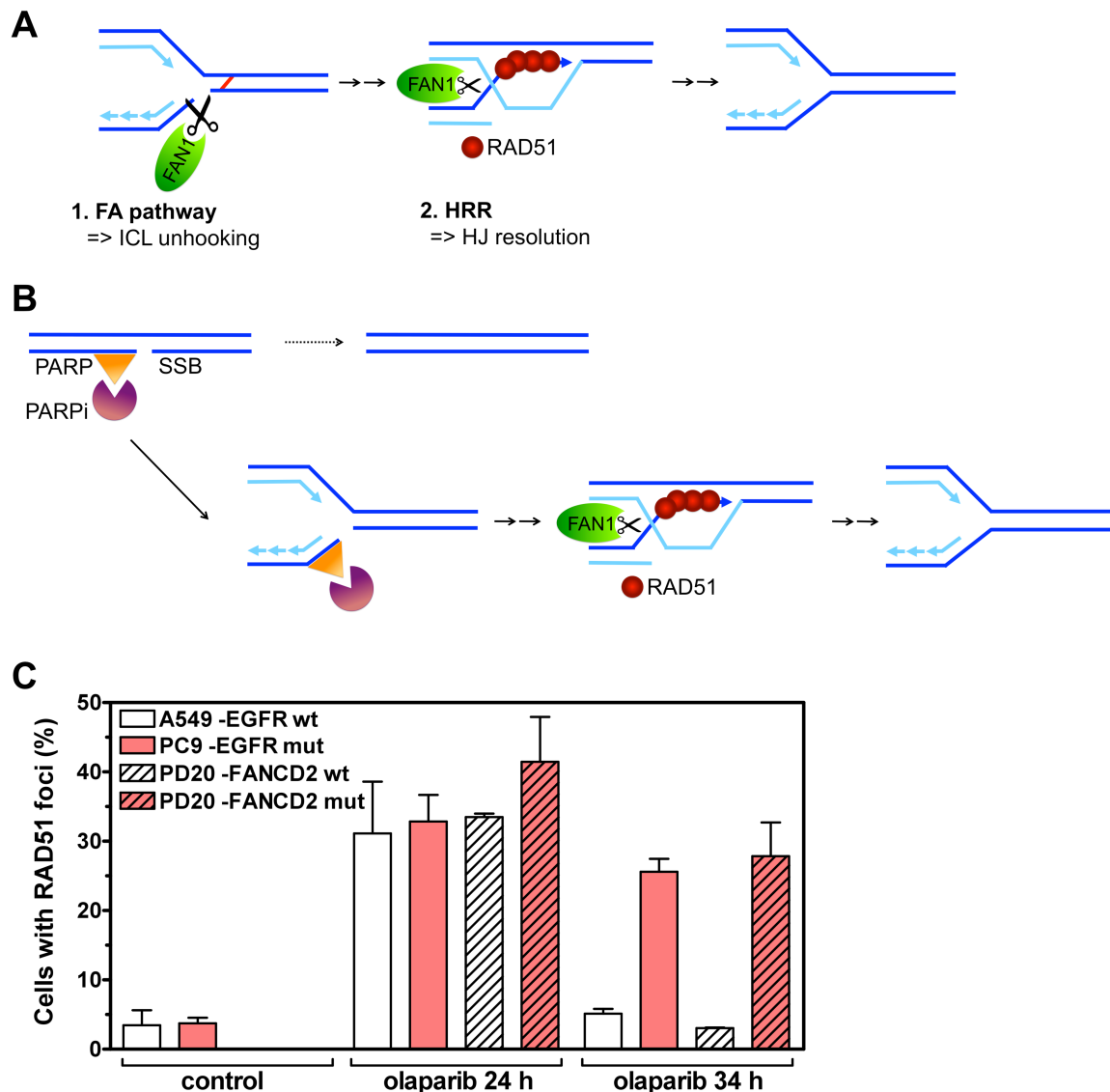


**Figure 23:** A) Panel shows FAN1's role in ICL unhooking and late stage HRR. B) Panel shows SSB repair, when PARP is inhibited. FAN1 is involved in late stage HRR. C) RAD51 foci formation in cell lines as indicated, treated with 10  $\mu$ M olaparib for 24 or 34 hours. Cells with  $\geq 10$  RAD51 foci/nucleus were scored. Bars represent mean  $\pm$  standard error based on 2-5 biological repeats.

### 3.4.3. EGFR-mutant cells treated with olaparib contain large amounts of unrepaired DNA damage

As a consequence of decreased FAN1 recruitment to DNA damage and impaired HRR we postulated increased unrepaired DNA damage in EGFR-mutant cells

treated with olaparib. Indeed we were able to show elevated levels of DNA damage, indicated by  $\gamma$ H2AX foci, in EGFR-mutant lung cancer cell lines after treatment with olaparib (Figure 24).  $\gamma$ H2AX foci are especially pronounced in PC9 and PC14 EGFR-mutant cell lines, which - as shown next - are also sensitive to olaparib treatment.

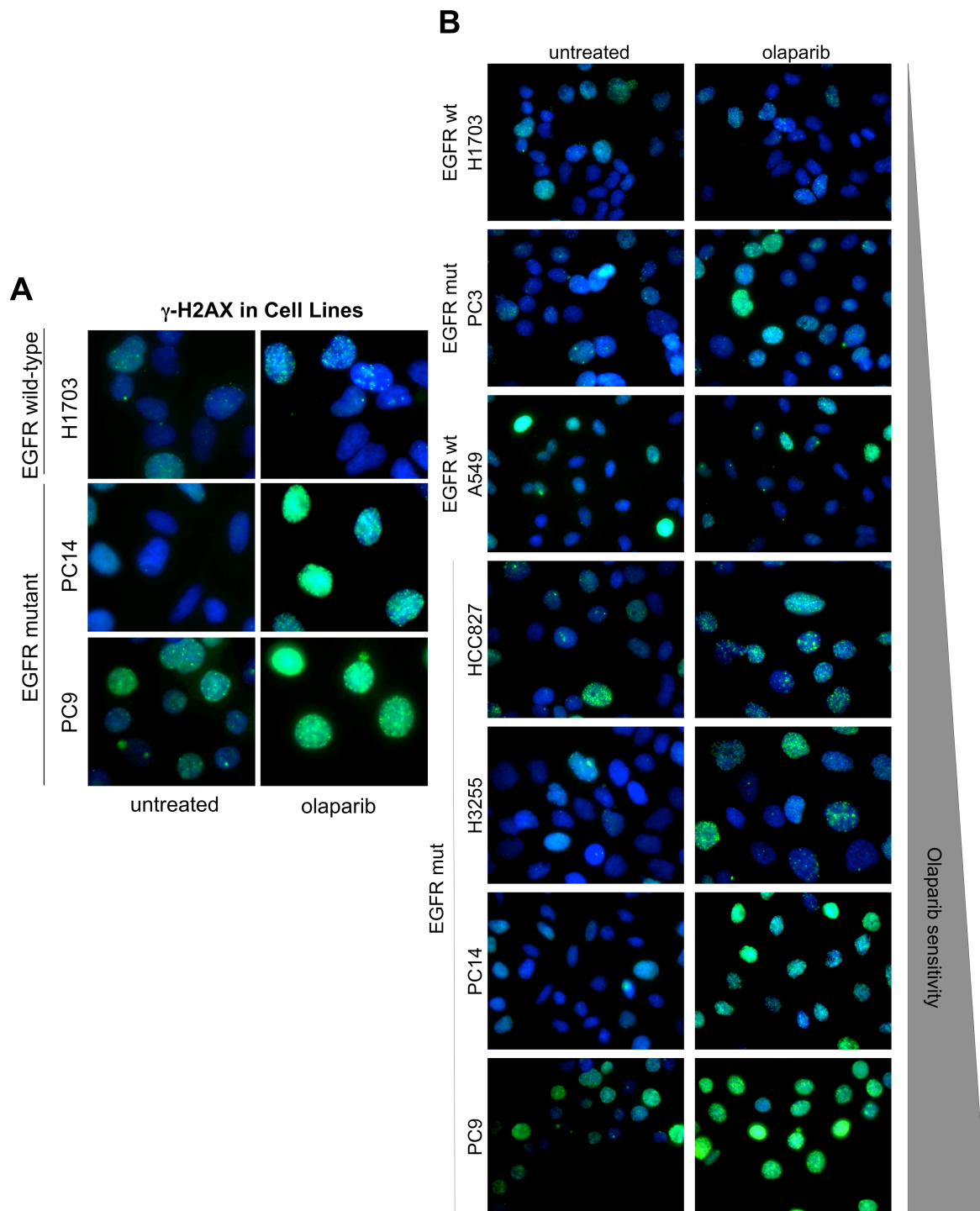


**Figure 24:** A) Representative images of  $\gamma$ H2AX foci in EGFR wild-type and mutant cell lines treated with 10  $\mu$ M olaparib for 24 hours. B) Subnuclear  $\gamma$ H2AX staining correlates

with increasing cellular sensitivity to olaparib based on data in Figure 25. Cell lines are ranked from top to bottom by increasing sensitivity to olaparib. Representative images with overlaid DAPI and  $\gamma$ H2AX stain are shown.

### 3.4.4. EGFR-mutant cell lines exhibit increased sensitivity to olaparib

However, is this HRR defect observed in EGFR-mutant cells severe enough to sensitize to treatment with PARP inhibitor? To answer this question, we performed colony formation assays, evaluating the sensitivity of EGFR wild-type and mutant lung cancer cell lines to olaparib (Figure 25). Indeed 3/6 EGFR-mutant cell lines showed decreased clonogenic survival of 1.0-7.6% at 10 $\mu$ M olaparib compared to 15.7-53.5% for wild-type cell lines. We could further confirm increased sensitivity of EGFR-mutant cells in an isogenic cell pair. Survival fractions were 5.0% for the EGFR-mutant cell line compared to 18.9% for the wild-type one. Thus mutant EGFR sensitizes to PARP inhibitor olaparib.

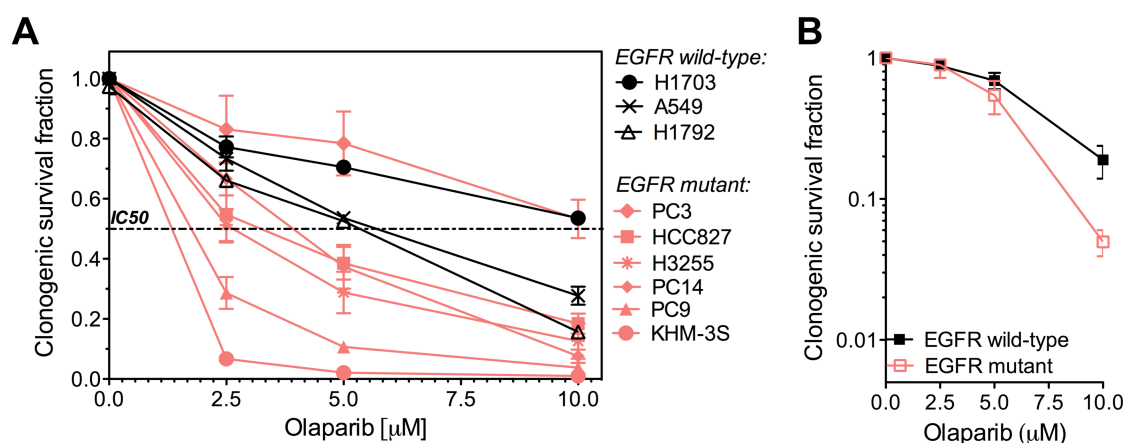


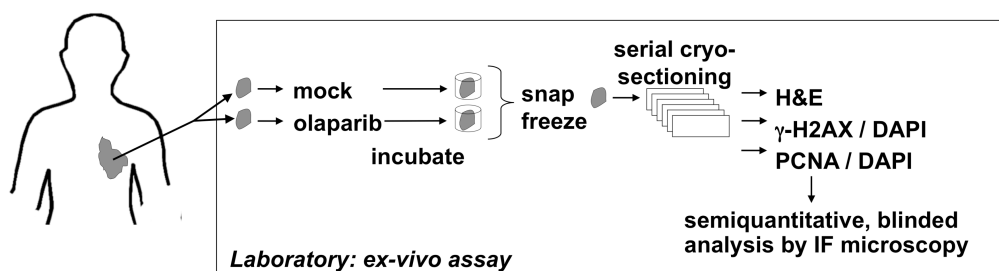
**Figure 25:** A) Clonogenic survival of lung cancer cell lines with wild-type or mutant EGFR after treatment with increasing concentrations of olaparib for 72 hours. Concentrations at which survival curves intercept with dotted horizontal line indicate IC50 (inhibitory concentrations to achieve 50% survival). Data points represent mean  $\pm$  standard error based on 2-3 biological repeats. B) Clonogenic survival of isogenic MEFs with wild-type or mutant (del19) EGFR. Cells were treated analogous to A. Data points represent mean  $\pm$  standard error based on 3 biological repeats.

### 3.4.5. EGFR-mutant sensitizes to olaparib in vivo

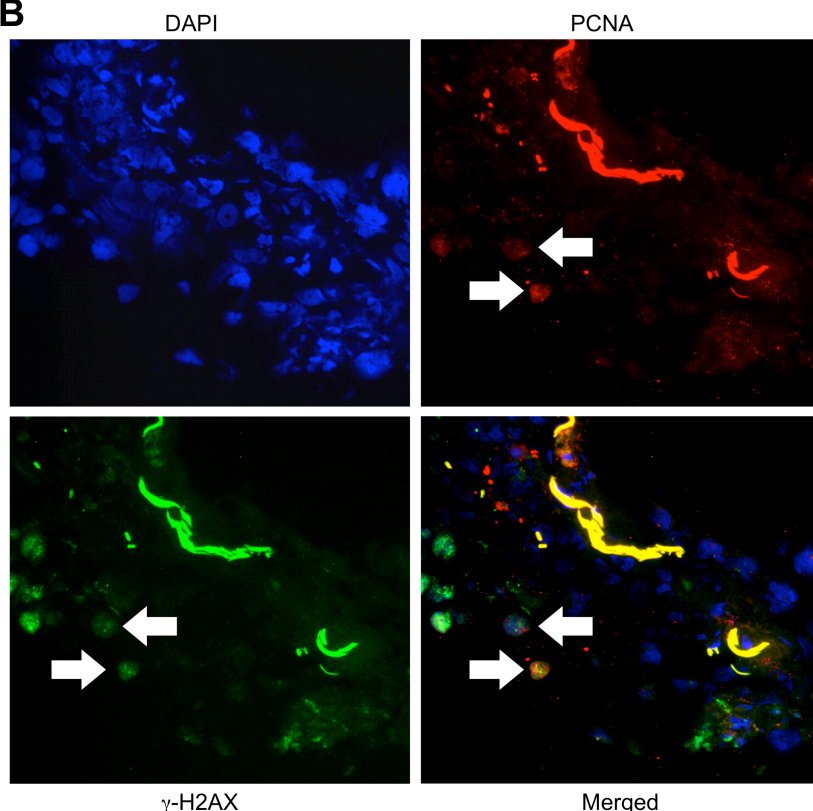
Finally we aimed to investigate the sensitization effect of mutant EGFR to olaparib in vivo. Therefore we obtained fresh tumor biopsies from lung cancer patients containing EGFR wild-type or mutant. We treated the samples with olaparib and

stained for  $\gamma$ H2AX foci formation using an ex-vivo foci assay, previously established by Birkelbach et al. [6] PARP inhibitors cause lethal DNA DSB only during S-phase. Keeping in mind that lung cancer tissue contains a much smaller S-phase fraction than cell lines, we identified olaparib-specific  $\gamma$ H2AX foci by co-staining with the S-phase marker PCNA (Figure 26) [6]. Indeed, quantification of  $\gamma$ H2AX foci in PCNA-positive cells confirmed in-vitro results, with elevated  $\gamma$ H2AX foci levels in EGFR-mutant lung cancer tissue compared to wild-type (21% versus 4%,  $p=0.03$ ).

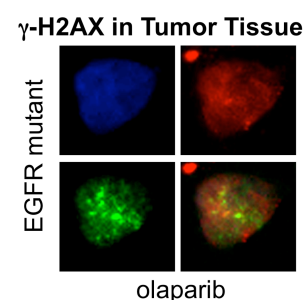
A



B



C



D

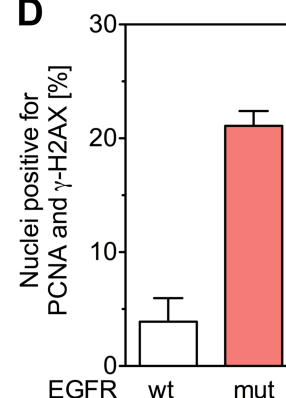


**Figure 26:** A) Ex-vivo assay for assessing DNA double-strand break formation in response to olaparib. Fresh tumor tissue is obtained from core biopsies or other methods. Viable tumor tissue not required for pathological diagnosis is placed in RPMI medium and hand-carried to the laboratory where it is aliquoted. Samples are subjected to mock or olaparib (10  $\mu$ M) treatment for 24 hours. Samples are then snap frozen and processed for

staining. B) Representative low-power images of a core biopsy section from a patient with an EGFR-mutant lung adenocarcinoma. Arrows indicate 2 cells double positive for a subnuclear PCNA staining patterns that is consistent with S-phase and  $\gamma$ H2AX foci. C) Pictures show a representative nucleus after counterstaining tumor tissue derived from a lung cancer patient with DAPI (blue), PCNA (red), and  $\gamma$ H2AX (green). D) Graph shows the fraction of PCNA positive nuclei containing  $\gamma$ H2AX foci following ex-vivo treatment of EGFR-mutant versus wild-type tumor tissue with 10  $\mu$ M olaparib for 24 hours. Bars represent average number of positive nuclei  $\pm$  95% confidence intervals. These data were gathered with great help from Liliana Gheorgiu.

### **3.5. Treatment with DNA damaging agents: Effect of EGFR TKI resistance on sensitivity**

Lung cancer patients with EGFR mutations currently receive EGFR inhibitors as first line treatment [87] [88] [89] [90] [91]. As mentioned earlier, initially impressive results can be achieved with these drugs, but unfortunately all patients relapse eventually [5]. Thus we investigated alterations in sensitivity to additional DNA damaging treatments, such as cisplatin, IR or PARP inhibitors.

#### **3.5.1. EGFR TKI resistance may not result in cisplatin resistance**

Utilizing colony formation assays we assessed sensitivity of EGFR-mutant lung cancers with acquired resistance to EGFR inhibitors erlotinib or gefitinib (Figure 27). Three EGFR TKI resistant cell lines showed slightly increased resistance to cisplatin. Survival fractions at 8  $\mu$ M cisplatin were 13%-18% compared to 4% for the EGFR TKI parental cell line (PC9). Cell lines with survival fractions of <20% can be considered sensitive given that several cisplatin-resistant EGFR wild-type cell lines show more than 70% survival at this dose. A fourth EGFR TKI resistant cell line was created from a pooled population (gtPC9-p). This cell line showed little increase in resistance to cisplatin when compared to the EGFR TKI sensitive parent cell line (5% versus 4% survival at 8 $\mu$ M cisplatin). We therefore concluded that EGFR TKI resistance does not confer cisplatin resistance back to the degree seen in EGFR wild-type cell lines.

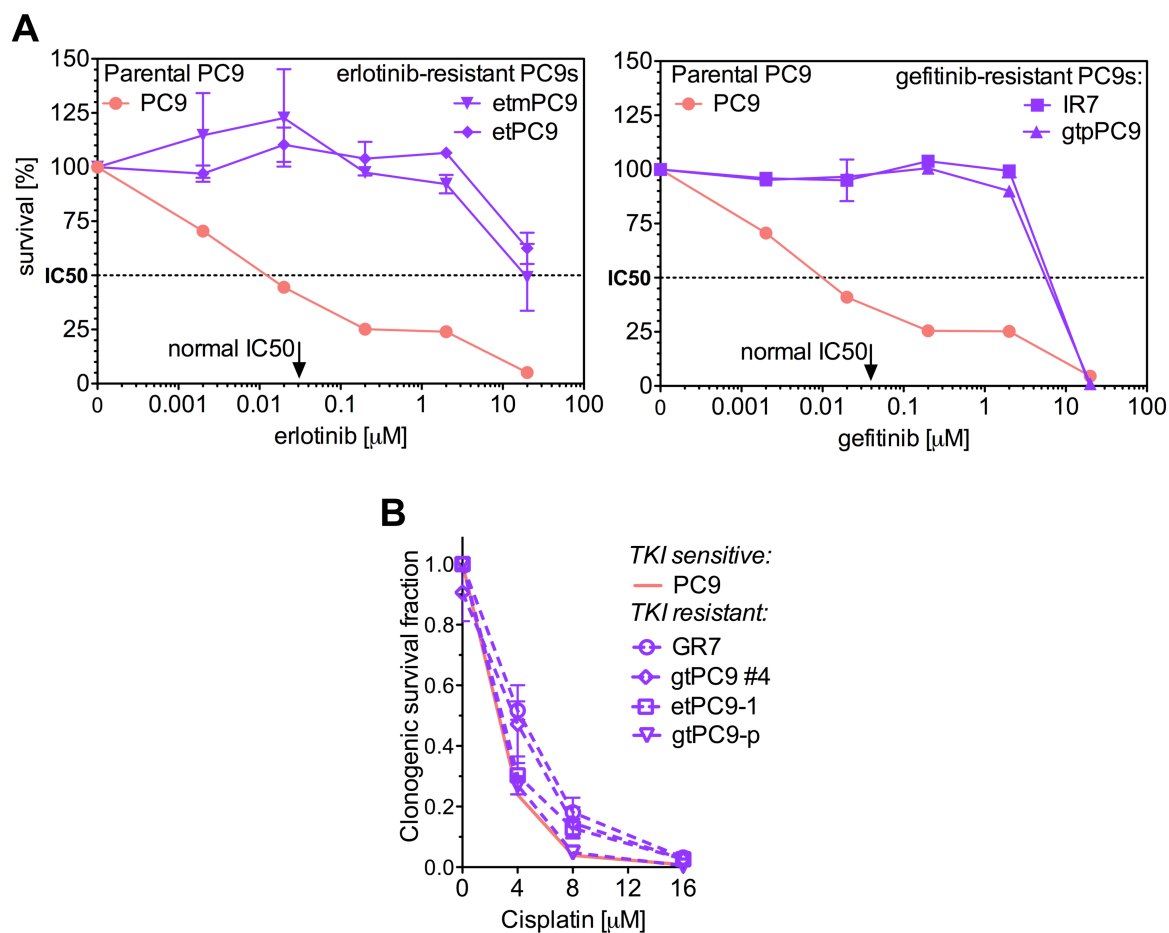


**Figure 27:** A) Left panel: Survival curves measured by Syto60 assay in response to increasing concentrations of EGFR inhibitor erlotinib. Depicted are the EGFR TKI sensitive lung cancer cell line (pink: PC9) and derived cell lines with acquired resistance to erlotinib (purple: etmPC9, etPC9). Right panel: Survival curves analogous to the left panel, but gefitinib was used and depicted are cell lines with acquired resistance to gefitinib (purple: IR7, gtpPC9) in addition to the sensitive parental line (pink: PC9). B) Clonogenic survival fractions of EGFR TKI sensitive (pink: PC9) and derived EGFR TKI resistant lines (purple) in response to increasing doses of cisplatin. Data points represent mean  $\pm$  standard error based on 3 biological repeats.

### 3.5.2. EGFR TKI resistance might sensitize to IR

We further assessed sensitivity of EGFR TKI resistant cell lines to radiation using colony formation assays (Figure 28). At 8 Gy there was a negligible increase in resistance to IR of 0.3% in a gefitinib-resistant cell line (HCCGR), which was derived from the EGFR TKI sensitive parental cell line “HCC827” (Figure 28A).

Interestingly EGFR TKI resistant cell lines derived from a different EGFR TKI sensitive parental cell line “PC9” showed a slight increase in sensitivity to IR (Figure 28B). Survival fractions at 8Gy dropped by more than half, from 4.6% to 0.9 – 2.0%. This increase in sensitivity may be due to more apoptosis in these

EGFR TKI resistant cells. Using western blotting increasing amounts of caspase 3 fragmentation can be found in TKI-resistant cells when treated with 8Gy (Figure 28C). In addition, TKI-resistant cells showed elevated sub G1 fractions of 21-29% after IR treatment compared to just 6.5% in the parental PC9 cell line (Figure 28D). We used PC9 cells treated with erlotinib as a positive control for caspase 3 cleavage, since this cell line is known to apoptose heavily upon EGFR TKI treatment. Thus, at least in this one cell pair, EGFR TKI resistance may increase sensitivity to IR by elevating apoptosis.

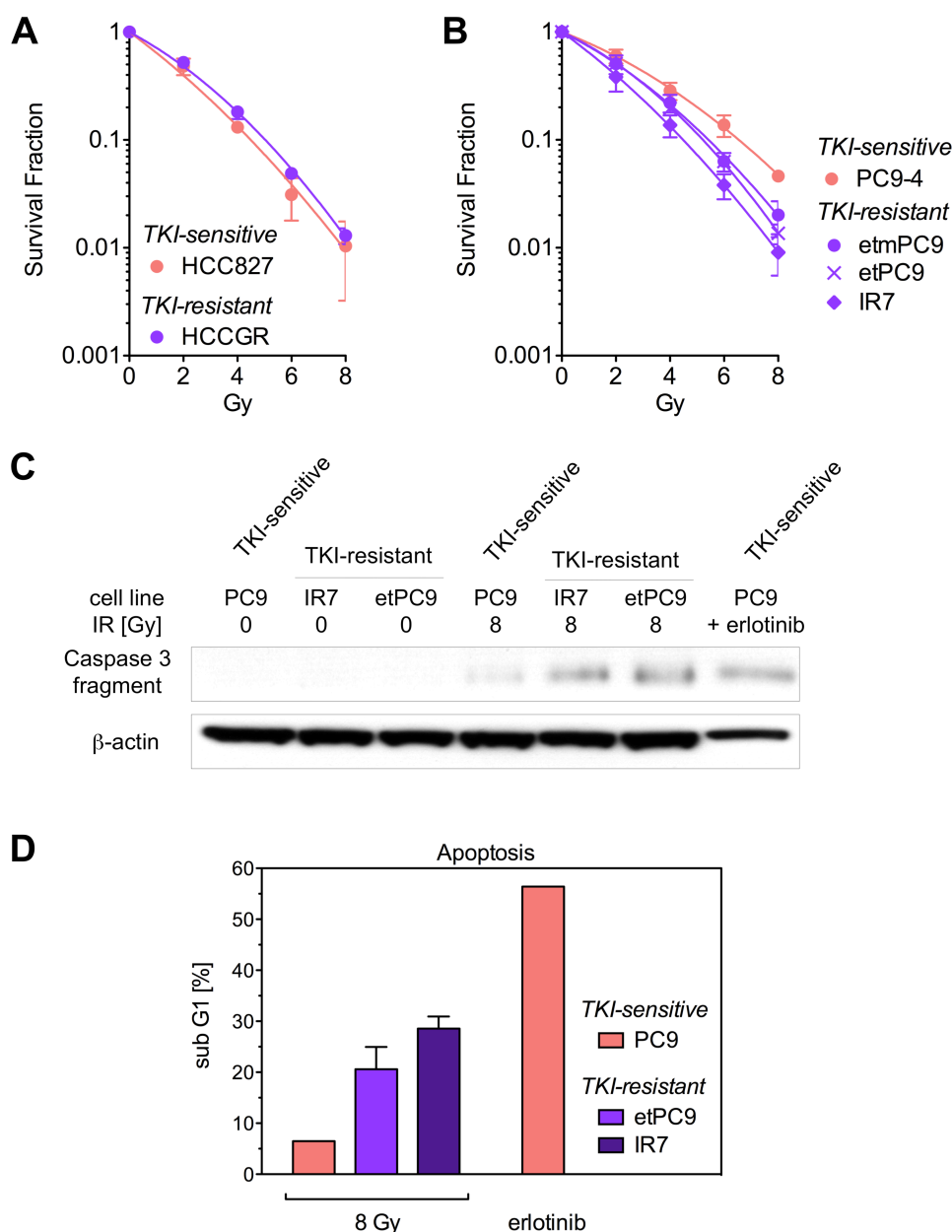


**Figure 28:** A) Clonogenic survival fractions of EGFR TKI sensitive cell line (pink: HCC827) and derived gefitinib-resistant cell line (purple: HCCGR) in response to increasing doses of irradiation. Data points represent mean  $\pm$  standard error based on 3 biological repeats. B) Clonogenic survival fractions of the parental EGFR TKI sensitive

cell line (pink: PC9) and derived gefitinib/erlotinib-resistant lines (purple) in response to increasing doses of irradiation. Data points represent mean  $\pm$  standard error based on 3 biological repeats. C) Western Blot depicting increased caspase 3 cleavage in TKI-resistant cell lines after 8Gy. Cell lines were irradiated with 8Gy and caspase 3 cleavage was assessed 48h after treatment. TKI sensitive cells treated with 2 $\mu$ M erlotinib are known to undergo apoptosis and are thus included as a positive control (last column). Note: 100 $\mu$ g protein was loaded except for the last column, which contains 40 $\mu$ g. D) Sub G1 cell cycle fractions were determined using flow cytometry. Cell lines were irradiated with 8Gy and sub G1 fractions were assessed at 72h after treatment. TKI sensitive cells treated with 2 $\mu$ M erlotinib are used as a positive control. Bars represent mean  $\pm$  standard error based on 4 biological repeats.

### **3.5.3. EGFR TKI-resistance sensitizes to PARP inhibitors possibly due to more endogenous SSB**

Lastly we investigated sensitivity of EGFR TKI resistant cell lines to treatment with PARP inhibitor olaparib. Strikingly we saw pronounced sensitization to olaparib in EGFR TKI resistant cell lines (Figure 29A). Survival fractions at 10  $\mu$ M olaparib dropped from 18% survival in the TKI-sensitive HCC827 lung cancer cell line to 1% in the TKI-resistant one. Similarly in the PC9 lung cancer cell line, survival dropped by >10x, from 4% to 0.4-0.06% in the TKI-resistant lines.

Sensitivity to olaparib was underscored by high levels of unrepaired DNA damage indicated by  $\gamma$ H2AX foci in EGFR TKI resistant cell lines. An increase in DNA damage levels is especially pronounced in HCCGR6 cells, when compared to its parental line HCC827 (Figure 29B). The EGFR TKI sensitive line PC9 is already considered sensitive to olaparib, thus containing high levels of  $\gamma$ H2AX foci. This makes any increase of foci in the derived EGFR TKI resistant lines hard to judge by eye.

PARP inhibitors prevent DNA SSB endogenously present from being repaired. We hypothesized EGFR TKI resistant cells may contain more endogenous DNA breaks than TKI sensitive cells, which could account for their increased sensitivity to PARP inhibition. Utilizing an alkaline comet assay we measured DNA breaks in an untreated EGFR TKI sensitive (PC9) and TKIR resistant (IR7) cell pair. In the absence of any drug the EGFR TKI resistant cell line (IR7) contains significantly

more DNA breaks than the EGFR TKI sensitive one (PC9),  $p = 0.0001$  (Figure 29C).

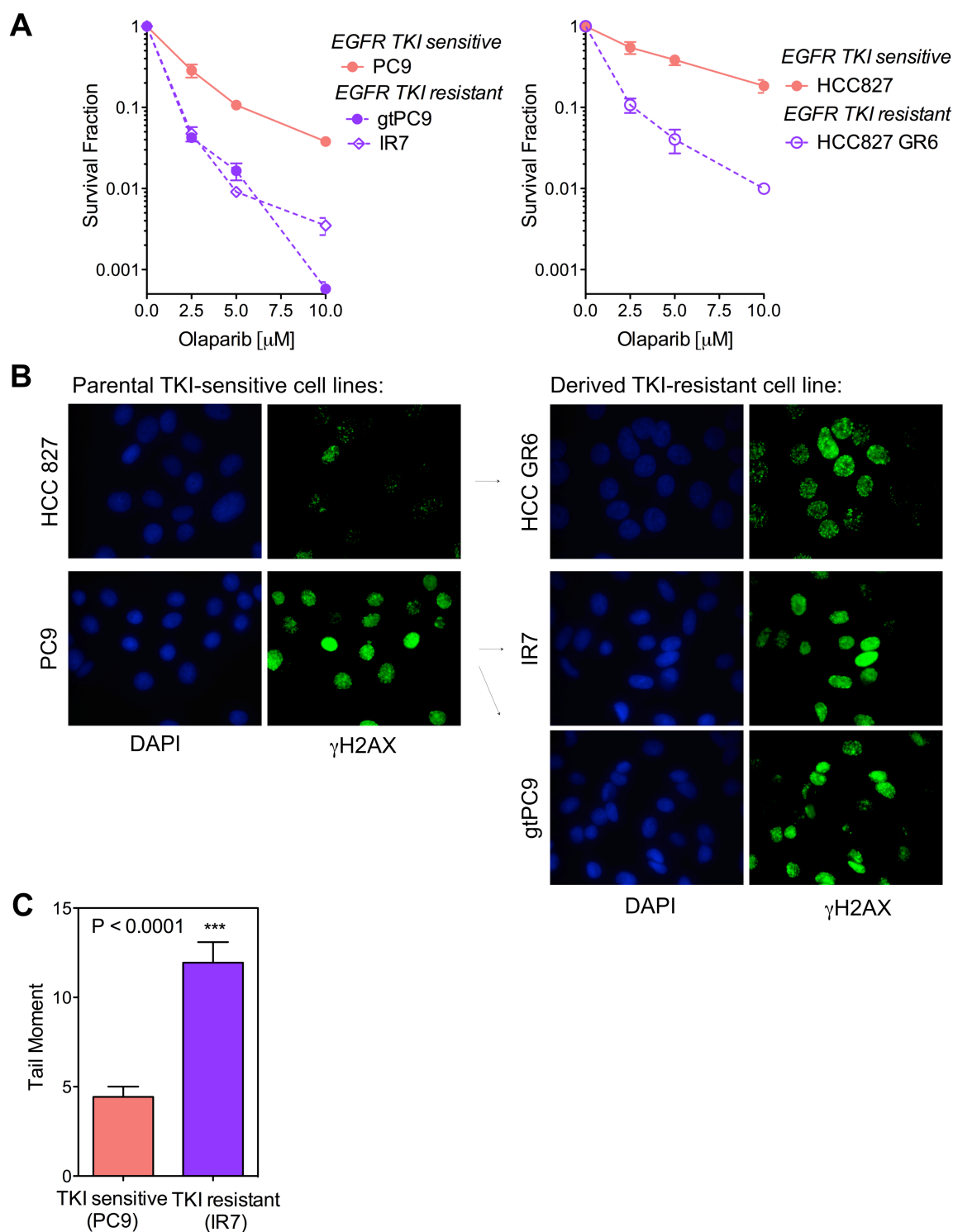


**Figure 29:** A) Left panel: clonogenic survival fractions of the parental EGFR TKI sensitive cell line (pink: PC9) and derived gefitinib/erlotinib-resistant lines (purple) in response to increasing doses of olaparib. Right panel: Clonogenic survival fractions of an EGFR TKI sensitive cell line (pink: HCC827) and derived gefitinib-resistant line (purple: HCCGR) in response to increasing doses of olaparib (72h). Data points represent mean  $\pm$  standard

error based on 3 biological repeats. B) Representative images of EGFR TKI sensitive and -resistant cell lines treated with 10 $\mu$ M olaparib and stained for  $\gamma$ H2AX foci 24h after starting treatment. C) Tail moment of untreated EGFR TKI-sensitive and -resistant cells as measured by alkaline comet assay. Increase in Tail Moment indicates significantly more DNA SSB/DSB in the TKI-resistant cell line. Bars represent mean  $\pm$  standard error based on 3 biological repeats.

## **4. DISCUSSION**

The dire statistics of lung cancer pose the need for improved therapy. In this work we focused on EGFR-mutant lung cancers and studied their ability to repair treatment inflicted DNA damage.

The key insights are the following:

EGFR-mutant cells show a FA-like DNA repair defect, which accounts for their increased sensitivity to ICL-inducing agents. The precise nature of the DNA repair defect renders EGFR-mutant cells defective in HRR, which can be exploited by targeted therapy with PARP inhibitors.

Investigating the influence of EGFR TKI resistance on sensitivity to DNA damaging agents in EGFR-mutant lung cancer cells, we found no adverse effect on sensitivity, in fact TKI resistance may have a sensitizing effect on treatment with radiation or PARP inhibitors.

### **4.1. Cells with mutant EGFR show impaired ICL repair and a FA-like phenotype**

We started out confirming the clinical observation of increased sensitivity to platinum-based chemotherapy in EGFR-mutant lung cancers [7] [8] [9]. In a panel of 9 human lung cancer cell lines, we saw decreased clonogenic survival in EGFR-mutant cell lines compared to EGFR wt cells when treated with cisplatin (Figure 1 A+B). Cisplatin causes different types of damage to the cell, but its toxicity is thought to be derived from detrimental DNA ICL [38]. In addition to cisplatin, EGFR-mutant lung cancer cell lines compared to EGFR wt cells show decreased clonogenic survival upon treatment with MMC, another crosslinking agent (Figure 1C). Even though there is a trend that EGFR-mutant cells are more sensitive to crosslinking agents, it should be noted that there is overlap in sensitivity between mutant and wild-type EGFR populations. Conceivably different genetic context between cell lines may dilute or emphasize the sensitizing effect of mutant EGFR to ICL-inducing drugs.

In an isogenic cell pair, we eliminated heterogenic background to tease out the sensitizing effect of mutant EGFR to ICL damage. We show that EGFR wild-type or mutant isogenic cell lines are sensitized to both cisplatin and MMC, if harboring

mutant EGFR (Figure 2). We acknowledge the sensitizing effect may be relatively small in vitro, however it seems to be clinically relevant, given that lung cancer patients with mutant EGFR respond better to platinum-based therapy [7] [8] [9].

Next we show that the increased sensitivity to cisplatin in EGFR-mutant cell lines may be due to unrepaired DNA damage. EGFR-mutant cells contain increased levels of DNA damage marked as  $\gamma$ H2AX foci when treated with cisplatin.  $\gamma$ H2AX foci levels further correlate with sensitivity to cisplatin (Figure 3).

$\gamma$ H2AX foci have long been established as a DNA damage marker and are most often used as an indicator for DNA DSB. Furthermore,  $\gamma$ H2AX foci are induced by ICL and foci associate with HRR factors required for ICL repair [92] [93] [94] [95] [96] [97] [98]. In the case of ICL damage,  $\gamma$ H2AX foci may be induced independent of DSB formation associated with ICL repair. Thus persisting  $\gamma$ H2AX foci may indicate remaining ICL as well as DSB resulting from unhooked ICL [92].  $\gamma$ H2AX is a very sensitive marker for detecting DNA damage associated with ICL-inducing agents. It is 6-10x more sensitive than the modified alkaline comet assay, which is another method to detect ICL [92].  $\gamma$ H2AX foci persist in cells defective in ICL unhooking (ERCC1 defective) or defective in HRR (XRCC3 defective) [92]. Persistence of  $\gamma$ H2AX foci correlates with prolonged ICL-unhooking and with increased sensitivity to the ICL-inducing drug (Figure 3) [92] [6].

ICL are repaired by the Fanconi Anemia pathway and subsequent HRR. Cells defective in the Fanconi Anemia pathway are impaired in repairing ICL and show specific phenotypic hallmarks such as increased sensitivity to ICL inducing drugs, damage induced chromosomal radials, as well as pronounced G2/M cell cycle arrest when challenged with crosslinking agents [57] [99].

We found EGFR-mutant cell lines to be positive for all three of these hallmarks indicating a defect in the FA pathway. EGFR-mutant cell lines arrest in G2/M cell cycle phase similarly to the FANCD2 deficient control cell line (Figure 4). Pronounced MMC-induced chromosomal radial formations can be observed in EGFR-mutant cells (Figure 5). Such an increase in aberrations can be caused by mutations of FANCD2, which we used as an assay control [84] [73]. We show increased sensitivity to ICL inducing drugs above, which has been previously

implicated with genetic or epigenetic defects in the FA pathway, such as mutations in FANCD2 sensitize to cisplatin and MMC [100] [36] [84] [101] [73] [44].

These results associate mutant EGFR with defective ICL repair resulting in hallmarks of FA defective cells, prolonged ICL damage visible by  $\gamma$ H2AX foci and increased sensitivity to ICL inducing drugs. These findings indicate a defect within the FA/HRR pathway.

## **4.2. Defect in FA/HRR pathway is independent of EGFR-mutant kinase function**

As the key player in HRR, RAD51 foci formation has been established as a biomarker for the integrity of this pathway [51] [52] [53] [6] [36]. After inducing ICL the FA pathway is activated followed by HRR. Intact RAD51 foci formation therefore reveals integrity of upstream events [38]. Thus we used RAD51 foci formation as a marker for proficiency of ICL repair. EGFR-mutant cells had reduced ability to form RAD51 foci when challenged with cisplatin and low foci levels correlated with sensitivity to cisplatin (Figure 7).

Interestingly, the RAD51 foci defect seen in EGFR-mutant cells is specific for ICL damage (Figure 9). EGFR-mutant cells are perfectly able to form RAD51 foci when challenged with IR. Unlike cisplatin, IR introduces DNA DSB and other DNA damage, but not ICL. ICL need to be unhooked via the FA-pathway before HRR can occur [40] [42]. EGFR-mutant cells show impaired RAD51 foci formation after treatment with cisplatin, but not with IR. Thus, when exposed to IR, which does not cause ICL, EGFR-mutant cells are able to form RAD51 foci. This indicates that there is no general RAD51 foci defect. Rather the repair defect in EGFR-mutant cells treated with a crosslinking agent needs to be upstream of RAD51 foci formation. A defect in the FA pathway upstream of HRR has been previously shown to lead to a RAD51 foci defect and we confirm this phenomenon (Figure 7D) [102] [69]. We therefore suspected EGFR-mutant cells harbor a repair defect in the FA-pathway upstream of RAD51 foci formation.

How does EGFR impair the FA/HRR pathway? Mutant EGFR downstream signaling is overactive and AKT among others is constitutively activated [5]. AKT has been reported to suppress HRR [80]. Thus overactive EGFR signaling may have an adverse effect on HRR. However, we did not see rescue of RAD51 foci formation in response to cisplatin when we inhibited EGFR signaling with an EGFR inhibitor or PI3K/AKT inhibitor (Figure 12). Furthermore inhibiting EGFR signaling in an EGFR wild-type cell line had no effect on cisplatin-induced RAD51 foci levels (Figure 13D). Thus EGFR signaling does not seem to influence the FA/HRR pathway.

Wild-type EGFR, but not the mutant receptor, has been shown to translocate to the nucleus, where it may activate transcription genes [103] [20]. It has been further suggested, that wild-type EGFR may increase DNA-PKcs activity in the nucleus. DNA-PK plays an important role in DSB repair through NHEJ, an alternative DSB repair pathway to HRR [20] [104]. DSB are an intermediate structure in ICL repair; it is therefore thought that NHEJ and HRR “compete” for the repair of these intermediates. It has been previously shown that EGFR-mutant cells are sensitized to IR and cisplatin [20]. This sensitization was attributed to an inability of mutant EGFR to translocate to the nucleus and thus reduced DNA-PK activity [20].

We tested this notion and confirmed that mutant EGFR does not translocate to the nucleus when challenged with cisplatin. We did observe some translocation of wild-type EGFR (Figure 10). However, such few cells contained the receptor in response to cisplatin that it is unlikely that EGFR nuclear translocation could cause the difference in sensitivity to cisplatin.

We further were not convinced that inability of EGFR-mutant cells to increase DNA-PK activity in the nucleus should account for sensitization to cisplatin, as previously claimed [20]. If this was the case, cells containing wild-type EGFR should be sensitized to cisplatin by inhibition of DNA-PK. However in our hands we show that there is no sensitization by DNA-PK inhibition to cisplatin in wild-type EGFR cells (Figure 11). In cells expressing mutant EGFR, DNA-PK inhibition may even increase resistance to cisplatin very slightly. We concluded from our results that loss of DNA-PK activity does not sensitize to ICL in either mutant or wild-type EGFR cell lines.

Increased DNA-PK activity previously seen in wild-type EGFR cells may account for IR resistance, but ICL repair differs greatly from repair of IR induced DNA damage [20] [105]. Supporting our results, increased DNA-PK activity has previously been shown to have an adverse effect on ICL-repair: DNA-PK is a key player in DSB repair by NHEJ, which is an error-prone alternative to HRR for DSB repair [104] [106] [38]. NHEJ is not required for ICL-repair [38] [107] [108]. It is believed to compete with HRR for the repair of DSB, occurring as intermediates in ICL-repair. The FA-pathway channels repair into high-fidelity HRR by inhibiting NHEJ [104] [38]. Thus FA deficiency leads to chromosomal radials and ICL sensitivity presumably through the lack of inhibition of NHEJ. Underscoring this idea are findings that inhibition of NHEJ in a FA deficient background reverses toxicity of ICL-inducing drugs [104] [109] [110] [38].

We discarded EGFR signaling, EGFR translocation, and EGFR's influence on DNA-PK activity as possible mechanisms for impairing the FA/HRR pathway. Surprisingly, overexpression of wild-type EGFR in a mutant EGFR cell line was able to rescue RAD51 foci in response to cisplatin (Figure 13). We concluded from these data that wild-type EGFR is capable of overriding the adverse effect of mutant EGFR on the FA/HRR pathway, resulting in rescue of RAD51 foci formation after treatment with cisplatin.

Furthermore EGFR silencing, but not kinase inhibition, triggered an "EGFR-mutant phenotype" in an EGFR wild-type cell line, as cisplatin-induced RAD51 foci levels were markedly reduced (Figure 13D).

Thus we concluded the repair defect is not genetically fixed. Wild-type EGFR may play a role in ICL repair, which is inhibited by mutant EGFR in a dominant negative fashion. Only when overexpressed can wild-type EGFR compete away the mutant version, resume its role in ICL repair and thus rescue RAD51 foci (see model). Since we have already studied EGFR signaling and nuclear translocation, future research could be done on EGFR dimerization. EGFR is known to form homo- or heterodimers with HER2 [15] [16]. It is conceivable that there may be differences in dimerization preference between the mutant and the wild-type receptor. It could be envisioned that distinct dimerization patterns may have different effects on cellular processes and possibly DNA repair. Thus, in a next step I would like to suggest performing immunoprecipitation of EGFR and HER2

to assess any differences in dimerization preferences between mutant and wild-type EGFR.

### **4.3. EGFR-mutant cells show reduced FAN1 recruitment and impaired ICL unhooking**

We confirmed our hypothesis of a defect within and not in parallel to the FA pathway by showing epistasis between mutant EGFR and disruption of the FA pathway by FANCD2 mutation (Figure 14). No matter whether cells had either or both mutations, after treatment with MMC we observed similar DNA damage levels, as measured by  $\gamma$ H2AX foci.

Narrowing down the defect, we concluded it to be downstream of the core complex, BRCA1 and FANCD2, since EGFR-mutant cells are proficient in forming both BRCA1 and FANCD2 foci in response to ICL-inducing drugs (Figure 16 + 17). Early in ICL repair BRCA1 promotes chromatin loading of FANCD2-Ub [42]. Later it promotes RAD51 loading [42]. FANCD2 foci on the other hand appear downstream of the core complex and are abrogated if the core complex is not intact [42]. To further strengthen intact FANCD2 function in EGFR-mutant cells, mono-ubiquitination of FANCD2 in response to cisplatin treatment could be checked by western blotting. In fact this experiment has been done in the meantime by my colleague Liliana Gheorghiu, and proper mono-ubiquitination of FANCD2 in cisplatin treated EGFR-mutant cells was confirmed [111].

We found the repair defect in EGFR-mutant cells to be at the stage of ICL unhooking (Figure 18). ICL can be indirectly quantified by a modified alkaline comet assay [20] [85] [86]. To further characterize this ICL unhooking defect we investigated the nucleases involved in the ICL unhooking step [40] [42]. EGFR-mutant NSCLC have previously been shown to contain low ERCC1 expression [112]. However, we do not see this in our cell lines (Figure 19). We did however observe low FAN1 expression (Figure 19 + 20). EGFR-mutant cells were further impaired to form FAN1 foci in response to ICL-inducing drugs (Figure 21). From these data we concluded that mutant EGFR is associated with reduced ability to

recruit FAN1 and impaired ICL unhooking, leading to defective ICL repair and increased sensitivity to ICL-inducing drugs.

Supporting this model are findings that silencing of FAN1 leads to persistence of  $\gamma$ H2AX foci and increased chromosomal radials similar to FANCD2 depleted cells in response to cisplatin [59]. FAN1 is not required for ubiquitination of FANCD2 or FANCI, thus FANCD2 foci are intact [59]. Additionally, FAN1 is not required for resection of DSB or RPA foci formation; in fact an increase in RPA foci may be observed [59]. We could detect the same phenomena in EGFR-mutant cells as described above. Furthermore the downstream RAD51 foci defect, which we observe in EGFR-mutant cells, is consistent with an unhooking defect or a defect within the FA pathway. Mutated FANCD2 leads to an abrogation of RAD51 foci (Figure 7D) [102] [113] [69]. Also, ICL unhooking and DSB resection is needed to create the 3' overhangs, which is the substrate for HRR and RAD51 foci formation [40] [114].

Yet lack of FAN1 recruitment may not be entirely responsible for failed ICL unhooking. Other nucleases involved in ICL-unhooking are XPF-ERCC1, MUS81-EME1 and SLX1 [40] [42]. SLX4/FANCP is responsible for recruiting those nucleases [40] [42]. Interestingly, others have reported RAD51 foci to be intact after depletion of either FAN1 or SLX4/FANCP [59]. Conceivably additional nucleases may be malfunctioning in EGFR-mutant cells. We see diminished RAD51 foci formation in EGFR-mutant cells, which suggests both FAN1 and SLX4/FANCP function may be disrupted. It would be interesting to study SLX4 foci formation in EGFR-mutant cells treated with cisplatin. In the meantime Mrs. Gheorghiu has been examining this, however so far, available SLX4 antibodies have not yielded results with adequate quality for publication. To circumvent the problem of poor SLX4 antibody one could transfect tagged SLX4/FANCP to study foci formation in wild-type versus mutant EGFR cells treated with cisplatin.

Assuming impaired function of several endonucleases, the question remains: how could mutant EGFR disrupt their recruitment? Ubiquitinated FANCD2 is responsible for delivering FAN1 and SLX4/FANCP to the site of damage [42]. It could be speculated that wild-type EGFR promotes the recruitment of these endonucleases by FANCD2 and this promoting role would be disrupted by the mutant version. We have already shown mutant EGFR to be able to impair FAN1

foci formation. In order to elucidate any influence of EGFR on direct interactions between ubiquitinated FANCD2 and FAN1 and/or SLX4/FANCP, immunoprecipitation of FANCD2 and FAN1 or SLX4/FANCP should shed light on possible differences in complex formation in wild-type and mutant EGFR cells.

#### **4.4. DNA repair defect in EGFR-mutant cells is exploitable with PARP inhibitors**

We aimed to exploit the DNA repair defect found in EGFR-mutant cells for targeted therapy. PARP inhibitors are a new group of targeted drugs, which exploit HRR defects [3]. They are currently tested for the treatment of HRR defective breast, ovarian and prostate cancer patients [61]. It has been previously reported that not only HRR defects but also impairments in the FA pathway sensitize to PARP inhibitors [65]. In addition, FAN1 seems to have a dual role in ICL unhooking and late stage HRR, where it may be involved in resolving Holliday junctions (Figure 23A) [58] [59] [60].

We hypothesized EGFR-mutant cells to harbor a general defect in FAN1 recruitment to sites of DNA damage. This would compromise not only ICL unhooking, but also late stage HRR, thus leading to sensitivity to PARP inhibitors.

Supporting the first part of our hypothesis we confirmed EGFR-mutant cells to be generally impaired in recruiting FAN1, which we concluded from their reduced ability to form FAN1 foci in response to the PARP inhibitor olaparib (Figure 22).

To investigate compromised HRR, we used RAD51 foci formation as a marker for any alterations of HRR in EGFR-mutant cells treated with olaparib (Figure 23). We observed intact RAD51 foci induction, but RAD51 foci persist at a later time point. We interpreted these results as follows: PARP inhibitor treatment results in unrepaired DNA SSB [65] [66]. SSB become DSB during DNA replication and require HRR for reliable repair [65] [66] [3]. Recall that EGFR-mutant cells are impaired in ICL unhooking, yet here there is no need to unhook any ICL to form DSB, which are the substrate for RAD51 loading. Thus, with DSB present after

PARP inhibitor treatment, RAD51 protein can be loaded onto DNA strands at DSB resulting in RAD51 foci formation in EGFR-mutant cells. Holliday junctions, which are late stage HRR structures, contain RAD51 protein filaments, which disassemble when the Holliday junction (HJ) is resolved [115] [116]. Persisting RAD51 foci have been previously established as a marker for unresolved HJ [115] [116]. Prolonged RAD51 foci formation in EGFR-mutant cells, as we have seen, may thus point to an inability to resolve Holliday junctions in response to olaparib. We further found that FANCD2 mutant cells, like EGFR-mutant ones, show persisting RAD51 foci after olaparib. FANCD2 is responsible for the recruitment of endonucleases, such as FAN1, to ICL and presumably to HJ as well [40] [42]. Therefore these data support our notion that RAD51 persistence and possibly unresolved HJ may be due to reduced presence of FANCD2-dependent endonucleases, such as FAN1, at the site of damage.

Again FAN1 may not be the only culprit for impairing late stage HRR and sensitization to PARP inhibitors. Like ICL unhooking, there are several nucleases involved in resolving HJ: BLM, MUS81-EME1, ID-complex, SLX4/FANCP-SLX1 complex, GEN1, and RAD51C/FANCO [56] [40] [42]. Similarly future research could investigate impaired recruitment of these nucleases by analyzing foci or, if that proves technically difficult, tagging the nuclease of interest.

What is the link between mutant EGFR and a replication-fork specific DNA repair defect? Here we can only speculate. Mutant EGFR has been previously associated with altered FA/BRCA function. EGFR-mutant lung cancers have been described in patients with BRCA germline mutations [117]. Furthermore increased EGFR expression has been reported in BRCA1 mutant breast cancers [118]. Mutated EGFR has oncogenic properties, such as increased proliferation [5]. It is tempting to suggest that mutated EGFR causes replication fork stress through increased proliferation in pre-cancerous cells. This could lead to mutations and malignant transformation in cells defective in replication-fork specific DNA repair and thus mutant EGFR would ultimately select for cells with defects in the FA/HRR pathway.

Finally, defective repair in EGFR-mutant cells treated with olaparib does indeed lead to increased sensitivity to the drug in vitro and in vivo. This is evident by

decreased clonogenic survival and increased DNA damage levels in EGFR-mutant cell lines challenged with olaparib (Figure 24 + 25). Similar to crosslinker sensitivity, not all EGFR-mutant cell lines show striking sensitivity to olaparib. As discussed above differences in genetic context might exacerbate or compensate for the repair defect associated with mutant EGFR. A clinical trial could determine the potential clinical significance of the association between olaparib sensitivity and EGFR mutation status.

In vivo, lung cancer tissue obtained from patients harboring mutant or wild-type EGFR shows significantly more DNA damage in the mutant tissue compared to the wild-type control tissue, when treated with olaparib (Figure 26). The ex-vivo foci method had been previously validated [6] [119]. We need to acknowledge that the patient sample of two is small. Ideally, follow up experiments would include mutant (e.g. PC9) and wild-type (e.g. A549) EGFR xenografts to further strengthen the difference in sensitivity to olaparib in vivo. Nevertheless these results show a trend and may raise hopes for some EGFR-mutant lung cancer patients to be able to benefit from targeted treatment with PARP inhibitors.

#### **4.5. DNA damaging treatments: No adverse influence of EGFR TKI resistance on sensitivity**

A secondary aim of this thesis project was to investigate any influence of resistance development to first line treatment with EGFR inhibitors on sensitivity to DNA damaging treatments, such as IR, cisplatin or olaparib.

We found no significant change in clonogenic survival between TKI sensitive and resistant EGFR-mutant lung cancer cell lines when treated with cisplatin (Figure 27B).

EGFR TKI resistance may have a sensitizing effect to IR, since clonogenic survival decreased and more apoptosis was seen in at least one EGFR-mutant cell line with acquired TKI resistance (Figure 28).

Strikingly EGFR TKI resistance had a pronounced sensitizing effect on treatment with olaparib, as evident by decreased clonogenic survival and increased levels of DNA damage indicated by  $\gamma$ H2AX foci in EGFR TKI resistant cell lines compared to sensitive ones when treated with olaparib (Figure 29B). While the difference in  $\gamma$ H2AX foci levels between EGFR TKI resistant and sensitive cell lines can be seen by eye, future experiments should further quantify that.

What could be the reason for increased sensitivity of EGFR TKI resistant cells to PARP inhibition? PARP is involved in SSB repair, which become DSB during S-phase, when PARP is inhibited [120] [3]. The more SSB are present endogenously the more can become DSB during S-phase, which require HRR for repair. Yet, as we have shown in this work, EGFR-mutants are defective in that pathway. The increase in sensitivity to olaparib seen in EGFR TKI resistant cells compared to TKI sensitive ones may therefore be due to more endogenous SSB. Utilizing an alkaline comet assay we did indeed observe more DNA breaks in EGFR TKI resistant cells (Figure 29C). It should be noted that with this assay both SSB and DSB are captured [121]. In future experiments one could single out the amount of SSB by performing an alkaline and neutral comet assay in parallel. The neutral comet assay measures DSB only [122]. Subtracting the amount of breaks found in the neutral assay from those yielded by the alkaline assay results in the amount of SSB.

What may be the connection between EGFR and increased amount of SSB in EGFR TKI resistant cells? It has been shown that, EGFR inhibition can cause oxidative stress [123] [124]. Oxidative stress can result in increased DNA damage including DNA SSB [120] [3]. EGFR TKI resistant cells are continuously cultured in the presence of EGFR inhibitor, which could be responsible for introducing SSB due to more oxidative stress. Assessing differences in oxidative stress among EGFR TKI resistant and sensitive cell lines, for example by measuring intracellular

reactive oxygen species (ROS), could be a valuable future experiment to further investigate this idea.

#### **4.6. Implications of findings for the clinic:**

The results of our study could be useful for making treatment choices in the clinic. It is of great interest to identify patients who may benefit from targeted therapy. Yet herein lays the difficulty. We acknowledge that EGFR mutation alone may not be a perfect biomarker for sensitivity to olaparib. Not all of our cell lines showed increased sensitivity to the drug, thus some may have evolved mechanisms to compensate for the DNA repair defect. Therefore one could perform a biopsy on lung cancer patients with mutant EGFR and utilize our ex-vivo foci assay to identify tumors with increased sensitivity to PARP inhibitor. Those patients should benefit from treatment with PARP inhibitors alone or in combination with a platinum-based chemotherapeutic. This would be a very interesting clinical study – one that we hope to see succeeding in the future.

# **5. SUMMARY**

## 5.1. Summary of findings

Lung cancer is the leading cause of cancer deaths, emphasizing the need for better treatments. In patients with EGFR-mutant NSCLC, increased responses to platinum-based chemotherapies have been seen, compared to EGFR wild-type cancers. However, the mechanisms underlying this association have remained elusive. Here, we confirmed in a panel of 9 lung cancer cell lines, that mutant EGFR was associated with a range of cisplatin sensitivities, with the most sensitive cell line displaying a more than 35-fold lower survival fraction than EGFR wild-type lines (for 16  $\mu$ M cisplatin).

Cisplatin sensitivity can be associated with defects in the Fanconi Anemia (FA) pathway, which functions in the detection and repair of DNA ICL at stalled replication forks. Strikingly, EGFR-mutant cells displayed the hallmarks of the FA phenotype, namely increased cell kill, damage-induced G2 cell-cycle arrest, and chromosomal radial formation in response to ICL introduced by mitomycin C.

In ICL repair the FA pathway produces DSB intermediates, which are subsequently repaired by HRR. RAD51 is the key mediator in HRR. EGFR-mutant cells exhibited an impaired RAD51 foci response specifically after ICL induction. Impaired RAD51 foci formation in EGFR-mutant cells was resistant to inhibition of EGFR downstream signaling, implying a kinase-independent regulation of HRR. Supporting this notion, overexpression of wild-type EGFR in EGFR-mutant cells was able to rescue RAD51 foci formation, while siRNA-mediated depletion of wild-type EGFR, but not kinase inhibition suppressed RAD51 foci.

The effect of EGFR mutation was epistatic with a defective FA pathway caused by mutated FANCD2, as the presence of either or both of these mutations resulted in virtually identical DNA damage levels. We identified a defect downstream of FANCD2 at the level of recruitment of the FAN1 nuclease and ICL unhooking.

FAN1 has a putative dual role in unhooking ICL and in resolving HJ late in HRR. HRR defects can be exploited by targeted treatment with PARP inhibitors. Indeed, in response to the PARP inhibitor olaparib, FAN1 foci failed to form in EGFR-mutant cells compared to wild-type cells (13% versus 29%). Interestingly RAD51 foci formed initially normally in EGFR-mutant cells, suggesting that the RAD51 foci defect seen after ICL induction was due to a lack of DNA substrate secondary to

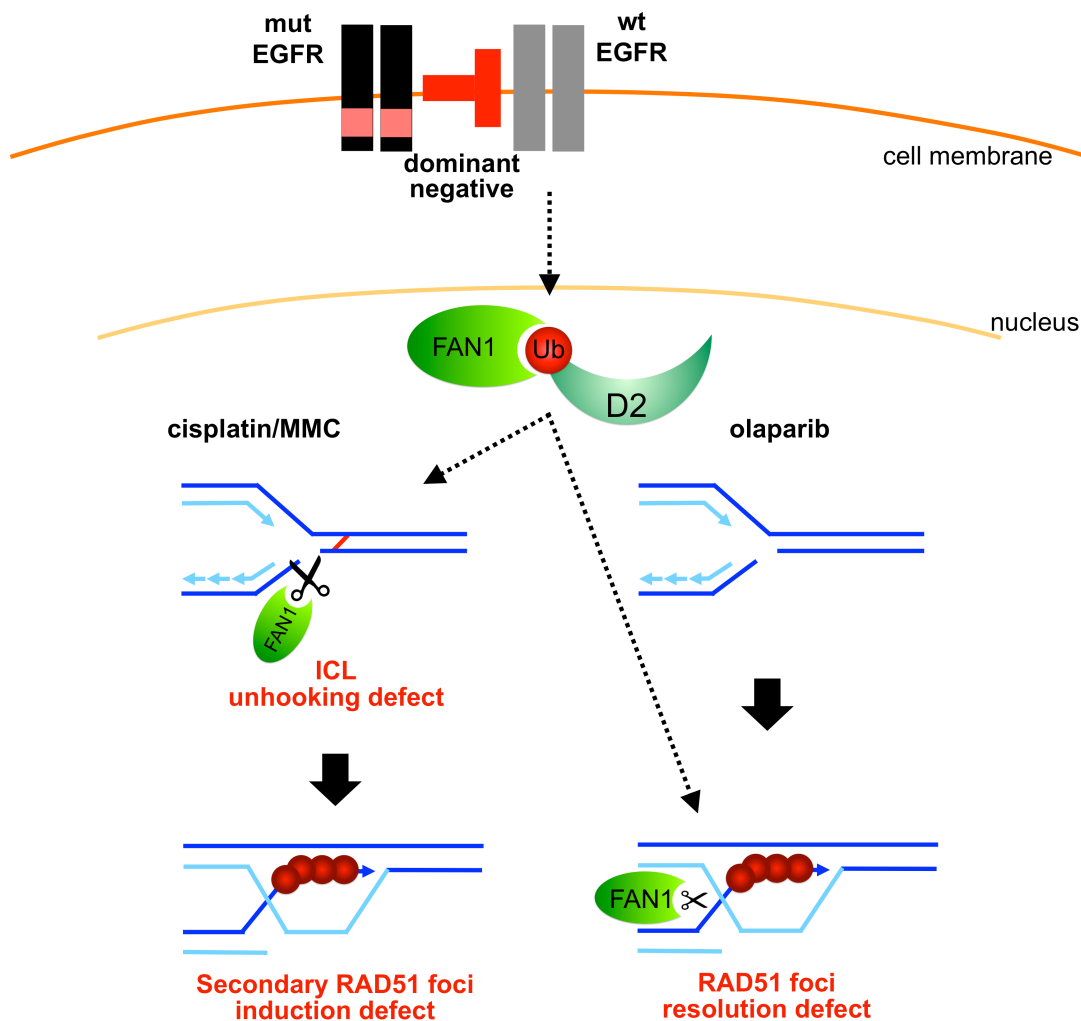
failed ICL incision. However, RAD51 foci persisted >24 hours (25.6% vs 5.1%) in EGFR-mutant cells, indicating an inability to complete HRR.

EGFR-mutant lung cancer cell lines demonstrated reduced clonogenic survival after olaparib treatment, with IC50 values < 6  $\mu$ M for 8/9 cell lines, compared to > 6  $\mu$ M for all EGFR wild-type cell lines. Consistent with this phenotype, we observed increased DNA damage levels in biopsy material from EGFR-mutant NSCLC treated with olaparib ex-vivo compared to wild-type tumor, i.e., 21% vs 4% cells with  $\gamma$ H2AX foci ( $p=0.03$ ).

In conclusion, we describe an EGFR kinase-independent disruption of the FA pathway downstream of FANCD2 in EGFR-mutant cells, which impairs ICL unhooking or completion of HRR in response to cisplatin or olaparib treatment, respectively. EGFR-mutant lung cancer patients thus may benefit from treatment with PARP inhibitors.

In a secondary aim we show that acquired resistance in EGFR-mutant cell lines to first line therapy with EGFR inhibitor may not have adverse effects on sensitivity to DNA damaging treatments, such as IR, cisplatin or olaparib.

## 5.2. Model



Wild-type EGFR promotes DNA repair. It may be involved in the recruitment of FAN1, and possibly other nucleases, by FANCD2 to the site of DNA damage. Mutant EGFR disrupts this function in a dominant negative fashion leading to impaired recruitment of FAN1 and possibly other nucleases to the site of damage.

In case of crosslinker damage, this results in failed ICL unhooking and blocked HRR, as indicated by a secondary RAD51 foci defect.

On the other hand in PARP inhibitor treated cells lack of FAN1 and other nucleases leads to unresolved Holliday junctions and persisting RAD51 foci.

Unrepaired DNA damage leads to cell death and thus increased sensitivity to crosslinking agents, as well as PARP inhibitors seen in EGFR-mutant cells.

## **6. REFERENCES**

1. American Cancer Society, *Cancer Facts & Figures 2013*. Atlanta: American Cancer Society, 2013.
2. Kaatsch, P., et al., *Krebs in Deutschland 2007/2008*. 8. Ausgabe ed2012: Robert Koch-Institut und die Gesellschaft der epidemiologischen Krebsregister in Deutschland e.V. .
3. Lord, C.J. and A. Ashworth, *The DNA damage response and cancer therapy*. Nature, 2012. **481**(7381): p. 287-94.
4. Lynch, T.J., et al., *Activating Mutations in the Epidermal Growth Factor Receptor Underlying Responsiveness of Non-Small-Cell Lung Cancer to Gefitinib*. New England Journal of Medicine, 2004. **350**(21): p. 2129-2139.
5. Sharma, S.V. and J. Settleman, *ErbBs in lung cancer*. Experimental Cell Research, 2009. **315**(4): p. 557-71.
6. Birkelbach, M., et al., *Detection of impaired homologous recombination repair in NSCLC cells and tissues*. J Thorac Oncol, 2013. **8**(3): p. 279-86.
7. Eberhard, D.A., et al., *Mutations in the Epidermal Growth Factor Receptor and in KRAS Are Predictive and Prognostic Indicators in Patients With Non-Small-Cell Lung Cancer Treated With Chemotherapy Alone and in Combination With Erlotinib*. Journal of Clinical Oncology, 2005. **23**(25): p. 5900-5909.
8. Mok, T.S., et al., *Gefitinib or carboplatin-paclitaxel in pulmonary adenocarcinoma*. The New England journal of medicine, 2009. **361**(10): p. 947-57.
9. Janne, P.A., et al., *Randomized phase II trial of erlotinib alone or with carboplatin and paclitaxel in patients who were never or light former smokers with advanced lung adenocarcinoma: CALGB 30406 trial*. Journal of clinical oncology : official journal of the American Society of Clinical Oncology, 2012. **30**(17): p. 2063-9.
10. Taylor, R., F. Najafi, and A. Dobson, *Meta-analysis of studies of passive smoking and lung cancer: effects of study type and continent*. International Journal of Epidemiology, 2007. **36**(5): p. 1048-1059.
11. Oxnard, G.R., et al., *Screening for germline EGFR T790M mutations through lung cancer genotyping*. J Thorac Oncol, 2012. **7**(6): p. 1049-52.
12. Ohashi, K., et al., *Epidermal growth factor receptor tyrosine kinase inhibitor-resistant disease*. Journal of clinical oncology : official journal of the American Society of Clinical Oncology, 2013. **31**(8): p. 1070-80.
13. Lee, Y.J., et al., *Lung cancer in never smokers: change of a mindset in the molecular era*. Lung cancer, 2011. **72**(1): p. 9-15.
14. Siegel, R., et al., *Cancer statistics, 2011: the impact of eliminating socioeconomic and racial disparities on premature cancer deaths*. CA: a cancer journal for clinicians, 2011. **61**(4): p. 212-36.
15. Nyati, M.K., et al., *Integration of EGFR inhibitors with radiochemotherapy*. Nature reviews. Cancer, 2006. **6**(11): p. 876-85.
16. Herbst, R.S., *Review of epidermal growth factor receptor biology*. International journal of radiation oncology, biology, physics, 2004. **59**(2 Suppl): p. 21-6.
17. Szumiel, I., *Epidermal growth factor receptor and DNA double strand break repair: the cell's self-defence*. Cellular signaling, 2006. **18**(10): p. 1537-48.
18. Dittmann, K., et al., *Radiation-induced epidermal growth factor receptor nuclear import is linked to activation of DNA-dependent protein kinase*. The Journal of biological chemistry, 2005. **280**(35): p. 31182-9.
19. Dittmann, K., C. Mayer, and H.P. Rodemann, *Inhibition of radiation-induced EGFR nuclear import by C225 (Cetuximab) suppresses DNA-PK activity*. Radiotherapy and oncology : journal of the European Society for Therapeutic Radiology and Oncology, 2005. **76**(2): p. 157-61.

20. Liccardi, G., J.A. Hartley, and D. Hochhauser, *EGFR nuclear translocation modulates DNA repair following cisplatin and ionizing radiation treatment*. *Cancer Research*, 2011. **71**(3): p. 1103-14.
21. Asahina, H., et al., *A phase II trial of gefitinib as first-line therapy for advanced non-small cell lung cancer with epidermal growth factor receptor mutations*. *British Journal of Cancer*, 2006. **95**(8): p. 998-1004.
22. Inoue, A., et al., *Prospective phase II study of gefitinib for chemotherapy-naive patients with advanced non-small-cell lung cancer with epidermal growth factor receptor gene mutations*. *Journal of clinical oncology : official journal of the American Society of Clinical Oncology*, 2006. **24**(21): p. 3340-6.
23. Costa, D.B. and S. Kobayashi, *Are exon 19 deletions and L858R EGFR mutations in non-small-cell lung cancer clinically different?* *British Journal of Cancer*, 2007. **96**(2): p. 399; author reply 400.
24. Sharma, S.V., et al., *"Oncogenic shock": explaining oncogene addiction through differential signal attenuation*. *Clinical cancer research : an official journal of the American Association for Cancer Research*, 2006. **12**(14 Pt 2): p. 4392s-4395s.
25. Weinstein, I.B., et al., *Disorders in cell circuitry associated with multistage carcinogenesis: exploitable targets for cancer prevention and therapy*. *Clinical cancer research : an official journal of the American Association for Cancer Research*, 1997. **3**(12 Pt 2): p. 2696-702.
26. Weinstein, I.B., *Disorders in cell circuitry during multistage carcinogenesis: the role of homeostasis*. *Carcinogenesis*, 2000. **21**(5): p. 857-64.
27. Weinstein, I.B., *Cancer. Addiction to oncogenes--the Achilles heel of cancer*. *Science*, 2002. **297**(5578): p. 63-4.
28. Sequist, L.V., et al., *Genotypic and histological evolution of lung cancers acquiring resistance to EGFR inhibitors*. *Science translational medicine*, 2011. **3**(75): p. 75ra26.
29. Kobayashi, S., et al., *EGFR mutation and resistance of non-small-cell lung cancer to gefitinib*. *The New England journal of medicine*, 2005. **352**(8): p. 786-92.
30. Ou, S.-H.I., *Second-generation irreversible epidermal growth factor receptor (EGFR) tyrosine kinase inhibitors (TKI): A better mousetrap? A review of the clinical evidence*. *Critical Reviews in Oncology/Hematology*, 2012. **83**(3): p. 407-421.
31. Chen, Y.M., *Update of epidermal growth factor receptor-tyrosine kinase inhibitors in non-small-cell lung cancer*. *J Chin Med Assoc*, 2013. **76**(5): p. 249-57.
32. Yang, J.C., et al., *Afatinib for patients with lung adenocarcinoma and epidermal growth factor receptor mutations (LUX-Lung 2): a phase 2 trial*. *The Lancet Oncology*, 2012. **13**(5): p. 539-48.
33. Miller, V.A., et al., *Afatinib versus placebo for patients with advanced, metastatic non-small-cell lung cancer after failure of erlotinib, gefitinib, or both, and one or two lines of chemotherapy (LUX-Lung 1): a phase 2b/3 randomised trial*. *The Lancet Oncology*, 2012. **13**(5): p. 528-38.
34. Engelman, J.A., et al., *MET Amplification Leads to Gefitinib Resistance in Lung Cancer by Activating ERBB3 Signaling*. *Science*, 2007. **316**(5827): p. 1039-1043.
35. Godin-Heymann, N., et al., *The T790M "gatekeeper" mutation in EGFR mediates resistance to low concentrations of an irreversible EGFR inhibitor*. *Molecular Cancer Therapeutics*, 2008. **7**(4): p. 874-9.
36. Willers, H., H.N. Pfäffle, and L. Zou, *Targeting Homologous Recombination Repair in Cancer*, in *DNA Repair in Cancer Therapy: Molecular Targets and*

- Clinical Applications*, M.R. Kelley, Editor 2011, Academic Press, Elsevier. p. 119-160.
37. Kelland, L., *The resurgence of platinum-based cancer chemotherapy*. *Nature Reviews Cancer*, 2007. **7**(8): p. 573-584.
  38. Deans, A.J. and S.C. West, *DNA interstrand crosslink repair and cancer*. *Nature Reviews Cancer*, 2011. **11**(7): p. 467-480.
  39. Hurley, L.H., *DNA and its associated processes as targets for cancer therapy*. *Nature reviews. Cancer*, 2002. **2**(3): p. 188-200.
  40. Kottemann, M.C. and A. Smogorzewska, *Fanconi anaemia and the repair of Watson and Crick DNA crosslinks*. *Nature*, 2013. **493**(7432): p. 356-363.
  41. Long, D.T., et al., *Mechanism of RAD51-dependent DNA interstrand cross-link repair*. *Science*, 2011. **333**(6038): p. 84-7.
  42. Kim, H. and A.D. D'Andrea, *Regulation of DNA cross-link repair by the Fanconi anemia/BRCA pathway*. *Genes & Development*, 2012. **26**(13): p. 1393-1408.
  43. Garcia-Higuera, I., et al., *Interaction of the Fanconi anemia proteins and BRCA1 in a common pathway*. *Molecular Cell*, 2001. **7**(2): p. 249-62.
  44. Kachnic, L.A., et al., *Fanconi anemia pathway heterogeneity revealed by cisplatin and oxaliplatin treatments*. *Cancer Letters*, 2010. **292**(1): p. 73-9.
  45. Kratz, K., et al., *Deficiency of FANCD2-associated nuclease KIAA1018/FANL sensitizes cells to interstrand crosslinking agents*. *Cell*, 2010. **142**(1): p. 77-88.
  46. Huang, M. and A.D. D'Andrea, *A new nuclease member of the FAN club*. *Nat Struct Mol Biol*, 2010. **17**(8): p. 926-928.
  47. Ciccía, A., N. McDonald, and S.C. West, *Structural and Functional Relationships of the XPF/MUS81 Family of Proteins*. *Annual Review of Biochemistry*, 2008. **77**(1): p. 259-287.
  48. Yoshikiyo, K., et al., *KIAA1018/FANL nuclease protects cells against genomic instability induced by interstrand cross-linking agents*. *Proceedings of the National Academy of Sciences*, 2010. **107**(50): p. 21553-21557.
  49. Ciccía, A. and S.J. Elledge, *The DNA Damage Response: Making It Safe to Play with Knives*. *Molecular Cell*, 2010. **40**(2): p. 179-204.
  50. Bryant, H.E., et al., *PARP is activated at stalled forks to mediate Mre11-dependent replication restart and recombination*. *The EMBO Journal*, 2009. **28**(17): p. 2601-15.
  51. Venkitaraman, A.R., *Cancer susceptibility and the functions of BRCA1 and BRCA2*. *Cell*, 2002. **108**(2): p. 171-82.
  52. McCabe, N., et al., *Deficiency in the repair of DNA damage by homologous recombination and sensitivity to poly(ADP-ribose) polymerase inhibition*. *Cancer Research*, 2006. **66**(16): p. 8109-15.
  53. Graeser, M., et al., *A marker of homologous recombination predicts pathologic complete response to neoadjuvant chemotherapy in primary breast cancer*. *Clinical cancer research : an official journal of the American Association for Cancer Research*, 2010. **16**(24): p. 6159-68.
  54. Heyer, W.-D., *Recombination: Holliday Junction Resolution and Crossover Formation*. *Current Biology*, 2004. **14**(2): p. R56-R58.
  55. Holliday, R., *A mechanism for gene conversion in fungi*. *Genetical research*, 2007. **89**(5-6): p. 285-307.
  56. Wechsler, T., S. Newman, and S.C. West, *Aberrant chromosome morphology in human cells defective for Holliday junction resolution*. *Nature*, 2011. **471**(7340): p. 642-646.

57. Deakayne, J.S. and A.V. Mazin, *Fanconi anemia: at the Crossroads of DNA repair*. Biochemistry (Moscow), 2011. **76**(1): p. 36-48.
58. Yamamoto, K.N., et al., *Involvement of SLX4 in interstrand cross-link repair is regulated by the Fanconi anemia pathway*. Proceedings of the National Academy of Sciences, 2011.
59. MacKay, C., et al., *Identification of KIAA1018/FAN1, a DNA repair nuclease recruited to DNA damage by monoubiquitinated FANCD2*. Cell, 2010. **142**(1): p. 65-76.
60. Sengerova, B., A.T. Wang, and P.J. McHugh, *Orchestrating the nucleases involved in DNA interstrand cross-link (ICL) repair*. Cell Cycle, 2011. **10**(23): p. 3999-4008.
61. De Vos, M., V. Schreiber, and F. Dantzer, *The diverse roles and clinical relevance of PARPs in DNA damage repair: current state of the art*. Biochemical Pharmacology, 2012. **84**(2): p. 137-46.
62. Nijman, S.M., *Synthetic lethality: general principles, utility and detection using genetic screens in human cells*. FEBS Letters, 2011. **585**(1): p. 1-6.
63. Dobzhansky, T., *Genetics of Natural Populations. Xiii. Recombination and Variability in Populations of Drosophila Pseudoobscura*. Genetics, 1946. **31**(3): p. 269-90.
64. Chan, D.A. and A.J. Giaccia, *Harnessing synthetic lethal interactions in anticancer drug discovery*. Nature reviews. Drug discovery, 2011. **10**(5): p. 351-64.
65. Murai, J., et al., *Trapping of PARP1 and PARP2 by Clinical PARP Inhibitors*. Cancer Research, 2012. **72**(21): p. 5588-99.
66. Strom, C.E., et al., *Poly (ADP-ribose) polymerase (PARP) is not involved in base excision repair but PARP inhibition traps a single-strand intermediate*. Nucleic Acids Research, 2011. **39**(8): p. 3166-75.
67. Bryant, H.E., et al., *Specific killing of BRCA2-deficient tumours with inhibitors of poly(ADP-ribose) polymerase*. Nature, 2005. **434**(7035): p. 913-7.
68. Farmer, H., et al., *Targeting the DNA repair defect in BRCA mutant cells as a therapeutic strategy*. Nature, 2005. **434**(7035): p. 917-21.
69. Willers, H., et al., *Biomarkers and Mechanisms of FANCD2 Function*. Journal of Biomedicine and Biotechnology, 2008. **2008**.
70. Wang, M., et al., *EGF receptor inhibition radiosensitizes NSCLC cells by inducing senescence in cells sustaining DNA double-strand breaks*. Cancer Research, 2011. **71**(19): p. 6261-9.
71. Sharma, S.V., et al., *A Chromatin-Mediated Reversible Drug-Tolerant State in Cancer Cell Subpopulations*. Cell, 2010. **141**(1): p. 69-80.
72. Bradford, M.M., *A rapid and sensitive method for the quantitation of microgram quantities of protein utilizing the principle of protein-dye binding*. Analytical biochemistry, 1976. **72**: p. 248-54.
73. Kachnic, L.A., et al., *FANCD2 but not FANCA promotes cellular resistance to type II topoisomerase poisons*. Cancer Letters, 2011. **305**(1): p. 86-93.
74. Borgmann, K., et al., *Genetic determination of chromosomal radiosensitivities in G0- and G2-phase human lymphocytes*. Radiotherapy and oncology : journal of the European Society for Therapeutic Radiology and Oncology, 2007. **83**(2): p. 196-202.
75. Sordella, R., et al., *Gefitinib-sensitizing EGFR mutations in lung cancer activate anti-apoptotic pathways*. Science, 2004. **305**(5687): p. 1163-7.

76. Smogorzewska, A., et al., *A genetic screen identifies FAN1, a Fanconi anemia-associated nuclease necessary for DNA interstrand crosslink repair*. *Molecular Cell*, 2010. **39**(1): p. 36-47.
77. Olive, P.L. and J.P. Banath, *Kinetics of H2AX phosphorylation after exposure to cisplatin*. *Cytometry. Part B, Clinical cytometry*, 2009. **76**(2): p. 79-90.
78. Kennedy, R.D., et al., *Fanconi anemia pathway-deficient tumor cells are hypersensitive to inhibition of ataxia telangiectasia mutated*. *The Journal of clinical investigation*, 2007. **117**(5): p. 1440-9.
79. Yamamoto, K., et al., *Upregulated ATM gene expression and activated DNA crosslink-induced damage response checkpoint in Fanconi anemia: implications for carcinogenesis*. *Molecular medicine*, 2008. **14**(3-4): p. 167-74.
80. Plo, I., et al., *AKT1 inhibits homologous recombination by inducing cytoplasmic retention of BRCA1 and RAD51*. *Cancer Research*, 2008. **68**(22): p. 9404-12.
81. Zou, Y., et al., *Functions of human replication protein A (RPA): from DNA replication to DNA damage and stress responses*. *Journal of Cellular Physiology*, 2006. **208**(2): p. 267-73.
82. Sleeth, K.M., et al., *RPA mediates recombination repair during replication stress and is displaced from DNA by checkpoint signaling in human cells*. *Journal of Molecular Biology*, 2007. **373**(1): p. 38-47.
83. Robison, J.G., et al., *DNA lesion-specific co-localization of the Mre11/Rad50/Nbs1 (MRN) complex and replication protein A (RPA) to repair foci*. *The Journal of biological chemistry*, 2005. **280**(13): p. 12927-34.
84. D'Andrea, A.D. and M. Grompe, *The Fanconi anaemia/BRCA pathway*. *Nature Reviews Cancer*, 2003. **3**(1): p. 23-34.
85. Almeida, G.M., et al., *Detection of oxaliplatin-induced DNA crosslinks in vitro and in cancer patients using the alkaline comet assay*. *DNA Repair*, 2006. **5**(2): p. 219-25.
86. Wu, J.H. and N.J. Jones, *Assessment of DNA Interstrand Crosslinks Using the Modified Alkaline Comet Assay*. 2012. **817**: p. 165-181.
87. Sgambato, A., et al., *The role of EGFR tyrosine kinase inhibitors in the first-line treatment of advanced non small cell lung cancer patients harboring EGFR mutation*. *Curr Med Chem*, 2012. **19**(20): p. 3337-52.
88. Mitsudomi, T., et al., *Gefitinib versus cisplatin plus docetaxel in patients with non-small-cell lung cancer harbouring mutations of the epidermal growth factor receptor (WJTOG3405): an open label, randomised phase 3 trial*. *The Lancet Oncology*, 2010. **11**(2): p. 121-8.
89. Maemondo, M., et al., *Gefitinib or chemotherapy for non-small-cell lung cancer with mutated EGFR*. *The New England journal of medicine*, 2010. **362**(25): p. 2380-8.
90. Zhou, C., et al., *Erlotinib versus chemotherapy as first-line treatment for patients with advanced EGFR mutation-positive non-small-cell lung cancer (OPTIMAL, CTONG-0802): a multicentre, open-label, randomised, phase 3 study*. *The Lancet Oncology*, 2011. **12**(8): p. 735-42.
91. Rosell, R., et al., *Erlotinib versus standard chemotherapy as first-line treatment for European patients with advanced EGFR mutation-positive non-small-cell lung cancer (EURTAC): a multicentre, open-label, randomised phase 3 trial*. *The Lancet Oncology*, 2012. **13**(3): p. 239-46.
92. Clingen, P.H., et al., *Histone H2AX phosphorylation as a molecular pharmacological marker for DNA interstrand crosslink cancer chemotherapy*. *Biochemical Pharmacology*, 2008. **76**(1): p. 19-27.

93. Rothfuss, A. and M. Grompe, *Repair kinetics of genomic interstrand DNA cross-links: evidence for DNA double-strand break-dependent activation of the Fanconi anemia/BRCA pathway*. *Molecular and Cellular Biology*, 2004. **24**(1): p. 123-34.
94. Fernandez-Capetillo, O., et al., *H2AX: the histone guardian of the genome*. *DNA Repair*, 2004. **3**(8-9): p. 959-67.
95. Lyakhovich, A. and J. Surrallés, *New roads to FA/BRCA pathway: H2AX*. *Cell Cycle*, 2007. **6**(9): p. 1019-23.
96. Huang, X., et al., *Assessment of histone H2AX phosphorylation induced by DNA topoisomerase I and II inhibitors topotecan and mitoxantrone and by the DNA cross-linking agent cisplatin*. *Cytometry. Part A : the journal of the International Society for Analytical Cytology*, 2004. **58**(2): p. 99-110.
97. Niedernhofer, L.J., et al., *The structure-specific endonuclease Ercc1-Xpf is required to resolve DNA interstrand cross-link-induced double-strand breaks*. *Molecular and Cellular Biology*, 2004. **24**(13): p. 5776-87.
98. Mogi, S. and D.H. Oh, *gamma-H2AX formation in response to interstrand crosslinks requires XPF in human cells*. *DNA Repair*, 2006. **5**(6): p. 731-40.
99. Oostra, A.B., et al., *Diagnosis of fanconi anemia: chromosomal breakage analysis*. *Anemia*, 2012. **2012**: p. 238731.
100. Taniguchi, T., et al., *Disruption of the Fanconi anemia–BRCA pathway in cisplatin-sensitive ovarian tumors*. *Nature Medicine*, 2003. **9**(5): p. 568-574.
101. Chirnomas, D., et al., *Chemosensitization to cisplatin by inhibitors of the Fanconi anemia/BRCA pathway*. *Molecular Cancer Therapeutics*, 2006. **5**(4): p. 952-61.
102. Digweed, M., et al., *Attenuation of the formation of DNA-repair foci containing RAD51 in Fanconi anaemia*. *Carcinogenesis*, 2002. **23**(7): p. 1121-6.
103. Lo, H.W. and M.C. Hung, *Nuclear EGFR signaling network in cancers: linking EGFR pathway to cell cycle progression, nitric oxide pathway and patient survival*. *Br J Cancer*, 2006. **94**(2): p. 184-188.
104. Bunting, S.F. and A. Nussenzweig, *Dangerous liaisons: Fanconi anemia and toxic nonhomologous end joining in DNA crosslink repair*. *Molecular Cell*, 2010. **39**(2): p. 164-6.
105. Jeggo, P. and M.F. Lavin, *Cellular radiosensitivity: How much better do we understand it?* *International Journal of Radiation Biology*, 2009. **85**(12): p. 1061-1081.
106. Nussenzweig, A. and M.C. Nussenzweig, *Origin of chromosomal translocations in lymphoid cancer*. *Cell*, 2010. **141**(1): p. 27-38.
107. Frankenberg-Schwager, M., et al., *Cisplatin-mediated DNA double-strand breaks in replicating but not in quiescent cells of the yeast *Saccharomyces cerevisiae**. *Toxicology*, 2005. **212**(2-3): p. 175-84.
108. Collins, A.R., *Mutant rodent cell lines sensitive to ultraviolet light, ionizing radiation and cross-linking agents: a comprehensive survey of genetic and biochemical characteristics*. *Mutation research*, 1993. **293**(2): p. 99-118.
109. Adamo, A., et al., *Preventing nonhomologous end joining suppresses DNA repair defects of Fanconi anemia*. *Molecular Cell*, 2010. **39**(1): p. 25-35.
110. Pace, P., et al., *Ku70 corrupts DNA repair in the absence of the Fanconi anemia pathway*. *Science*, 2010. **329**(5988): p. 219-23.
111. Pfäffle, H.N., et al., *EGFR activating mutations correlate with a Fanconi anemia-like cellular phenotype that includes PARP inhibitor sensitivity*. *Cancer Research*, 2013.
112. Gandara, D.R., et al., *Association of Epidermal Growth Factor Receptor Activating Mutations with Low ERCC1 Gene Expression in Non-small Cell Lung Cancer*.

- Journal of Thoracic Oncology, 2010. **5**(12): p. 1933-1938  
10.1097/JTO.0b013e3181fd418d.
113. Wang, X., P.R. Andreassen, and A.D. D'Andrea, *Functional Interaction of Monoubiquitinated FANCD2 and BRCA2/FANCD1 in Chromatin*. Molecular and Cellular Biology, 2004. **24**(13): p. 5850-5862.
  114. Symington, L.S. and J. Gautier, *Double-Strand Break End Resection and Repair Pathway Choice*. Annual Review of Genetics, 2011. **45**(1): p. 247-271.
  115. Liberi, G., et al., *Rad51-dependent DNA structures accumulate at damaged replication forks in sgs1 mutants defective in the yeast ortholog of BLM RecQ helicase*. Genes & Development, 2005. **19**(3): p. 339-50.
  116. Svendsen, J.M. and J.W. Harper, *GEN1/Yen1 and the SLX4 complex: Solutions to the problem of Holliday junction resolution*. Genes & Development, 2010. **24**(6): p. 521-36.
  117. Marks, J.L., et al., *EGFR mutant lung adenocarcinomas in patients with germline BRCA mutations*. Journal of thoracic oncology : official publication of the International Association for the Study of Lung Cancer, 2008. **3**(7): p. 805.
  118. Lakhani, S.R., et al., *Prediction of BRCA1 status in patients with breast cancer using estrogen receptor and basal phenotype*. Clinical cancer research : an official journal of the American Association for Cancer Research, 2005. **11**(14): p. 5175-80.
  119. Willers, H., et al., *Utility of DNA repair protein foci for the detection of putative BRCA1 pathway defects in breast cancer biopsies*. Molecular cancer research : MCR, 2009. **7**(8): p. 1304-9.
  120. Hegde, M.L., et al., *Oxidative genome damage and its repair: implications in aging and neurodegenerative diseases*. Mechanisms of ageing and development, 2012. **133**(4): p. 157-68.
  121. Speit, G. and A. Rothfuss, *The comet assay: a sensitive genotoxicity test for the detection of DNA damage and repair*. Methods in molecular biology, 2012. **920**: p. 79-90.
  122. Olive, P.L., *Cell proliferation as a requirement for development of the contact effect in Chinese hamster V79 spheroids*. Radiation research, 1989. **117**(1): p. 79-92.
  123. Orcutt, K.P., et al., *Erlotinib-mediated inhibition of EGFR signaling induces metabolic oxidative stress through NOX4*. Cancer Research, 2011. **71**(11): p. 3932-40.
  124. Sancho, P., et al., *The inhibition of the epidermal growth factor (EGF) pathway enhances TGF-beta-induced apoptosis in rat hepatoma cells through inducing oxidative stress coincident with a change in the expression pattern of the NADPH oxidases (NOX) isoforms*. Biochimica et biophysica acta, 2009. **1793**(2): p. 253-63.

# **7. APPENDIX**

## 7.1. Abbreviations

Abbreviations	
ATM	ataxia telangiectasia mutated
BRCA1/2	breast cancer 1/2, early onset
BSA	bovine serum albumin
cp	cisplatin
DDR	DNA damage response
dH <sub>2</sub> O	deionized H <sub>2</sub> O
DNA	Deoxyribonucleic acid
DSB	double strand break
EGFR	epidermal growth factor receptor
FA	Fanconi Anemia
FAN1	FANCD2-associated nuclease 1, KIAA1018
FANCA/B/C/...	Fanconi Anemia complementation group A/B/C...
HJ	Holliday junction
HRR	homologous recombination repair
ICL	interstrand crosslink
IR	irradiation
mAb	monoclonal antibody
MAPK	mitogen-activated protein kinase
max	maximum
MEF	mouse embryonic fibroblasts
min	minutes
MMC	mitomycin C
MRN complex	Mre11, Rad50 and NSB1
Ms	mouse
mut	mutant
NER	nucleotide excision repair
NSCLC	Non-small cell lung cancer
pAb	polyclonal antibody
PARP	poly(ADP-ribose) polymerase
Pen-Strep	penicillin streptomycin
PFA	paraformaldehyde
PI3K	phosphatidylinositol 3-kinase
q.s.	quantum satis
Rb	rabbit
RPA	replication protein A
RT	room temperature
SCLC	Small cell lung cancer
ser	serine
SF	survival fraction
SOC medium	Super optimal broth with catabolite repression
SSB	single-strand break

---

SSBR	single-strand break repair
STAT	signal transducer and activator of transcription
TBST	Tris-Buffered Saline and Tween20) Solution
TKI	tyrosine kinase inhibitor
TLS	translesion synthesis
UBZ4	ubiquitin-binding zinc finger 4
wt	wild-type

## 7.2. Publications

### Journal Articles:

Heike N. Pfäffle, Meng Wang, Liliana Gheroghiu, Natalie Ferraiolo, Patricica Greninger, Kerstin Borgmann, Jeffrey Settleman, Cyril H. Benes, Lecia V. Sequist, Lee Zou, and Henning Willers, **EGFR activating mutations correlate with a Fanconi anemia-like cellular phenotype that includes PARP inhibitor sensitivity**. Cancer Research, epub ahead of print 2013

Birkelbach, M.\*, Ferraiolo, N.\*, Gheorghiu, L., Pfäffle, H. N., Daly, B., Ebright, M. I., Spencer, C., O'Hara, C., Whetstine, J. R., Benes, C. H., Sequist, L. V., Zou, L., Dahm-Daphi, J., Kachnic, L. A., Willers, H., **Detection of impaired homologous recombination repair in NSCLC cells and tissues**. J Thorac Oncol, 2013. **8**(3): p. 279-86.

\*authors contributed equally to this article.

### Book Chapter:

Willers, H., H.N. Pfäffle, and L. Zou, **Targeting Homologous Recombination Repair in Cancer**, in DNA Repair in Cancer Therapy: Molecular Targets and Clinical Applications, M.R. Kelley, Editor 2011, Academic Press, Elsevier. p. 119-160.

### Poster and Oral Presentation:

Heike N. Pfäffle, Meng Wang, Liliana Gheroghiu, Natalie Ferraiolo, Patricica Greninger, Kerstin Borgmann, Jeffrey Settleman, Cyril H. Benes, Lecia V. Sequist, Lee Zou, and Henning Willers, **EGFR-mutant lung cancer cells exhibit a Fanconi Anemia-like phenotype including PARP inhibitor sensitivity**. Dana-Farber/Harvard Cancer Center Lung Cancer Program Symposium, Harvard Medical School, Boston, USA

In a poster abstract competition this work received the highest score among 26 entries and was awarded a 500\$ cash prize by the Governance Committee of the Dana-Farber/Harvard Cancer Center Lung Cancer Program. The award included the invitation as a speaker to present the findings at the Lung Cancer Program Symposium.

## 7.3. Curriculum vitae

### Personal data:

Name Heike Natalie Pfäffle  
Nationality German  
Email Heike.Pfaeffle@gmail.com

### Academic Education:

2009 - 2013	<b>Harvard Medical School/Massachusetts General Hospital</b> <b>Ludwig Maximilian University</b> <i>Ph.D. Student in Pharmaceutical Biology</i> Thesis project: "Exploiting DNA repair defects in Non-Small Cell Lung Cancer (NSCLC) for targeted therapy"	<b>Boston, USA</b> <b>Munich, Germany</b>
2007 - 2008	<b>National Institutes of Health (NIH)</b> <i>Research Intern</i> 6-month research internship on viral vectors capable of delivering a gene of interest to non-dividing cells.	<b>Bethesda, USA</b>
2003 - 2007	<b>Albert-Ludwigs University</b> <i>Pharmacy Student</i> Degree: Approbation (German equivalent to Pharm.D.) – Pharmacy License for Europe	<b>Freiburg, Germany</b>

## 7.4. Acknowledgments

I would like to express my sincere gratitude to my advisor Prof. Dr. Henning Willers. This project would not have been possible without his valuable guidance and advice. No matter how busy times were, he always found time for me when I needed his expertise.

I am deeply thankful to Prof. Dr. Angelika Vollmar for supervising and advising me on this Ph.D. thesis. Thanks to her support and open mind I was able to conduct all my research for this dissertation abroad. Without her this external Ph.D. would not have been possible.

Furthermore, I would like to thank Prof. Dr. Wagner, Prof. Dr. Zahler, Prof. Dr. Biel and Prof. Dr. Wahl-Schott for taking the time to be on my thesis committee. I greatly appreciate the interest in my work.

Many, many thanks go to my colleagues at Massachusetts General Hospital Meng Wang, Liliana Gheorghiu, and Natalie Ferraiolo. Besides contributing to this work, they were always there for me not only in scientific matters, but also as great friends.

I am also very thankful for the help from Chake Tokadjian. She has great experience with colony formation assays and keeps our lab running.

Moreover, I would like to thank Prof. Dr. Kathryn Held for her great advice, her lab and everyone else in the Willers's lab for creating such a fun learning environment. I consider myself truly lucky to have been part of this unique research group.

Thank you to Saman for making work at lab all the more fun and for being such an amazing friend.

I would like to thank Christian, who patiently listened to all my science problems. He was always there to support and encourage me, whenever I needed it most.

Finally, many thanks go to my whole family, my parents and sister Nicole. They gave me their unlimited support and encouragement on all my endeavors, and I am deeply grateful for that.